Experimental evaluation of the PHY layer of WSN focused on smart city applications

PhD Dissertation by Albert Angles Vazquez

aangles1984@gmail.com

Supervisors: Xavi Vilajosana and Jose Lopez Vicario

Department of Telecommunications and Systems Engineering

Universitat Autonoma de Barcelona

Bellaterra, June, 2013

Resum

Els ràpids avenços en les tecnologies de la informació i de les comunicacions ha permès avui en dia poder dissenyar i construïr per separat o compacte microcontroladors i transceptors de baix consum i baixa potència en un sol chip de silici (un sistema en un chip, en anglès conegut com *System on Chip*). Simultàniament el continu augment de la demanda de utilitats degudes a les activitats econòmiques i a l'expansió de la població ha conduït a un ús insostenible dels recursos naturals de la Terra amb un afecte advers sobre l'entorn. El poder mantenir l'equilibri entre la disponibilitat dels recursos i utilitats amb l'entorn és un dels desafiaments més grans que les ciutats, Europa i el món estan fent front avui dia. Per tal de fer front les problemàtiques causades per la falta de recursos suficient tals com la electricitat, l'aigua, el transport i proporcionar les necessitats a una area urbana amb un enorme continu creixement de la població, és important fer ciutats energèticament eficients i sostenibles. A partir d'aquí neix el concepte de ciutat intel·ligent. La idea bàsica d'aquest concepte es la presència omnipresent d'un conjunt de xarxes sense fils formades per dispositius inalàmbrics petits de baix consum operant amb bateries, són programables (intel·ligents), coneguts com DCA (Dispositius de Curt Abast, en anglès SRD-Short Range Devices) que s'integren a les coses i són capaços d'interactuar amb l'entorn i amb els nodes veïns per tal de proporcionar les necessitats a les ciutats, dintre del context de les tecnologies sense fils M2M (Machine to Machine). Les ciutats intel·ligents són alhora un dels pardigmes que formen part del context de Internet de les coses (IoT-Internet of Things) tals que la informació relacionada amb les coses podrà ser monitoritzada, gestionada i controlada (ex: contenidors, enllumenat públic, places d'aparcament, l'aigua, etc.) sense la intervenció humana. En aquest context les xarxes de sensors sense fils tenen un paper important. El paper d'aquestes xarxes de sensors sense fils en el futur IoT és un dels camps de recerca interessants i emergents per diverses raons: primera, aquests dispositius inalàmbrics tenen restriccions energètiques, el consum de potència és un factor important que s'ha de tenir en consideració. Segon, donat que aquests dispositius poden ser desplegats a qualssevol lloc, la màxima potència de transmissió legal de 14 dBm (25 mW) a Europa és un gran repte amb impediments en escenarios on no hi ha visió directa entre transmissor i receptor. Per exemple, un gran repte és la comunicació entre nodes desplegats a prop del terra, donat que el mateix terra introdueix unes pèrdues de potència considerables en funció de la freqüència, difultant la propagació de les ones electromagnètiques i

per tant la dificultat d'aconseguir distàncies de comunicació elevades. Tercer, el gran número de nodes que poden arribar a ser desplegats en una area urbana pot causar interferències entre ells provocant pèrdues de paquets, retransmissions i per tant un augment del consum energètic degut a les retransmissions. Per aquestes raons, aquesta tesis es centra en estudiar aspectes capa física, amb una modelització teòrica de l'entorn amb el suport de mesures. En concret aquesta tesi evalua primerament la propagació (a gran escala) en la banda de Europa 868 MHz en escenaris de comunicació típics en entorns urbans. Posteriorment s'evalua i es compara els aspectes de propagació (a gran escala i a petita escala) de les bandes ISM (Industrial, Scientific and Medical) 433 MHz i 2.4 GHz a partir de fonaments teòrics i pràctics. La banda de 433 MHz és una possible banda candidata pel futur de les WSN oferint major alcanç i menor probabilitat d'interferència que la banda de 2.4 GHz donat a que hi ha menys dispositius operant a la banda de 433 MHz. Tots els anàlisis dels resultats obtinguts han surgit a partir d'un conjunt de campanyes de mesura amb fenòmens de propagació reals i dades reals.

Resumen

Los rápidos avances en las tecnologías de la información y de las comunicaciones ha permitido hoy en día poder diseñar y construir por separado o compacto microcontroladores y transceptors de bajo consumo y baja potencia en un solo chip de silicio (un sistema en un chip, en inglés conocido como *System on Chip*). Simultáneamente el continuo aumento de la demanda de utilidades debidas a las actividades económicas y a la expansión de la población ha conducido a un uso insostenible de los recursos naturales de la Tierra con un afecto adverso sobre el entorno. El poder mantener el equilibrio entre la disponibilidad de los recursos y utilidades con el entorno es uno de los desafíos más grandes que las ciudades, Europa y el mundo están haciendo frente hoy en día. Para hacer frente las problemáticas causadas por la falta de recursos suficiente tales como la electricidad, el agua, el transporte y proporcionar las necesidades a una área urbana con un enorme continuo crecimiento de la población, es importante hacer ciudades energéticamente eficientes y sostenibles. A partir de aquí nace el concepto de ciudad inteligentes. La idea básica de este concepto se la presencia omnipresente de un conjunto de redes inalámbricas formadas por dispositivos inalámbricos pequeños de bajo consumo que operan con baterías, son programables (inteligentes), conocidos como DCA (Dispositivos de Corto Alcance, en inglés SRD-Short Range Devices) que se integran a las cosas y son capaces de interactuar con el entorno y con los nodos vecinos para proporcionar las necesidades a las ciudades, dentro del contexto de las tecnologías inalámbricas M2M (Machine to Machine). Las ciudades inteligentes es a la vez uno de los paradigmas que forman parte del contexto de Internet de las cosas (IoT-Internet of Things) tales que la información relacionada con las cosas podrá ser monitoritzada, gestionada y controlada (ej: contenedores, alumbrado público, plazas de aparcamiento, el agua, etc.) sin la intervención humana. En este contexto las redes de sensores inalámbricos juegan un papel importante. El papel de estas redes de sensores inalámbricos en el futuro del IoT es uno de los campos de investigación interesantes y emergentes por varias razones: primera, estos dispositivos inalámbrics tienen restricciones energéticas, el consumo de potencia es un factor importante que se tiene que tener en consideración. Segundo, dado que estos dispositivos pueden ser desplegados en cualquier lugar, la máxima potencia de transmisión legal de 14 dBm (25 mW) en Europa es un gran reto con impedimentos en escenarios donde no existe visión directa entre transmisor y receptor. Por ejemplo, un gran reto es la comunicación entre nodos desplegados cerca del suelo,

dado que el mismo suelo introduce unas pérdidas de potencia considerables en función de la frecuencia difultando la propagación de las ondas electromagnéticas y por lo tanto la dificultad de conseguir distancias de comunicación elevadas. Tercero, el gran número de nodos que pueden llegar a ser desplegados en una área urbana puede causar interferencias entre ellos provocando pérdidas de paquetes, retransmisiones y por lo tanto un aumento del consumo energético debido a las retransmisiones. Por estas razones, esta tesis se centra al estudiar aspectos capa física, con una modelización teórica del entorno respaldada con medidas. En concreto esta tesis evalua la propagación (a gran escala) en la banda de Europa 868 MHz en escenarios de comunicación típicos en entornos urbanos. Posteriormente se evalua y se compara los aspectos de propagación (a gran escala y a pequeña escala) de las bandas ISM(Industrial, Scientific and Medical) 433 MHz y 2.4 GHz a partir de fundamentos teóricos y prácticos. La banda de 433 MHz es una posible banda candidata para el futuro de las WSN ofreciendo mayor alcance y menor probabilidad de interferencia que la banda de 2.4 GHz dado a que hay menos dispositivos haciendo uso de la banda 433 MHz. Todos los análisis de los resultados obtenidos han surgido a partir de un conjunto de campañas de medida con fenómenos de propagación reales y datos reales.

Abstract

The fast advances in the Information and Telecommunication technologies has allowed nowadays to design and build embedded low power microcontrollers and low power transceivers on a Chip (System on Chip). In parallel, the increasing demand of utilities due to economic activities and population expansion has led to an unsustainable use of the earth natural resources with an adverse effect on the environment. Sustaining the utilities availability in balance with the environment is one of the biggest challenges that cities, Europe and the world are facing today. To face the problematics caused by the lack of enough resources such as electricity, water, transportation and to supply the needs of an urban area with a continuous tremendous growth of the population, it is crucial to make energy efficient and sustainable cities and hence smart. The basic idea of the smart cities is the ubiquitous presence of a set of networks composed by tiny battery-powered smart wireless autonomous devices, known as SRD's (Short Range Devices) which are embedded to the "things" capable to interact with each to provide the needs of the cities, in the context of Machine-to-Machine wireless communications. The smart cities is one of the paradigms in the future Internet Of Things, such that "things will be able to send information to be monitored " without human intervention. Wireless Sensor Networks plays an important role in the context of Internet of Things. The role of the WSN in the future Internet of Things is one of the interesting research fields for several reasons: first, since these tiny wireless devices have power constraints, the power consumption is an important factor that must be taken into consideration. Second, since devices can be deployed anywhere the low transmit power, i.e. maximum 14 dBm (25mW) in Europe, is challenge for those applications where there is not Line Of Sight between the transmitter and the receiver. For instance a big challenge is the propagation between near ground nodes since the ground itself causes a significant amount of power losses as a function of frequency making difficult to achieve long communication distances. Third, the large number of deployed devices may cause interference themselves and hence the loss of packets, retransmissions and an increase of the power consumption owed to the retransmissions. For that reason, this PhD dissertation is focused on the physical layer with the environment theoretical modeling supported with measurements. Specifically this PhD thesis is devoted first to evaluate the behavior of the propagation characteristics at the European 868 MHz band focused on low power wireless communications scenarios that may be typical in urban environments. Second

an evaluation and a comparison in terms of propagation aspects (both large and small scale) between the 433 MHz and 2.45 GHz ISM (Industrial, Scientific and Medical) bands is provided from a theoretical and experimental point of view. The 433 MHz band is a possible candidate band for the future WSN offering higher wireless range and lower interference probability than the actual 2.4 GHz band due to the low number of devices making use of the 433 MHz band. All the analysis of the obtained results come from a set of experimental measurement campaigns with real phenomenons and real data.

This PhD dissertation has been partially founded by TALENT-EMPRESA grant (TEM-DGR2009).

Dedicated to my parents and to Damià, Jorgina and Claudia.

"It is dangerous to put limits on wireless."
Gugliemlo Marconi (1937).

Agraïments

La vida és un llarg camí a recórrer amb diferents entrebancs de diferents nivells de dificultat que s'han de superar amb empenta i energia per tal de poder aconseguir coneixements enriquidors i enfrontar-se amb un futur desconegut i alhora difícil. Aquesta etapa doctoral, com una part de la vida, m'ha donat la oportunitat de trobar-m'he amb reptes els quals he hagut de superar. Primer de tot vull agraïr als meus pares ja que sense ells no estaría on estic ara i m'han donat empenta i autoestima per aconseguir els objectius. També vull agraïr als meus amics Carlos, Ivàn, Marc, Joan, Luí, Eneritz, Isa, Míriam i Susana (incloent les companyes de pis Marta, Roser, Lola i Sara) ja que durant aquesta llarga etapa m'han proporcionat moments de distracció i diversió (sopars, cinema, teatres, cases rurals, partits del Barça, etc.) que mai s'olvidaràn. Els coneixements consolidats en aquesta Tesis Doctoral han estat adquirits funamentalment pel co-director de Tesi José López Vicario que m'ha estat donant suport quan l'he necessitat i a més em va dónar a conèixer l'empresa on he estat cursant el Doctorat: WorldSensing, S.L. Vull agraïr doncs a tota la plantilla de l'empresa, especialment a Ignasi Vilajosana Guillèn com a director executiu, Jordi Llosa Melich com a coordinador d'enginyeria i Xavier Vilajosana Guillèn com a coordinador de les tecnologies de la informacó (i al mateix temps director de Tesi) per haver-me donat la oportunitat d'adquirir nous coneixements, d'especialitzar-me en el món de les xarxes de sensors sense fils i d'haver colaborat en un equip d'intel.lectuals i competents en el món de les TIC (Tecnologies de la Informació i Comunicacions) que ha fet possible la consolidat productes innovadors, un dels quals ha format part en el àmbit de recerca de la meva Tesis Doctoral. Per acabar, vull agraïr també a Pere Tuset Peiró, també doctorant de Xavier Vilajosana, qui m'ha donat la oportunitat de poder evaluar la banda de 433 MHz amb motes experimentals.

Albert Anglès
Barcelona, 17 de abril del 2013.

Many thanks to WorldSensing company!

Contents

List of Figures

List of Tables

Acronyms

RFID	Radio Frequency Identification
M2M	Machine to Machine
IoT	Internet Of Things
WSN	Wireless Sensor Network
IEEE	Institute of Electrics and Electronics Engineers
LR-WPAN	Low Rate Wireless Personal Area Networks
PHY	Physical layer
BPSK	Binary Phase Shift Keying
OQPSK	Offset Quaternary Phase Shift Keying
DSSS	Direct Sequence Spread Spectrum
FHSS	Frequency Hopping Spread Spectrum
FHSS	Frequency Hopping Spread Spectrum
ED	Energy Detection
CCA	Clear Channel Assessment
MAC	Medium Access Layer
LQI	Link Quality Indicator
SNR	Signal to Noise Ratio
CSMA-CA	Carrier Sense Multiple Access with Collision Avoidance
ETSI	European Telecommunications Standard Institute
SRD	Short Range Device
NLoS	Non Line Of Sight
LoS	Line Of Sight
RSS	Received Signal Strength

RSSI	Received Signal Strength Indicator
RMSE	Root Mean Square Error
EIRP	Equivalent Isotropic Radiated Power
LMP	Local Mean Power
MMSE	Minimum Mean Square Error
LBT	Listen Before Talk
AFA	Adaptive Frequency Agility
RBW	Resolution Bandwidth
SoC	System on Chip
RC	Raised Cosine
PER	Packet Error Rate
AWGN	Additive White Gaussian Noise
PDR	Packet Delivery Ratio
PER	Packet Error Rate
TX	Transmitter
RX	Receiver
FPCB	Flexible Printed Circuit Board
PCB	Printed Circuit Board
PSD	Power Spectral Density
VSWR	Voltage Standing Wave Ratio
FSPL	Free Space Path Loss
FS	Free Space
SMD	Surface Mount Device
CRC	Cyclic Redundancy Check
PA	Power Amplifier
LNA	Low Noise Amplifier
LS	Least Squares

Chapter 1

Introduction and Objectives

1.1 Motivation

Urban population is presenting a tremendous growth. Today more than 50% of the population lives in cities. In 2050 about 70% of global population will be living in cities [4, 5]. Every day 3 megalopolis like New York are being build in ASIA. Every citizen and every business in Europe relies on the availability of utilities such as water, waste removal or electricity as well as transportation in order to carry out their day to day activities and operations [6]. Their continuous supply is essential for the growth of global economy and well-being of world society in general. The increasing demand of utilities due to economic activities and population expansion has led to an unsustainable use of the earth natural resources with an adverse effect on the environment [7]. Sustaining the utilities availability in balance with the environment is one of the biggest challenges that cities, Europe and the world are facing today. To face the urban complexity and build more sustainable, and efficient cities we need to make them more smart. The smart cities or digital cities are a novel paradigm that is rapidly gaining ground in the scenario of modern wireless telecommunications in the century XXI.

The smart cities or the Internet of Things become nowadays one of the interesting research fields. The basic idea of this concepts is the pervasive presence of a variety of smart tiny things or IoT devices -such as RFID tags, sensors, actuators, etc- placed randomly in a urban region that are able to interact with each other and cooperate with their neighbors to reach common goals i.e [7]: smart waste management, smart water and sewage management, citizens and objects smart transport, smart metering and street lighting, smart parking spot management, smart urban traffic management, smart grid, etc. Applications for smart cities can be found in [8] and a platform for analyzing emergent phenomena in future power systems, based on the electricity infrastructure of a smart city is described by [9]. The use of modern wireless sensing M2M (Machine-to-Machine) technologies such as RFID (Radio Frequency Identification) and

WSN (Wireless Sensor Networks), addressed for low power tiny devices contribute to sustainable and optimized supply and intelligent digital access to services and resources in urban areas. Furthermore the use of Internet Protocol (IP)-based smart tiny devices which have access to Internet will allow the remotely monitoring of urban resources. For instance, experimental works of structural monitoring are carried out by [10] and [11]. Smart cities will help to make cities more sustainable by the use of IT technologies and managing the limited urban services and resources (i.e. waste, water, parking spots, electricity, etc.) in a efficient way to reduce costs, pollution and providing comfortable live to citizen. Device manufacturers, integrators or operators of urban services require propagation models as well as solutions that help them to ensure proper communication of the IoT devices.

Propagation models are a valuable tool for designing and deploying wireless communication devices. In addition to the propagation models, the choice of the frequency band or the PHY (Physical Layer) standard is crucial for future deployment purposes. The most common frequency bands covered by the standard IEEE 802.15.4[12] designated for low power wireless communications (WSN for instance) are 915 MHz(used in United States) with 10 channels and 2 MHz Bandwidth/channel, 868 MHz(used in Europe) with one 400 KHz channel and 2.4 GHz(worldwide ISM-Industrial-Scientific and Medical band) with 15 channels and 5 MHz/channel. Both 915 MHz and 868 MHz are not ISM bands since they are not worldwide available. The 868 MHz band in Europe is prone to high interference because the low number of available channels and the high number of devices making use of this band. The 2.4 GHz band has several disadvantages, despite of being an ISM band available worldwide for low power wireless applications: high propagation losses, high attenuation in obstacles penetration and high interferences with a large number of wireless technologies that are making use of it. In order to combat this problematic there is another ISM band that provides lower propagation losses as well as lower interferences because it is less crowded than the 2.4 GHz band. This is the 433 MHz ISM band that is also available worldwide, has a total bandwidth of 1.74 MHz and 15 channels with 108 KHz of bandwidth per channel.

1.2 Goals

Given the motivation stated above, the main goal of this thesis is to evaluate an discuss from a given theoretical background the PHY wireless propagation phenomenons by means of developed propagation models focused on typical smart city applications (i.e. nodes placed near ground). To the best of our knowledge most of the existing work in the literature do not cover in detail the propagation aspects that we cover in depth in this thesis.

In this thesis we provided a propagation model to understand the behavior of low power wireless communications operating at the 868 MHz band. Furthermore, given the advantages

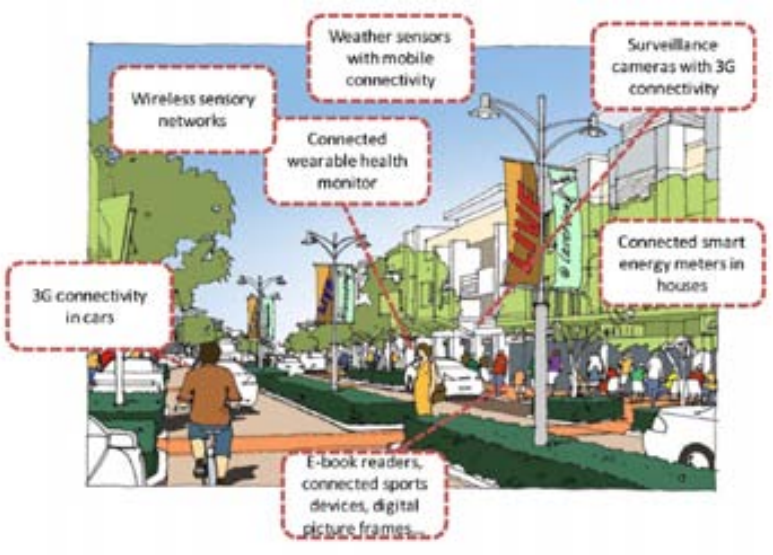

Figure 1.1: Concept of a Smart City where citizens, objects, utilities, etc, connect in a seamless manner using ubiquitous technologies, so as to significantly enhance the living experience in 21st century urban environments [1]

of the 433 MHz ISM band with respect to 868 MHz band and 2.4 GHz ISM band in terms of lower propagation losses, we experimentally demonstrate and compare its propagation aspects with the 2.4 GHz band and confirm our hypothesis.

The summary of the achieved goals in this thesis, which are based on PHY aspects is the following:

- We developed a generic propagation model conducted at the 868 MHz band that takes into account the antenna height from ground. The developed propagation model is suitable for smart city applications where either the transmitter and the receiver can be deployed at different heights from ground (e.g. smart waste management, smart street-lighting, smart water management, smart parking applications).
- We evaluated and discussed the propagation aspects of the 433 MHz band in comparison to the 2.4 GHz band in different environments in order to confirm its advantage in terms of lower propagation losses and higher wireless range with the same transmit power.

1.3 Document organization

This PhD dissertation is organized as follows. Chapter 2 introduces the IEEE 802.15.4 standard for short-range low power wireless communications and provides a theoretical background on wireless communications phenomenons. Chapter 3 focuses to understand the PHY wireless

propagation behavior at the 868 MHz in typical low power communication scenarios under urban environments. Chapter 4 focuses to understand the wireless propagation behavior at the 433 MHz band providing a comparison with the 2.45 GHz band. To this end, Chapter 5 concludes and this PhD dissertation.

1.4 Contributions

Chapter 3

The main contribution in this Chapter is a generic empiric propagation model addressed to low power lossy networks operating at the 868 MHz band for deployments in urban environments.

- A.Angles, X.Vilajosana, J.L.Vicario, A.Morell, P.Tuset, I.Vilajosana. " A generical empirical channel model for low power lossy networks at the 868 MHz band for smart cities ", IET Microwaves, Antennas & Propagation, 2013. (Under Review)

Chapter 4

The main contribution in this Chapter is the understanding of the propagation characteristics at the 433 MHz band and demonstrating that, under the same conditions, 433 MHz propagation is better in terms of range than 2.45 GHz. In addition, the empiric propagation model obtained in Chapter 4 is validated with two other frequency bands: 433 MHz and 2.45 GHz in both outdoor and indoor environments.

- P.Tuset, A.Angles, J.L.Vicario, X.Vilajosana. " On the suitability of the 433 Mhz band for M2M wireless communications: propagation aspects ". European Transactions on Telecommunications, 2013. (accepted)

Other Research Contributions

The author of this PhD dissertation has contributed as a co-author in other research contributions related to smart cities whose content is not included in the present document.

- I.Vilajosana X.Vilajosana, J.Llosa, B.Martinez, M.Domingo, and A.Angles. "Bootstrapping Smart Cities Through A Self-Sustainable Model Based On Big Data Flows. IEEE communications society, 2013. (accepted) "

Chapter 2

Background on wireless communications and IEEE 802.15.4 standard's overview

2.1 Introduction

In this Chapter we introduce the IEEE 802.15.4 standard for short-range low power wireless communications. Next we discuss the theory of wireless communications phenomenons.

The rest of the Chapter is organized as follows. In section 2.2 we introduce the main standards focused on low power wireless devices. In section 2.3 we give a theoretical background about wireless communications.

2.2 IEEE 802.15.4 international standard for low power wireless devices.

The IEEE 802.15.4 standard was created in 2003 with the first revision by the IEEE 802.15 Task 4 group to investigate a low data rate solution with multi-month to multi-year battery lifetime and very low complexity. It was called then the so called IEEE 802.15.4-2003. The last revision was made in 2011, so called as IEEE 802.15.4-2011 with additional improvements. Although the standard was focused for LR-WPAN it was accepted also for WSN because of the similar features. The standard defines both the PHY and the MAC layers. The PHY layer is responsible for the following tasks [12, 13]:

- Data transmission and reception: the PHY specifies three frequency bands with different

data rates as well as two kinds of modulation (BPSK and QPSK) and spreading techniques (DSSS and FHSS).

The three frequency bands are: 868-868.6 MHz (Europe) with only one channel, 902 MHz-928 MHz (Americas) with 10 channels of 2 MHz channel spacing and the global ISM band 2.4 GHz with 16 channels of 5 MHz channel spacing.

The data rates differ with respect to the frequency band under operation: 20 Kbps with BPSK at the 868 MHz band, 40 Kbps with BPSK at the 915 MHz band and 250 Kbps with OQPSK at the 2.4 GHz band. These data rates are compatible with the previous standard IEEE 802.15.4-2003. The further revision added improvements in the data rate: 100 kbps with OQPSK at the 868 MHz and 250 kbps also with OQPSK at the 915 MHz band. Table 2.1 summarizes all these information [12] being the data rates (*) as optional. In addition to the standard data rates the manufacturers of commercial equipments can offer higher data rates.

Frequency band (MHz)	**Spreading Parameters**			
	Chip Rate	**Modulation**	**Pulse Shaping**	**Bit Rate (Kb/s)**
868-868.6	300	BPSK	RC-1	20
	400*	ASK	SRRC-0.2	250
	400*	OQPSK	half-sine	100
902-928.6	600	BPSK	RC-1	40
	1600*	ASK	SRRC-0.2	250
	1000*	OQPSK	half-sine	250
2400-2483.5	2000	OQPSK	half-sine	250

Table 2.1: Frequency bands and data rates

The IEEE Std 802.15.4-2011 is amended by the standard IEEE Std 802.15.4e-2012 [14]. The IEEE802.15.4e is a working group by the IEEE which defines a MAC amendment to the existing standard 802.15.4-2006 to better support industrial markets. The key element of the solution proposed by 802.15.4e is channel hopping, which significantly increases robustness against external interference and persistent multi-path fading.

The IEEE 802.15.4f [2] Active RFID System Task Group is chartered to define new wireless Physical (PHY) layer(s) and enhancements to the 802.15.4-2006 standard MAC layer which are required to support new PHY(s) for Active RFID System bi-directional and location determination applications. This standard propose the use of the 433 MHz chan-

Parameter	Value
Frequency band	433.05MHz-434.79MHz
Number of supported Channels	3 @ 250kbps
Channel Bandwidth	540KHz @ 250kbps
Channel space	20KHz
Data Rate	250 kbps (other data rates are proposed: 1.2b/s, 38.4kbps and 500 kbps)
Modulation	MSK

Table 2.2: IEEE 433 MHz Channel Parameters [2]

nel as alternate 802.15.4-2006 PHY and MAC modification. This band has the following advantages:

- It is useful as the number of interfering transmitters is lower than 2.4 GHz band.
- Low cost and increased battery life as the energy per bit is minimized
- Optimal RF performance: low path loss and low signal attenuation (good range).
- Seamless Indoor and Outdoor use.
- Acceptable frequency band in most regions.

The IEEE 802.15.4f defines the channel parameters shown in Table 2.2. The default data rate of the PHY shall be 250 kbps and the longer communication range can be achieved with the data rate of 31.25 kbps. Additional optional data rates for the 433 MHz frequency band can be obtained with a mapping to the corresponding non-overlapping channels that are allowed to be used for each data rate. This standard is focused on the operation at the 433 MHz ISM band, which has 1.74 MHz of bandwidth, from 433.04 MHz to 433.79 MHz. Nevertheless, the actual bandwidth occupied by the standard extends from 433.056 MHz to 433.784 MHz, as there are two 6-kHz guard bands located at the beginning and the end of the spectrum. This standard defines 15 channels basic channels that are 108 kHz wide each, thus offering channel hopping.

2.3 Physical Propagation phenomenons in Wireless Communications

Wireless communications typically have the following behavior: the receiver power fluctuation around the mean is attributed to the contribution of one or several physical phenomenons such as shadowing, multipath (due to reflections) as shown in Figure 2.1 and diffraction. A brief discussion of these phenomenons is given below.

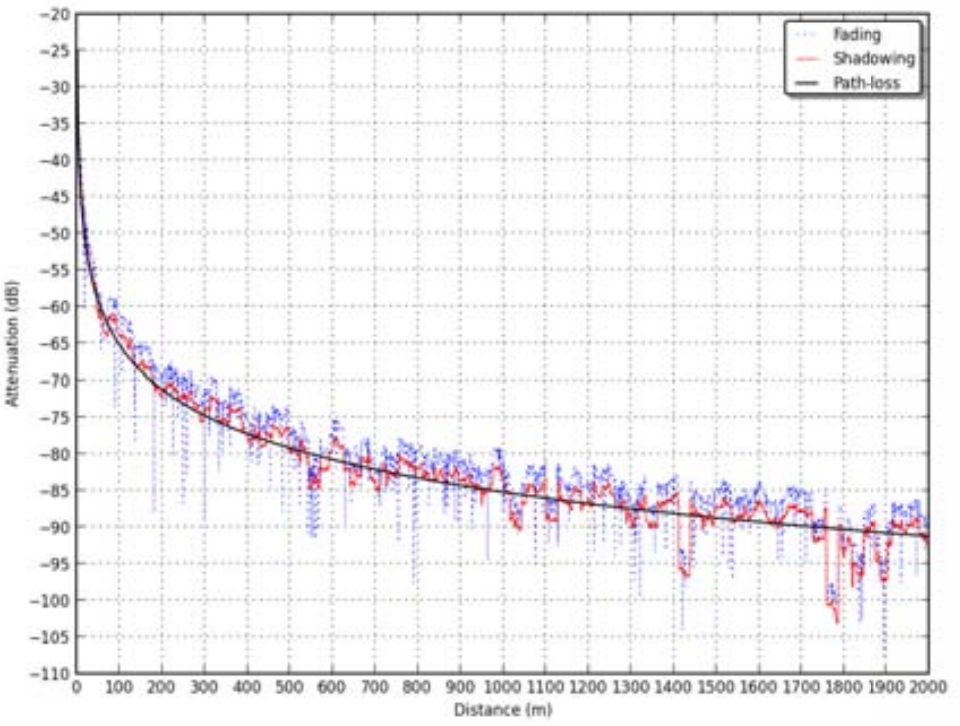

Figure 2.1: Path Loss, Shadowing and Multipath versus Distance. The fadings are caused by multipath. .

2.3.1 Shadowing (a.k.a large-width fading)

The shadowing effect is common when TX and RX antennas are at heights lower than the obstacles. Shadowing occurs in NLOS, when the visibility between the transmitter and receiver is obstructed. The shadowing effect induces high fluctuations over the path loss-predicting attenuations or gains in the received signal [15]. The statistical distribution of the random received power due to shadowing is log-normal with mean μ_{dBm} and standard deviation σ_{dBm} both in dBm units. The mean can be based on empirical measurements which equals the averaged received power in order to remove the multipath and shadowing contribution. In fact the shadowing can be treated as a log-normal random variable with zero-mean and standard deviation σ_{dB} [16, 17, 18]. Hence the shadowing incorporates reflection, diffraction and scattering for both LOS and NLOS paths[16]. Most empirical studies show standard deviations between 3 dB and 4 dB [17, 19]. However there are not enough shadowing empirical measurements for sensor networks at the band 868 MHz.

Since variations due to path loss combined with shadowing occur over relatively large distances (100-10000m), these variations are sometimes referred to as **large-width fading.**

2.3.2 Multipath (a.k.a small-scale fading)

The nature of any wireless media makes that the transmitted signal reaches the receiver with other m replicas (m extends from 0 to) due to surface reflection. In Figure 2.2 we show an urban environments with several buildings around the wireless link between TX and RX. One can consider these buildings as objects. The main ray is the blue one and the other rays reaching the receiver are reflections from the other objects except the ground reflection being the dark one.

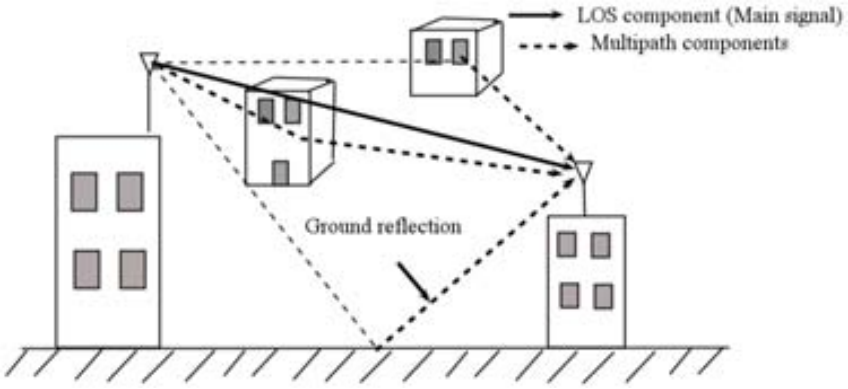

Figure 2.2: Multipath wireless phenomenon

Each of these replicas reaches the receiver through different paths or angles γ and different path lengths L_m with a delay of τ_m. The maximum τ_m is refereed to as channel delay spread. All the received signals from paths other than the direct path become attenuated experimenting a phase shift of $\pm\theta_n$ radiants in each reflection. This phase shift is Gaussian distributed from $[-\pi\ \pi]$ [18]. Hence the combined signal components at the receiver causes positive and negative variations with respect to the main signal received from the direct path. It is known as constructive and destructive interference. For example if m received interference signals are in-phase the result is the sum of these m signal replicas; if they are out-of phase they cancel each other.Hence, a statistical model for the received signal in a multipath wireless channel is defined by (2.1)[18, 20]:

$$r(t) = \mathbb{R}\left\{ s(t)e^{j(2\pi f_c t+\phi)} \left(\sum_{n=1}^{M} \alpha_n(t) e^{-j\theta_n} \delta(t-\tau_n) \right) \right\} \tag{2.1}$$

being $s(t)$ the transmitted signal at the center frequency f_c with an arbitrary phase γ, α_n is the attenuation coefficient associated to the n signal replica, θ_n is the phase shift of the n signal replica and $\delta(t-\tau_n)$ is the Dirac delta delayed τ_n.

Multipath effect occurs over short distances at the order of λ 2 so these variations are sometimes refereed to as **small-scale fading**. We call this short movement as coherence length [21, 18].

A way to to take advantage of multipath is the use of spatial diversity with several antennas separated λ 2 [22].

2.3.3 Diffraction (Fresnel Zone)

The condition of visibility or Line Of Sight between the transmitter antenna and the receiver antenna applies when there is no obstruction inside the first Fresnel zone and thus the diffraction phenomenon is null. In any wireless link there appears n Fresnel zones. These have a form like a revolution ellipsoid with the major axis equals to $R + n\lambda$ 2. The intersection of an infinite plane P with the revolution ellipsoids defines a set of concentric circles with radius R_n known as Fresnel zone radius. These radius of the n Fresnel zones theoretically can be found by the formula (2.2)[23].

$$R_n = \sqrt{n\lambda \frac{d_1 d_2}{d_1 + d_2}} \tag{2.2}$$

being d_1 d_2 the distances from both TX and RX antennas to the plane P. Figure 2.3 shows an intuitive idea with the plane located at the middle, as well as the set of Fresnel zones. The received field at the receiver antenna is the contribution of all the fields coming from each of the Fresnel zones. However the main wavefront is the first Fresnel zone since the other zones are canceled each other because of the phase lag of 180°. The radio link between TX and RX in Figure 2.3 is considered to be obstructed or in LOS when the top of the obstacle is at $h < 0$. When $h \geq 0$ the losses increases significantly much greater than in free space causing thus a drastic diminution of the received power.

The formula is known as **Fresnel knife edge diffraction model** because assumes an asymptotically thin diffraction object between TX and RX.

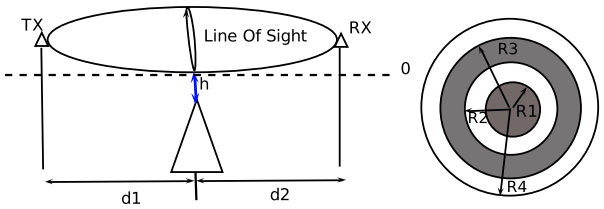

Figure 2.3: Diffraction model (left) and the radio Fresnel zones (right)

2.3.3.1 Path loss models description

The path loss is a wireless channel characteristic which accounts for the power losses of a traveling electromagnetic wave through space. Path loss models are useful to predict the

coverage in terms of mean RSS in any scenario and thus defining transmit power, network topology, inter-node distance and so on.

As aforementioned in section 2.3 the RSS variation due to path loss and shadowing occurs over very large distances, whereas the RSS variation due to multipath occurs over distances on the order of the λ or signal wavelength. The path loss is the mean RSS which decays lineally with distance.

There exists both theoretical and empirical path loss models each of them is useful in its own conditions. Theoretical models can be useful if the environment is known and not complex. However most of the outdoor environments are complex and in practice it is not suitable to use theoretical models due to the number of multipath components as well as dielectric properties of the propagation environment are unknown. Therefore in such cases it is more practice to use empirical models with parameters based on measurements. Models usually find these parameters by means of LS (Least Squares)[17, 13, 18]. LS method find the corresponding model that best fits to the measurement data, i.e. LS finds the model parameters that minimizes the RMSE between the model and the measurements.

The linear mean path loss is defined as the ratio between the power of the transmitted signal (P_t) to the mean power of the received signal ($\overline{RSS}$) assuming real antennas with transmitter and receiver antennas peak gains G_{Tx} and G_{Rx} respectively[18]:

$$\overline{P_L(dB)} = 10log_{10}(\frac{P_t(mW)}{\overline{RSS(mW)}})\,dB \;=\; P_t\,(dBm) + G_{Tx}(dB) + G_{Rx}(dB) - \overline{RSS(dBm)} \tag{2.3}$$

2.3.3.2 Theoretical Models

We start defining the most simple model and then we follow with more complex models [18]:

Free-space path loss model This model is the basic one because it accounts only for the losses due to the frequency and the distance assuming that the TX and RX are in LOS (Line-Of-Sight). The received signal power is defined as in (2.4):

$$RSS\,(dBm) = P_{Tx}(dBm) + 10log_{10}(G_{Tx}G_{Rx}) - 20log_{10}(\frac{4\pi d}{\lambda}) \tag{2.4}$$

The dependency of the RSS to λ as well as to G_{Rx} is due to receiver antenna effective area with peak gain G_{Rx}. Also the dependency with of the RSS with the peak gain G_{Tx} is due to the EIRP (Equivalent Isotropic Radiated Power). The EIRP is defined as the amount of power that a theoretical isotropic antenna (which evenly distributes power in

all directions) would emit to produce the peak power density observed in the direction of maximum antenna gain 2.5:

$$EIRP(dBm) = P_{Tx}(dBm) + G_{Tx} \tag{2.5}$$

Higher frequencies add higher losses and thus to increase the coverage we can do by transmitting more power or by using directive antennas (higher gains).

It can be stated that the RSS falls off inversely proportional to the square of the distance (d) between TX and RX. Thus according to (2.4) the free space path loss model (FSPL) is (2.6):

$$P_{L-FSPL}(dB) = 10log_{10}(\frac{4\pi d}{\lambda})^2 = 20log_{10}(\frac{4\pi d}{\lambda}) \tag{2.6}$$

Two-ray model (a.k.a Plane Earth Model) This model is more realistic when the transmitter and receiver antenna are at a known height from ground. It can be used when the only contribution to the RSS variation is the ground. The model takes into account the existence of a reflecting path component from ground in addition to the direct path as shown in Figure 2.4 where theta equals θ.

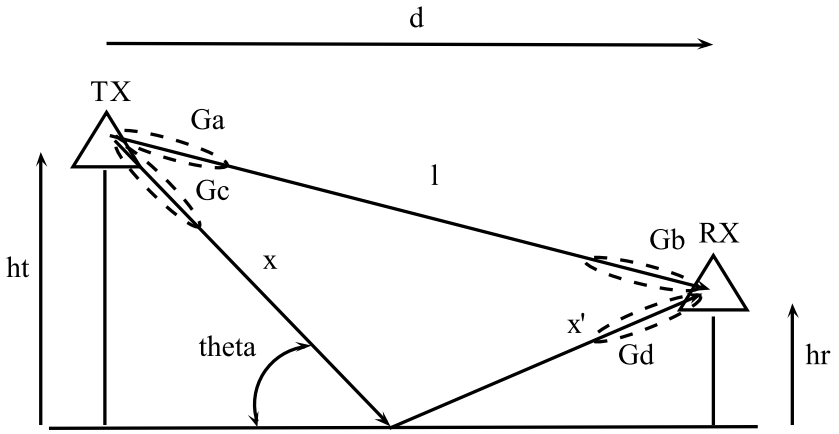

Figure 2.4: Two-Ray Model

The multipath signal component with a delay spread of $\tau = (x + x - l)\ c$ changes its phase by γ degrees. Thus the RSS is defined as shown by (2.7), assuming that the transmitted signal is narrowband (i.e. $\tau < BW^{-1}$):

$$RSS = P_{_{Tx}}(\frac{\lambda}{4\pi d}) \left| \frac{\overline{G_a G_b}}{l} e^{-jkl} + \Gamma(\beta) \frac{\overline{G_c G_d}}{x + x} e^{jk(x+x')} \right|^2 \tag{2.7}$$

where $\Gamma(\theta)$ is the ground reflection coefficient related to the angle of incidence and to the ground dielectric constant according to the Snell law as shown in (2.8).

$$\Gamma = \frac{sin(\theta) - Z(\theta\ \epsilon_r)}{sin(\theta) - Z(\theta\ \epsilon_r)} \tag{2.8}$$

Equation (2.7) can be simplified with the one shown by (2.9) expressed in dBm units with the assumptions that d , $\theta = 0°$ and $\Gamma(\theta = 0°) = -1$

$$RSS = P_{Tx} + 10log_{10}(G_{Tx}G_{Rx}) + 20log_{10}(h_t h_r) - 40log_{10}(d) \tag{2.9}$$

Thus the two-ray path loss model is 2.10.

$$PL_{2ray} = 40log_{10}(d) - 10log_{10}(G_{Tx}G_{Rx}) + 20log_{10}(h_t h_r) \tag{2.10}$$

One can see in (2.10) that the path loss falls off with d^{-4} after a critical distance d_c given by (2.11) and is independent of λ The reason why the RSS is inversely proportional to the quarter of the distance is due to the destructive interference between the LOS ray and the reflected ray.

$$d_c = \frac{4h_t h_r}{\lambda} \tag{2.11}$$

However the RSS experiences peaks and valleys due to the small-scale fading and falls off as d^{-2} at the interval $d = [h_t - d_c]$ [18]. Two-ray model is applicable to LOS open flat fields such in rural flat areas because the only contribution is the ground.

2.3.4 Empirical Path Loss Models

The above described theoretical path loss models can be used to foretell approximately the receiver power at any distance and at any open field environment. The two-ray model is environment specific and needs to know the dielectric properties of the ground, as well as the path length of the reflected path. In practice in scenarios where transmitter and receiver can be in NLOS conditions such as in urban areas the diffraction, the multipath, and the shadowing are common. In such cases the theoretical models can be unsuitable to use. In such complex environments it is best to use empirical models from the received power measurements and hence analyzing the behavior of the received signals with respect to the distance. The difference with the theoretical models is that these ones can be used in any geographical area with similar characteristics such as: urban wide streets, urban narrow streets, rural areas, indoor offices, suburban environments with small buildings and so on. For each kind of environment an empirical model is found from the measurements and shared among the wireless community for future wireless deployments.

All the empirical path loss models are linear with respect to the logarithmic of the distance or $log_{10}(d)$. In contrast with theoretical models, they include the channel variations (shadowing, multipath,...) for each $P_L(d)$ resulting from the average of a set of mean empirical power measurements known as LMP measurements. The LMP measurements at a given distance d remove the RSS variations. With the discrete mean empirical path loss the model is found by means of linear regression such as Least Squares or MMSE.

Empirical path loss models can be classified as:

– **One-slope path loss model**: these model has the following form (2.12)[13, 17, 18, 24]

$$\begin{aligned} RSS &= P_t - A - 10\gamma log_{10}(d) - {}_{shad};\ d \geq d_0 \\ P_L(d) &= A + 10\gamma log_{10}(d) + {}_{shad} \end{aligned} \tag{2.12}$$

,where A is a constant called intercept factor which depends on the antenna effective area as well as the average channel attenuation at a given initial distance $d_0$shown by (2.13)

$$A = 20log_{10}(\frac{4\pi d_0}{\lambda}) \tag{2.13}$$

,γ is called **path loss exponent** which represents the falloff of the RSS with the distance (the slope). The path loss exponent is environment specific. For environments close to free space $\gamma = 2$, the two-ray model has either $\gamma = 2$ or $\gamma = 4$ respectively. For more complex environments, it is best to estimate γ together with A to minimize the MSE between the model and the empirical measurements. Mathematically it is demonstrated by (2.14):

$$\begin{bmatrix} A \\ \gamma \end{bmatrix} = \begin{bmatrix} 1 & 10log_{10}(d_1) \\ 1 & 10log_{10}(d_2) \\ & \end{bmatrix}^{+} \cdot \begin{bmatrix} P_L(d_1) \\ P_L(d_2) \\ \end{bmatrix} \tag{2.14}$$

being $P_L(d_n)$ the local mean path loss measurements at the distance d_n, and ${}_{shad}(dB) \sim N(0\ \sigma_{shad})$ is a zero mean log-normally distributed random variable with standard deviation $\sigma_{shad}\ dB$ representing the received power variations around the path loss model caused by either shadow fading, multipath or both combined.

– **Multi-Slope path loss model (a.k.a piecewise path loss models)**: Most of the outdoor environments can have one or more critical distances or breakpoints (for example the separation between LOS and NLOS conditions). In such environments

the one-slope model cannot be suitable. Hence, a two-slope path loss model as the one shown by 2.15 [13, 18, 17] can be useful. This generic model can be generalized by n slopes and $n-1$ breakpoints. As an example, Figure 2.5 shows a example of a piecewise path loss model with two slopes and one breakpoint.

$$P_r(dB) = \begin{cases} P_t + A - 10\gamma_1 log_{10}(d) & d \leq d_c \\ P_t + A - 10\gamma_1 log_{10}(d) - 10\gamma_2 log_{10}(d) & d_c < d \end{cases} \tag{2.15}$$

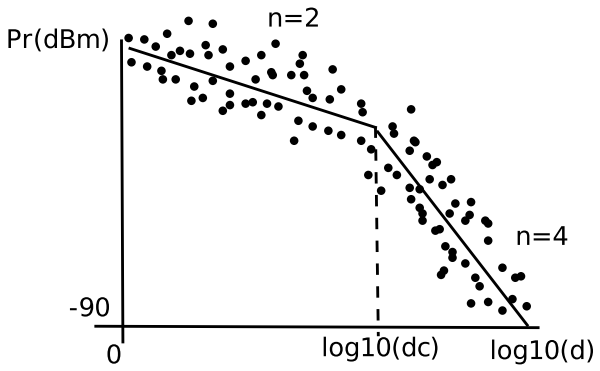

Figure 2.5: Picewise linear model for path loss

A special case of multi-slope path loss model is the two-ray path loss model for $d > h_t$ with two slopes of $\gamma_1 = n = 2$ before and $\gamma_2 = n = 4$ and one critical distance.

Chapter 3

A generic empirical channel model for low power lossy networks at the 868 MHz band for smart cities

3.1 Introduction

In the previous Chapter we focused to obtain a specific channel model targeted to smart parking applications, which the transmitter antenna is placed at ground level, $h = 0$ m and the receiver antenna is placed at h =3 m. In this Chapter we generalize the specific channel model for any smart city application, i.e. smart waste management and smart street-lighting, which either the transmitter or receiver antenna can be placed at any height h from ground.

This Chapter contains the work carried out to determine a unified propagation model that is focused on typical applications in urban environments, which low power and energy constrained devices can be deployed at any height from ground. The model parameters are found in real experimentation using experimental motes operating at the 868 MHz band. We have used the 868 MHz band because it has lower propagation losses and less interference effects than the 2.4 GHz band. The propagation characteristics and conclusions can be also extended to 915 MHz because frequency variation is very low, around 5%.

This Chapter presents an in-depth analysis of the wireless propagation behavior from the devices communication perspective. It also provides a unified empiric propagation model that takes into account the node height from ground.

The main contributions of this Chapter are the following. It presents a unified propagation model for typical communication scenarios in urban environments: ground-to-ground and ground-to-air. The propagation model is derived from theoretic knowledge, i.e. from the one-

slope log-normal path loss model [18] [23]. It provides the model parameters obtained from real experimentation for the described communication scenarios. It presents an in-depth analysis of the propagation model parameters from an extensive measurement campaign in the defined communication scenarios. It is worth to note that the analyzed ground to air scenario, where the receiver is always higher than the transmitter, is not covered in depth in the existing literature.

The rest of the Chapter is organized as follows. Section 3.2 presents the related work. Section 3.3 presents the modeling of some typical communication scenarios in urban environments in terms of devices communication scenarios perspective. Section 3.4 introduces the propagation model. Section 3.5 describes the measurement setup. Section 3.6 provides a description of the set of measurement campaigns that have been used to analyze the propagation in the described communication scenarios. Section 3.7 are the experimental results. Section 3.8 validates the propagation model. Finally, Section 3.9 concludes this Chapter.

3.2 State of art

There are some experimental studies that have already focused to obtain propagation models for low power wireless technologies, specially near ground. According to the Fresnel zone theory, the authors in [25] develop a novel theoretical channel model for near ground-antenna propagation generalized for different transmitter and receiver antenna heights. Their near ground theoretical channel model is the sum of the free space model and a diffraction model that is considered to be the sum between the knife-edge model and an additional diffraction loss that is dependent on the antenna height, wavelength and antenna distance, and is derived from hypothesis. However, they fail in stating that the near-ground path-loss slope is the same than in free space, since they consider the diffraction loss as a constant.

[26] evaluates the one slope and the two slope parametrized models at the 868 MHz band for near ground scenarios in three different environments. They empirically show that near ground, the power decay factor with distance is in the interval $[3-3\ 7]$ for the one slope model. However, the two slope model fits better real data. A particular case of this model is the two ray model. In this model the power decay factor is around 2 before a certain breakpoint distance and 4 after this breakpoint distance. This is because the LOS (Line-of-Sight) signal and the signals reflected from ground are out of phase, combining destructively. The two ray model is valid when $h_t >> h_r$, being h_t and h_r the heights of the TX and RX with respect to ground [18]. The dependence of the breakpoint distance with the environment is empirically validated.

The authors in [27] provide a channel model validated at the 868 MHz and 915 MHz for street-light telemetry applications where the transmitter and receiver are far away from ground. Their channel model is empiric and is shown and validated with measurements.

[13] follows the same approach than [26] evaluating the one slope and the two slope models at the 2.4 GHz band in LOS environments with different types of ground and NLOS environments. Their model takes into account the antenna height from ground.

[28] uses a standard procedure to find the corresponding propagation model parameters for each case and environment. They compare the wireless propagation model at 2.4 GHz in three different locations with three different ground surfaces. They also evaluate the impact of antenna height and the antenna orientation on the propagation model characteristics. Their results mainly demonstrate that the near ground path loss exponent is in the interval $[2\ 90 - 3\ 47]$. Additionally, they analyze the effects of the different variations in the received signal caused by multipath in distinct situations and environments using different statistics distributions.

[29] presents a practical propagation model from experimental measurements conducted at the 2.4 GHz band that combines four different factors. These factors are: free space path loss, ground reflection, received power uncertainty and antenna pattern irregularity.

[30] provides the wireless range at the ground level for the 915 MHz and 2.4 GHz bands with different types of ground (grass, asphalt, stone, concrete) and different configurations as we do in this Chapter: equal antenna heights and different antenna heights. However, they fail in evaluating the propagation behavior in these configurations. They demonstrate that in most of the environments the fadings nature follow a Ricean distribution.

[31] provides a one slope empiric propagation model for the worldwide 433 MHz and 2.4 GHz ISM (Industrial, Scientific and Medical) bands taking into account the antenna height. They demonstrate that the influence of the antenna height on 433 MHz frequency band is slightly larger than at 2.4 GHz. This is because the first Fresnel zone radius is bigger at the 433 MHz band. Nevertheless the initial path loss at 2.4 GHz is higher. Their experimental results demonstrate that the optimal height for their specific environment is 3.5 m to ensure LOS conditions independently of the used frequency band.

The presented work in [32] studies in detail in the time-domain the LOS blockage and shadowing characteristics of multiple time-varying wireless channels for different links caused by a pedestrian moving. Their experimental setup is near-ground at the 2.6 GHz band for typical surveillance and pedestrian tracking applications.

Besides, many other propagation models obtained in urban environments exist. Some of them are sub-empiric, such as Cost-231 or Okumura-Hata models, whereas the remaining are empiric, that is, model parameters are obtained from regression fitting of measurement data. Nevertheless most of them require the transmitter (or Base Station) placed at heights higher than 30 m and the receiver (or mobile device) placed higher than 1 m. These models are valid for distances above 1 km [18]. Examples of some technologies that meet these requirements are cellular and WiMAX networks [33], [34], [35], [36], [37]. Unfortunately, these models are not

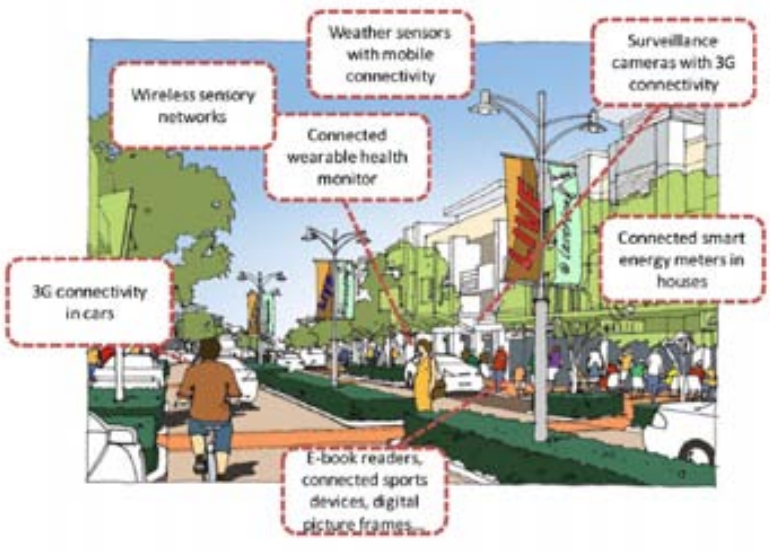

Figure 3.1: Concept of a Smart City where citizens, objects, utilities, etc, connect in a seamless manner using ubiquitous technologies, so as to significantly enhance the living experience in 21st century urban environments [1]

suitable for low power wireless technologies operating near ground.

Despite all the research works existing in the literature, to the best of authors knowledge, to the best of our knowledge, there is not a unified propagation model targeted to smart city applications. For that reason, we provide and validate in this Chapter a generic empiric propagation model focused on typical communication scenarios under urban environments described in Section 3.3 with an in-depth analysis using the available RSSI (Received Signal Strength Indicator) parameter given by low power transceivers [3] embedded in commercial wireless motes such as TelosB [38] or Zolertia z1 [39]. An advantage of using our method to obtain channel measurements is the low cost, weight and high autonomy of wireless motes in comparison to dedicated hardware, i.e. an Spectrum Analyzer, at the expense of a worse RSS resolution, typically equal or higher than 1 dB.

3.3 Modeling the communication scenarios under urban environments

As illustrated in Figure 3.1, common applications that use smart wireless devices in urban environments include 3G connectivity in cars, Wireless sensory networks, weather sensors with mobile connectivity, connected wearable health monitor, surveillance cameras with 3G connectivity, connected smart energy meters in houses, E-book readers, connected sports devices, digital picture frames, and so on.

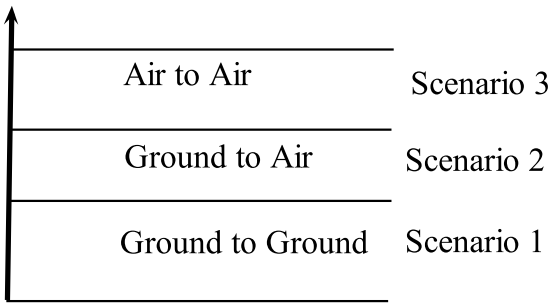

Figure 3.2: Urban Environment Scenarios

All of these applications from the communication perspective can be modeled by 3 different communication scenarios which depend on the transmitter and receiver height from ground. The later, has effects on the communication capabilities which may be reflected on the propagation model. We believe that the position of the devices in relation to the ground is the main responsible for propagation characteristics [13, 28, 31]. Thus we propose to have a unified one-slope propagation model derived from the theory of wireless propagation that takes into account the node height in relation to ground.

The above classification can be generically modeled as in Figure 3.2, in terms of devices communication perspective:

- Air to air: in this communication scenario both TX and RX are placed high enough from ground at a certain h such that the Fresnel zone is not obstructed by ground. Therefore $h >> r$ or $h - r > 0$, being r the first Fresnel zone radius. A particular smart city application of this scenario is the smart street lighting.

- Ground (Near) to air: in this communication scenario, the height of the receiver is always fixed and above the height of the transmitter. In other words, the TX and RX antennas are not aligned. The first Fresnel zone is not obstructed by ground. A particular smart city application of this scenario is the smart waste management, where the nodes placed on the top of waste containers communicate to the nodes placed at higher heights at the street lampposts.

- Ground to ground: in this communication scenario, both the transmitter and the receiver are placed at the same height h in relation to ground. We emphasize those situations when the transmitter and the receiver are placed near ground, that is when $h - r <= 0$. Particular smart city applications of this scenario are the traffic applications where the nodes are placed at ground level.

These communication scenarios have the following characteristics:

- The EM (Electro-Magnetic) model of the environment where signal propagates is complex and unknown.
- Wireless propagation can be classified in Line-of-Sight or LOS (when the first Fresnel zone is free) and Non LOS (when the first Fresnel zone is obstructed).
- The physical environment where signal propagates is heterogeneous: the wireless devices can be placed anywhere in a city (near ground/above ground).
- The physical environment can be dynamic specially for the near ground devices (e.g. traffic applications). Objects placed temporally on the near ground antenna may modify its radiation pattern and thus the antenna gain in the propagation direction and may block the LOS.

According to these characteristics the propagation model parameters will be different for every communication scenario resulting in multiple propagation models.

3.4 Theoretical propagation model

In this section we first define a unified propagation model based on the theoretic one-slope log-normal propagation model [18], which is focused on the communication scenarios described in Section 3.3. Specific theory of wave propagation, i.e. diffraction, shadowing and multipath, is already covered in Section 2.5 of Chapter 2. For more information refer to [18, 23]. It is worth noting that there is not any unified model in the SOA.

The theory of wireless communications [18], [23] states that the received power decays linearly with the logarithmic of the distance by a certain slope (γ) known as path loss exponent. The reference of all wireless communications is the free space propagation law or Friis model which has γ=2. The generic form of the proposed propagation model presented in Equation (3.1) is based on the one-slope propagation model [18, 23, 13, 17, 31, 24].

$$\begin{aligned} RSS(d\ h)(dBm) = RSS(d0) - 10\gamma(h)log(d\ \ d0) \\ -L_g^{dB}(h) - L_e(dB) + \quad (dB) \end{aligned} \tag{3.1}$$

In Equation (3.1), RSS is the received signal strength or received power at a distance d expressed in meters from the transmitter, $RSS(d0)$ expressed in dBm units is the received power at the first measured distance $d0$ in meters from the transmitter. The transmitter antenna gain G_{TX} and the receiver antenna gain G_{RX} are included in this parameter. γ is the path loss exponent, which accounts for the RSS decay as a function of the distance. L_g expressed in

dB units accounts for the attenuation or diffraction power losses due to the first Fresnel zone obstruction by ground. This parameter is dependent on the height such that the lower the height the higher the diffraction losses. The parameter L_e also expressed in dB units accounts for the attenuation caused by obstacles that temporally block the LOS between the transmitter and the receiver. The lower the node the higher the attenuation due to a changing environment. This parameter should be taken into account in near ground sensing applications (i.e. traffic apps). The parameter also dependent on the height of the node expressed in dB units is considered a zero mean log-normally distributed random variable with standard deviation σ in dB representing the received power variations caused by either shadowing, multipath effects and other non-expected channel impairments.

As stated in Section 3.2, the corresponding model parameters $RSS(d0)$ and $\gamma(h)$ are obtained using linear regression, i.e. Least Square fitting from the measurements as described by Equation (2.14):

$$\begin{bmatrix} RSS(d0) \\ \gamma(h) \end{bmatrix} = \begin{bmatrix} 1 & -10log_{10}(d_1\ d0) \\ 1 & -10log_{10}(d_2\ d0) \\ & \\ 1 & -10log_{10}(d_n\ d0) \end{bmatrix}^{+} \cdot \begin{bmatrix} RSS(d_1\ h) \\ RSS(d_2\ h) \\ \\ RSS(d_n\ h) \end{bmatrix} \tag{3.2}$$

In Equation (2.14) $RSS(d_n\ h)\ n = 1\ 2$ is the mean of the received power measurements at the known distances $d_1\ d_2\ d_3\ d_4$ d_n and height h.

3.5 Measurement setup

In order to conduct the set of experiments we use a custom device, named COU868 mote. In the current section we present a detailed description of the used device and the configuration parameters (e.g. transmit power, receiver sensitivity, signal modulation, data rate, etc.) that have been used to conduct the different experiments.

3.5.1 Equipment

The set of experiments at the 868 MHz band are conducted using two COU868 motes, as depicted in Figure 3.3. The COU868 motes are equipped with an Atmel 8-bit ATmega-1281 microcontroller running TinyOS and an Atmel AT86RF212 transceiver that is connected to a Texas Instruments CC1190 external RF front end. The CC1190 RF front end has a 25 dB PA (Power Amplifier) and a 11 dB LNA (Low Noise Amplifier). The microcontroller operates at 4 MHz

and features 8 Kbytes RAM, 128 Kbytes of Flash and 4 Kbytes EEPROM memory respectively. The transceiver is fully compliant with IEEE 802.15.4-2011 [12] standard, e.g. 100 kbps with OQPSK modulation and DSSS, and is connected to a whip antenna through an SMA antenna connector.

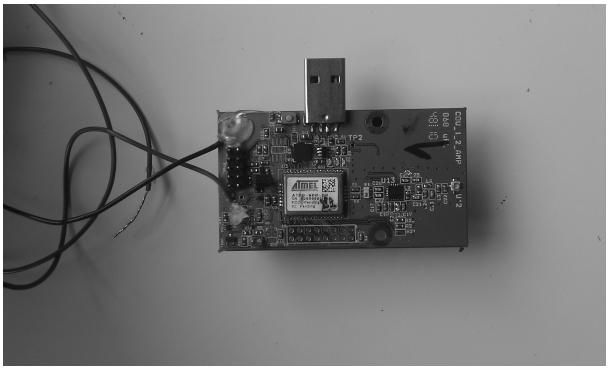

Figure 3.3: A COU868 development board featuring an Atmel ATmega-1281 microcontroller, an Atmel AT86RF212 transceiver and a Texas Instruments CC1190 TI RF front end.

3.5.2 Configuration

The configuration parameters used in the experimental measurements campaigns are presented in Table 3.1. The chosen data rate and modulation scheme are in accordance with the IEEE 802.15.4-2011 standard. Transmit power at the output of the SMA connector is 12 dBm, which is in accordance with the European Regulations where the maximum allowed transmit power is 14 dBm at the 868 MHz band.

Two metrics have been used throughout the measurement camping to evaluate the propagation aspects at the 868 MHz band. One is the RSS (Received Signal Strength) and the other is the PDR (Packet Delivery Ratio). The RSS measures the received power level at the input of the signal demodulator given the receiver filter bandwidth and Low Noise Amplifier (LNA) gain. On its behalf the PDR is a measure of the number of successfully received packets with respect to the number of transmitted packets. The transmitter sends 800 packets of 127 bytes and for each measure the receiver computes the PDR as well as the average of the RSS of the received packets in order to remove contributions from shadowing, multipath and other non-expected channel impairments.

3.6 Measurement campaigns description

In this section we present a description of the set of measurement campaigns where RSS measurements are obtained to validate the generic propagation model shown by Equation (3.1).

	COU868
Standard	IEEE 802.15.4
Modulation	OQPSK
Data rate (kbps)	100
Transmit power (dBm)	12
Channel bandwidth	400 KHz
Antenna type	-2 dBi λ 2 whip
RSSI resolution (dB)	3
Transmitted packets	800
Packet length (bytes)	127
RX sensitivity (dBm)	-98

Table 3.1: Configuration parameters for COU868 mote. The RX sensitivity is obtained from the transceiver datasheet [3].

Additionally, these measurement campaigns were carried out to find the different propagation model parameters for each communication scenario and evaluate its propagation characteristics.

3.6.1 Ground to Ground Scenario

In this section we describe the procedure to obtain $L_g^{dB}(h)$, i.e. the diffraction model. Next we describe how to obtain $RSS(d0)$ and $\gamma(h)$ as a function of height.

3.6.1.1 Measurement campaign I

In order to find the corresponding diffraction model, we set the distance between TX and RX to i.e. $d = 5$ m. Next we take RSS measurements changing both TX and RX heights from $h = 0$ m to $h = 1\ 2$ m ($>> 3\lambda$) in steps of 5 cm as depicted in Figure 3.4. This parameter has an impact on $RSS(d0)$ at the initial distance $d0$ and accounts for the first Fresnel zone obstruction by ground. The selected distance is well above the far-field distance. In the far-field region, the antennas radiation pattern do not vary with distance between TX-RX. Since the TX and RX antennas physical dimensions D is 0.018 m and $\lambda = 0\ 3455$ m the far-field distance, df is [24]:

$$d_f = \frac{2 \times D^2}{\lambda} = 0\ 0019m = 1\ 87\ cm \tag{3.3}$$

For this scenario the model described by Equation (3.1) simplifies to Equation (3.4) if we consider that $L_e = 0$ dB and $d = d0$.

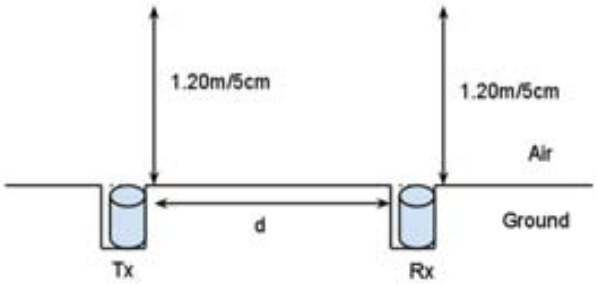

Figure 3.4: Ground node-to ground node scenario description. The equipment with the antenna on the top is buried such that the antenna is flushed with ground.

$$RSS(d0\ h) = RSS(d0) - L_g(h) + \tag{3.4}$$

We force $L_e = 0$ dB because we are interested to evaluate the dependency of either L_g or $RSS(d0)$ with the height. The expected value of the simplified model in Equation (3.4) is depicted by Equation (3.5) taking into account that $\bar{} = 0$ dB.

$$\overline{RSS}(h) = \overline{RSS}(d0) - L_g(h) \tag{3.5}$$

It is worth noting that $RSS(d0)$ and L_g are inversely proportional and if we analyze $RSS(d0)$ we also analyze L_g.

3.6.1.2 Measurement campaign II

In order to find the path loss exponent $\gamma(h)$ we measure the RSS for different measurement distances and heights as shown in Figure 3.5. We choose 4 heights: $h = 2$ m, 70 cm, 30 cm and 0 m. We choose in purpose not equidistant measurements due to the log-distance decay of the received power [33]. Moreover shorter measurement distances will allow an accurate analysis. The measurements for $h = 0$ m where obtained up to $d = 40$ m because the measured RSS was close to the receiver sensitivity. This measurement campaign was carried out in two different environments below described to confirm the validation of the model parameters. In these environments there were not obstructions other than ground between the transmitter and the receiver.

- **Open field**: as a reference with few surrounding objects.
- **An urban park**: with some surrounding trees, buildings and other non-metallic structures.

The expected value of the propagation model is (3.6) if we consider again that $L_e = 0$ dB because we only study the dependency of γ with height.

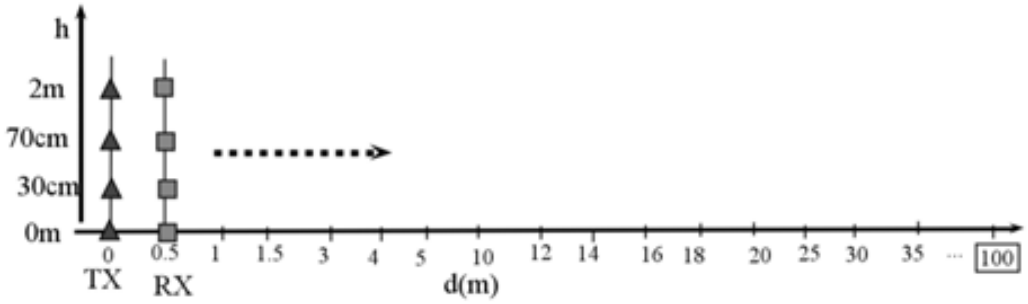

Figure 3.5: Description of the ground to ground scenario measurement campaign II.

$$\overline{RSS}(h) = \overline{RSS}(d0) - 10\gamma(h)log_{10}(d\ d0) - L_g(h) \tag{3.6}$$

3.6.2 Ground to Air Scenario

As stated in Section 3.3 the height of RX is always above the height of TX. The height of RX was fixed at $h = 3$ m. The rest of heights and distances are the same as in the ground to ground communication scenario:

- From $h = 0$ m up to $h = 1$ 2 m in steps of $h = 5$ cm for the measurement campaign I.
- $h = 2$ m, 70 cm, 30 cm and 0 m for the measurement campaign II.

It is worth noting that in this scenario $L_g = 0$ dB because the Fresnel zone is never obstructed by ground (TX and RX are always in LOS conditions). In Section 3.6.2.1 we describe the procedure to obtain $RSS(d0)$. In Section 3.6.2.2 we present the method to obtain $RSS(d0\ h)$ and $\gamma(h)$. Finally, in Section 3.6.2.3 we describe how to find the L_e parameter with an example of a smart city application where this parameter is contemplated.

3.6.2.1 Measurement campaign I

In order to obtain $RSS(d0\ h)$ we measure the RSS for the same TX heights as in Section 3.6.1.1 and as depicted in Figure 3.6. We are interested in evidencing the dependency between $RSS(d0\ h)$ and height at $d = d0$. The results obtained in this measurement campaign for this communication scenario have nothing to do with the ground to ground diffraction model because there is not diffraction caused by ground.

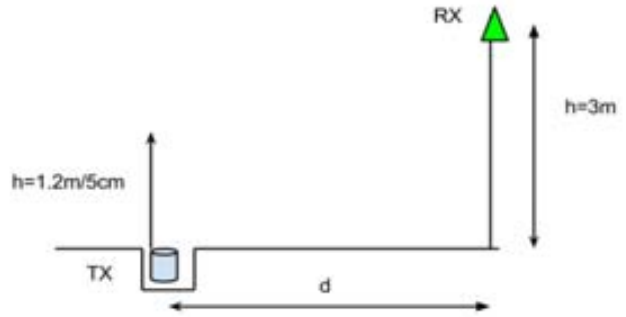

Figure 3.6: Description of the ground to air measurement campaign I.

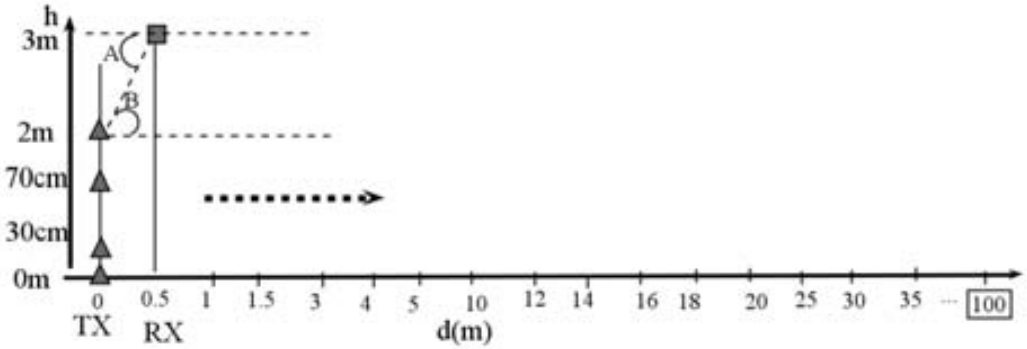

Figure 3.7: Description of the ground to air scenario measurement campaign II.

3.6.2.2 Measurement campaign II

In order to obtain $\gamma(h)$ we take RSS measurements in the same measurement distances and TX heights as in the ground to ground scenario, as shown in Figure 3.7. This measurement campaign is also carried out in the open field and urban park environments, to evaluate and validate the unified propagation model. The measurements for $h = 0$ m in the open field environment where obtained up to $d = 40$ m.

In Figure 3.7 it is observed that the RX antenna height is fixed and it is always different and higher than the TX antenna height. It makes that the elevation angle θ formed between TX and RX (in Figure 3.7 , $B = \theta$) changes with the distance. Therefore, we expect certain RSS variations with distance due to a change of the TX and RX antennas gain at the propagation direction. As a result the slopes of the obtained propagation model will be masked by this effect. The expected value of the propagation model will be (3.7) if we consider again that $L_e = 0$ dB because we are interested in evidencing the dependency between γ and height.

$$\overline{RSS}(h) = \overline{RSS}(d0\ h) - 10\gamma(h)log_{10}(d\ d0) \tag{3.7}$$

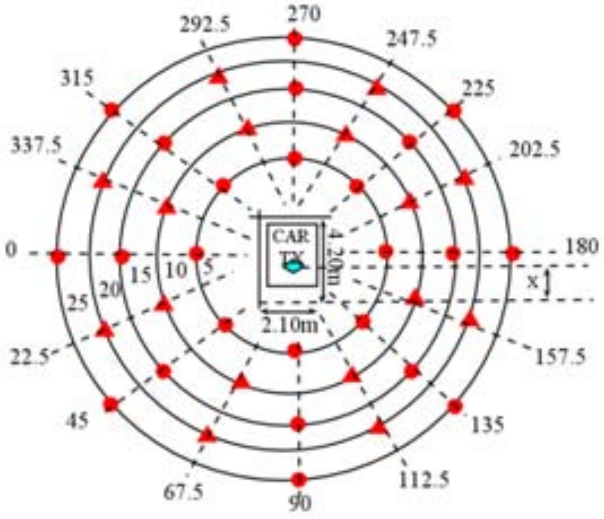

Figure 3.8: Description of the ground to air scenario measurement campaign III. The dots are the measurement positions. The circles radius are: 5 m, 10 m, 15 m and 25 m respectively.

Note in Equation (3.7) that $\gamma(h)$ still may have a dependency on TX height. Also the parameter L_g is not considered in this scenario because as stated above the first Fresnel zone is not obstructed by ground (TX and RX are always in LOS conditions). Nevertheless $RSS(d0\ h)$ has a certain dependency with TX height. It is attributed to the variation of the antennas gain for each pair of $(h\ d)$ which depend on the angle between TX and RX.

3.6.2.3 Measurement campaign III

In this measurement campaign depicted in Figure 3.8 we show how to obtain the parameter L_e with an example of a car above the transmitter. In order to obtain the L_e parameter owing to the vehicle we take measurements of RSS around the buried transmitter in the open field environment in different angles and circles with radius: 5 m, 10 m, 15 m and 25 m. The RSS measurements are taken for the conditions with a car above the transmitter (in NLOS) and without car (in LOS). Next we obtain the L_e for each circle as the difference in the RSS between the cases without car ($L_e = 0$ dB) and with car ($L_e >> 0$ dB). Thus we can proof whether L_e changes significantly or not with distance.

3.6.3 Air to Air Scenario

In this section we describe the procedure to find the propagation characteristics in terms of $RSS(d0)$ and γ. As observed in Figure 3.9 we take RSS measurements for the heights $h = 3$ m and 4 m. The measurement distances are 5 m equidistant. This measurement campaign was also conducted in the same open field environment than the ground to ground and ground to air

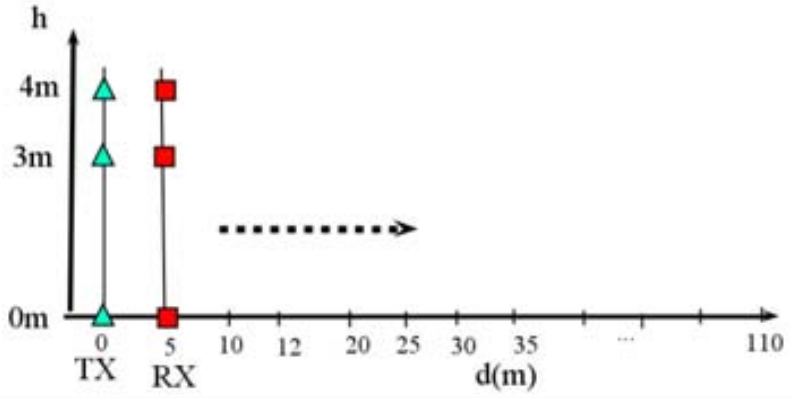

Figure 3.9: Description of the air to air scenario measurement campaign I.

scenarios.

Next the same measurement campaign in the open field is carried out in two distinct urban streets with different widths to evaluate the effects to the propagation model characteristics. In principle a narrow street should offer higher communication distance possibilities than a wider street, because multipath is more emphasized i.e. the reflections from surrounding buildings reach the receiver with higher power levels as they travel less distance. The environment of both streets is illustrated in Figure 3.10. In it the wide street is shown with a solid line whereas the narrow street is shown with a dashed line. Figure 3.10 also depicts the LOS and NLOS regions of both streets. The characteristics of these streets are the following:

- A wider street with traffic in two ways and higher traffic density.
- A narrow street with traffic in one way and low traffic density .

The particularity of these environments with respect to the open field is that the distinct impairments between TX and RX (trees, street lampposts, containers, telephone booths, etc) obstruct the first Fresnel zone.

In this communication scenario the model in Equation (3.1) simplifies to Equation (3.8):

$$RSS(d) = RSS(d0) - 10\gamma log_{10}(d\ \ d0) + \tag{3.8}$$

The propagation model parameters L_g and L_e are not considered in this measurement campaign because the following reasons. The first Fresnel zone is not obstructed by ground, so $L_g = 0$ dB because TX and RX are high enough from ground. $L_e = 0$ dB because the higher the nodes, the fewer obstructions between TX and RX (the environment is less dynamic). As aforementioned, in this communication scenario there is not a dependency between γ and h because there is not diffraction caused by ground. The procedure to obtain the parameters $RSS(d0)$ and

Figure 3.10: Urban environment.

γ is the same as for the ground to ground and ground to air communication scenarios. In this measurement campaign we measure the RSS along the streets.

We start the next section with the results of the described measurements campaigns of the three distinct communication scenarios. Propagation models for the ground to ground, ground to air nodes and air to air communication scenarios are useful for data analysis as well as to determine for each of them the wireless range.

3.7 Data analysis and experimental results

This section presents the data analysis and the experimental results with the obtained model parameters for each of the described scenarios in Section 3.5 of the proposed propagation model in Equation (3.1).

3.7.1 Ground to Ground

3.7.1.1 Measurement Campaign I

The results of this measurement campaign are illustrated in Figure 3.11. In it the evolution of the RSS as a function of TX and RX height with a decrease from $h = 0.8$ to $h = 0$ m is observed. This reduction in the received power is attributed to the first Fresnel zone obstruction by ground. Under this scenario the expected value of the proposed model in Equation (3.1) is reduced to Equation (3.6) taking into account that $d = d0$, $h0 = 1.2$ m and $L_e = 0$ dB since no obstacles

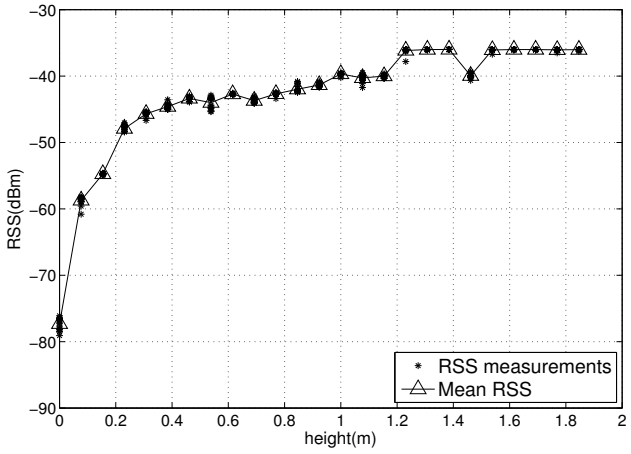

Figure 3.11: Ground to ground diffraction model. TX and RX are separated a distance of d=5 m.

other than ground were present.

$$RSS(d0\ h) = RSS(d0\ h0) - L_g(h) \tag{3.9}$$

The L_g parameter in dB can be obtained by subtracting the value of $RSS(h = 1\ 2$ m) to each of the $RSS(h)$ values. As observed in Figure 3.11, $L_g(dB)$ takes the values from 42 dB to 0 dB comprising the RSS values from -78 dBm to -36 dBm.

Following we conclude this section in comparing the empirical results with a theoretical analysis using the FS (Free Space) [18] model. For example the RSS at a h=1.2 m and at d =5 m is shown by Equation (3.10) assuming that the cable losses are zero:

$$\begin{aligned} RSS(d0 = 5\ m\ \ h = 1\ 20\ m) &= 12\ 5 - 20log10(\tfrac{20\pi}{0.3456}) \\ &= -32\ 69\ dBm \end{aligned} \tag{3.10}$$

which is close to the empirical measurement (-36.03 dBm). This small difference is caused by the cable losses and the RSS resolution of the transceiver (3 dB). Additionally, the RSS at a height of $h = 40$ cm, $RSS(d = 5$ m, $h = 0\ 4$ m) using the FS model and assuming null the cable losses is represented by Equation (3.11):

$$\begin{aligned} RSS(d0 = 5\ m\ \ h = 0\ 4\ m) &= RSS(h = 1\ 20\ m) - L_g(h = 0\ 40\ m) \\ &= RSS(h = 1\ 20\ m) - (RSS(h = 1\ 20\ m) - RSS(h = 0\ 4\ m)) \\ &= -32\ 69\ dBm - 6\ 68\ dB \\ &= -39\ 37\ dBm \end{aligned} \tag{3.11}$$

which approximates to the empirical measurement (-42.71 dBm). Therefore, this brief theoretical foundation confirms the diffraction model represented by Equation (3.9) and Figure 3.11.

3.7.1.2 Measurement Campaign II

The goal of this subsection is to obtain the parameters $RSS(d0)$, γ and by adopting the Least Squares criterion (2.14) for the different TX and RX antenna positions as described in section 3.6.1.2. The parameter L_g is already included in the RSS measurements. The experimental results are validated with two different environments: an open field with few surrounding objects and an urban park.

- **Open field environment**: In Figure 3.12a is observed that $\gamma(h = 2$ m)=1.82, which is slightly smaller than the theoretical value in free space ($\gamma = 2$). Below $h = 80$ cm and according to the obtained diffraction model depicted in Figure 3.11, the LOS condition is never satisfied, i.e. the first Fresnel zone becomes obstructed by ground and the closer to it the higher the slope. It is worth noting that near ground heights corresponding to $h <= 30$ cm the multipath effect due to the diffraction phenomenon induces higher RSS variations at large distances. Additionally, at $h = 0$ m, half of the Fresnel zone is obstructed causing a drastic diminution of $RSS(d0\ h)$ by an amount of 41 dB from $RSS(d0\ h = 30cm) = -10\ 12$ dBm to $RSS(d0\ h = 0$ m)$= -50\ 55$ dBm. This value is consistent with the results presented in Section 3.7.1.1. In Figure 3.12a the parameter L_g is already included in the RSS measurements such that $RSS = RSS(d0) - L_g$. Moreover, near ground positions shows a γ around 3, which is consistent with the literature [26, 28]. However a significant variation of γ for $h = 0$ m with respect to $h = 30$ cm is not observed. Besides, the theoretical two ray model [18, 23] is not satisfied for any of the heights since critical distances (slope breakpoints) are not observed in our experimental results. Concerning the PDR behavior depicted in Figure 3.12b it is possible to see that the sizes of the connected region and transition region are in this case height dependent. When the Fresnel zone is not obstructed by ground all the positions appear in the connected region resulting in zero packet loss. Hence the higher the Fresnel zone obstruction, the smaller the connected and transition regions and the larger the disconnected region. Moreover, the abrupt transitions of the PDR that appear only appear in the transition region is attributed to the contribution of both an RSS close to the receiver sensitivity (between -65 dBm and -70 dBm) and the destructive interferences caused by multipath in certain positions. For instance, as observed in Figure 3.12a the three abrupt variations in the RSS of 10 dB between $log10(d\ d_0) = 1\ 5$ and $log10(d\ d_0) = 2$ caused by multipath conduces the three abrupt transitions in the PDR shown in Figure 3.12b.

  Figures 3.13a and 3.13b illustrate the histogram of the RSS measurements collected in this experiment for the heights 2 m and 0.3 m respectively. These Figures show the RSS variations modeled by with respect to the linear regression model. The observed variations are caused by reflections from ground. Additionally, the behavior of follows a Gaussian distribution. For that reason we can consider the Gaussian distribution to model the

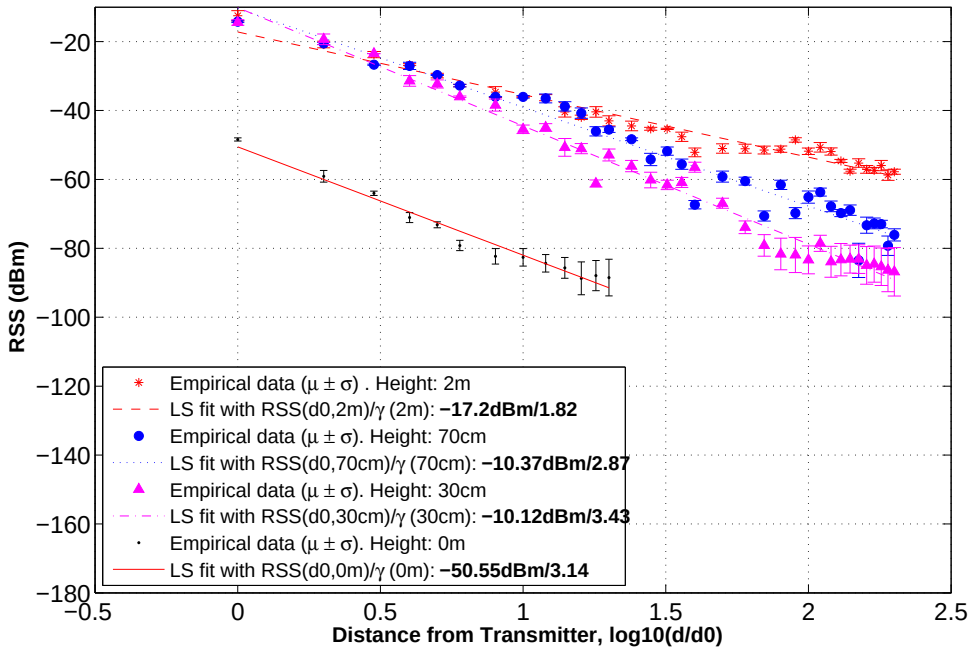

(a)

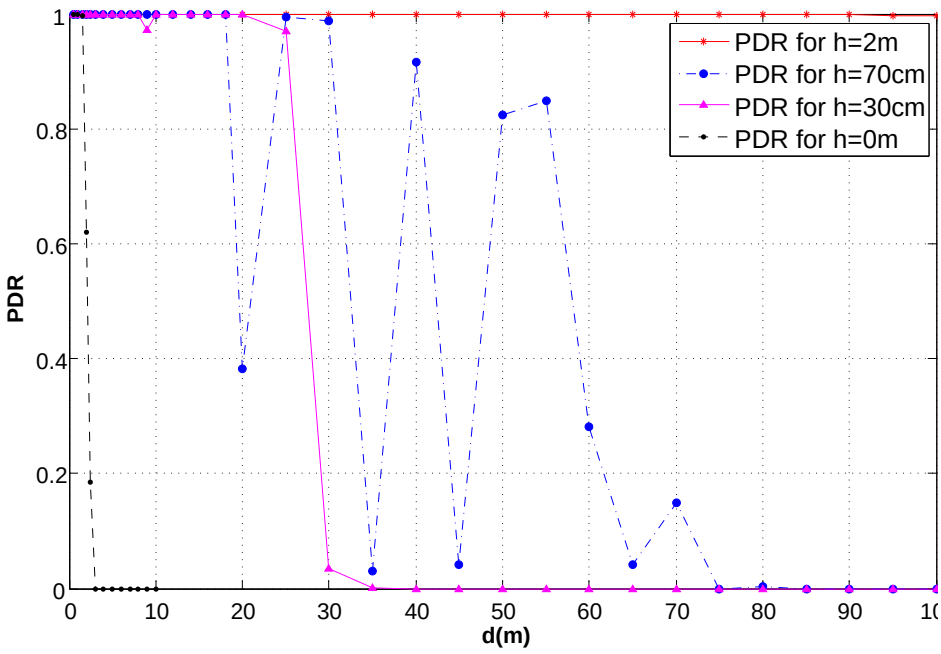

(b)

Figure 3.12: 3.12a: Empiric propagation models for the heights $h = [2\text{ m}, 0.7\text{ m}, 0.3\text{ m}, 0\text{ m}]$. Open field environment. 3.12b: PDR as a function of distance

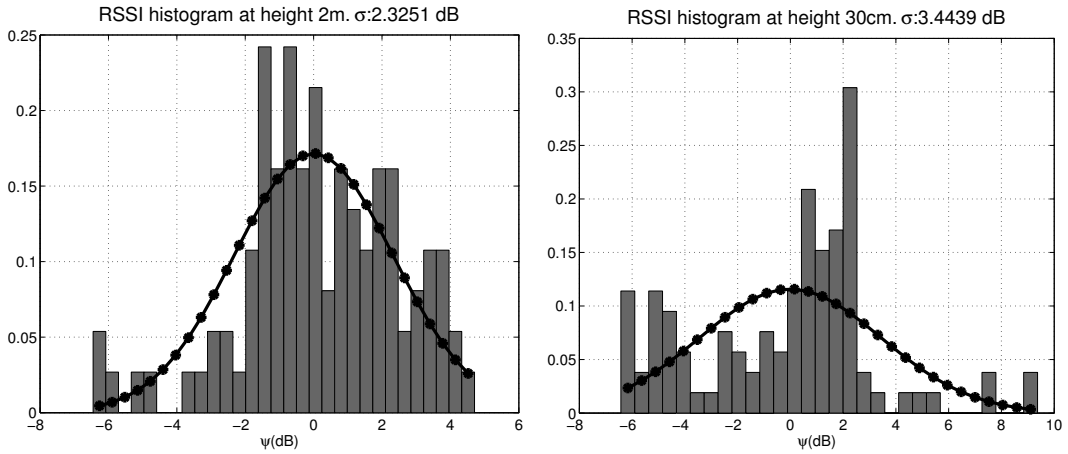

(a) $h = 2$ m (b) $h = 0.3$ m

Figure 3.13: distribution for heights 2 m and 0.3 m in open field environment.

behavior in order to have a generalized model. Due to several non expected random channel impairments in real world and according to the Central Limit Theorem the Gaussian distribution is suitable to model . Additionally $\mu = 0$ dB and the standard deviation of increases from 2.33 dB to 3.44 dB when h goes from 2 m to 0.3 m.

- **Urban park environment**: We repeat the same experiments carried out in the open field environment in this environment surrounded mainly by buildings and trees. In this environment there are less measurement distances due to the environment dimensions constraints. The aim is to see how much the environment affect the propagation model characteristics. The experimental results are depicted in Figure 3.14a. The measurements for the height $h = 0$ m were not carried out due to the difficulties to make holes in the ground was composed by rocks. The same effect than in the open field is observed in this environment. At $h = 2$ m the path loss exponent is $\gamma(h = 2 \text{ m}) \sim 2$ which is close to the free space. When the height is closer to the ground γ increases around 3. Note that large RSS variations due to the multipath effects from ground are not observed because they occur at larger distances. These effects that are shown in the RSS are also given in the PDR, see Figure 3.14b. As it is possible to see, the measurements for the node heights 70 cm and 2 m respectively appear inside the connected region of the PDR whereas for the height of 30 cm, the transition region starts at a distance of 18 m despite of a high RSS (-63 dBm). Additionally, in comparison to Figure 3.12b, the size of the connected region is similar for the heights of $h = 2\ m$ and $h = 70\ cm$ whereas due to a different environment the transition region begins 7 m before. Thus we demonstrate that the model of the PDR(d) is also dependent on the environment.

  As we demonstrated above, the $RSS(d0\ h)$ in LOS conditions can be predicted using the FS

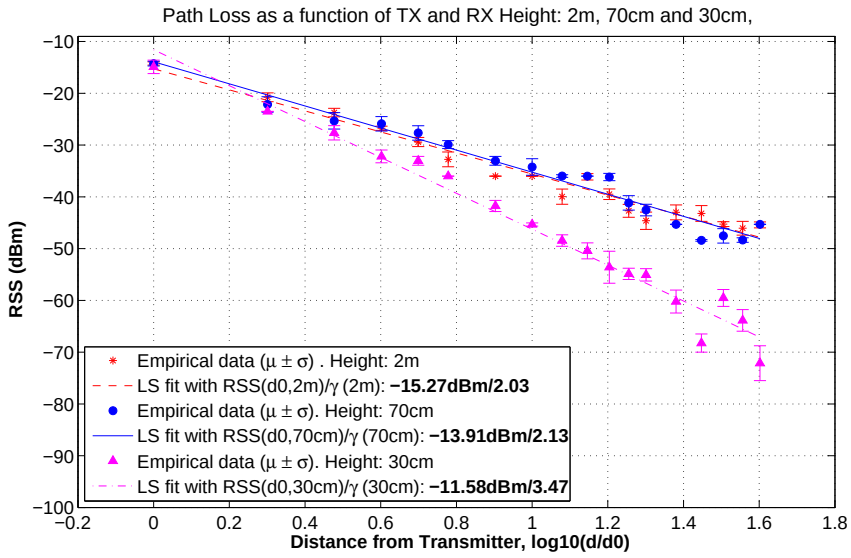

(a)

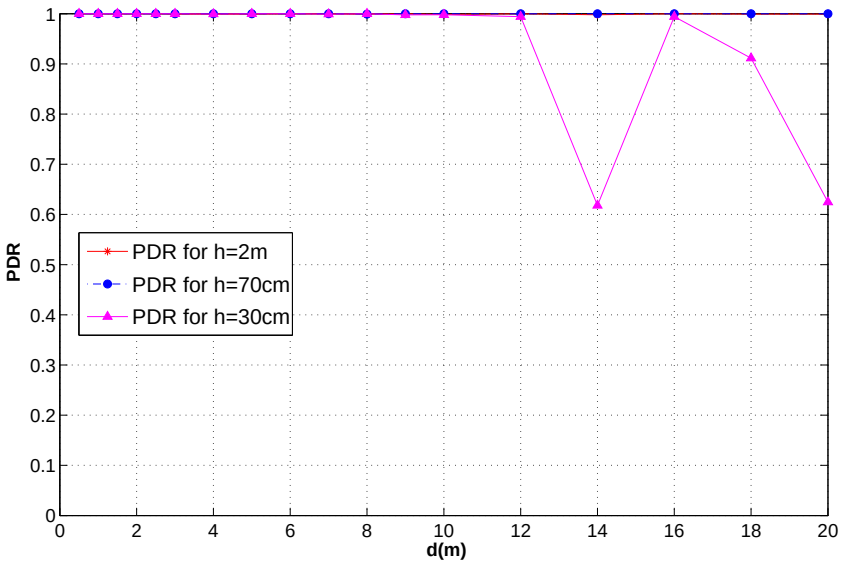

(b)

Figure 3.14: 3.14a: Empiric propagation models for the heights h = [2 m,0.7 m,0.3 m] respectively. Urban park environment. 3.14b: Wireless range in terms of PDR.

Table 3.2: Ground to ground model parameters (γ and $RSS(d0)$ with its 95% confidence bounds). Open field.

h	**2 m**	**0.7 m**	**0.3 m**	**0 m**
γ	1.817(1.69,1.945)	2.869(2.651,3.087)	3.434(3.249,3.619)	3.144(2.79,3.498)
$RSS(d0)$	-17.2(-19.29,-15.11)	-10.37(-13.93,-6.804)	-10.12(-13.15,-7.099)	-50.55(-53.77,-47.33)
μ	0	0	0	0
σ_ψ	2.33	4.22	3.44	2.14
R^2	96.32	95.72	97.81	97.21
$RMSE$	2.3	3.93	3.33	2.24

model or using our model because in both models γ is extremely close. For instance, using the FS model for $h = 2$ m, $d = d0 = 0\ 5$ m we obtain the result shown in Equation (3.12), which is quite close to the empirical value (-12.49 dBm), whereas for $h = 2$ m, $d = 40$ m ($log10(d\ \ d0) = 1\ 9$) we obtain the result in Equation (3.13), which is also quite similar to the empirical measurement (-51.79 dBm).

$$RSS(d0 = 0\ 5) = 12\ 5 - 25\ 1916 = -12\ 69\ dBm \tag{3.12}$$

$$RSS(d = 40) = 12\ 5 - 63\ 25 = -50\ 75\ dBm \tag{3.13}$$

Hence it is well demonstrated that the theoretical FS model is accurate to predict the RSS at a certain distance when the Fresnel zone is not obstructed, i.e. in LOS conditions. This is because the FS model assumes a $\gamma = 2$ (free space), that is close to our obtained γ (1.82 in open field and 2.03 in urban park). For scenarios with the first Fresnel zone obstructed by ground, the empiric propagation model is more accurate. As observed there is higher multipath contribution in the open field than in the urban park environment (smaller γ).

The histograms of the linear regression models corresponding to the heights $h = 2$ m and $h = 0\ 3$ m are shown in Figures 3.15a and 3.15b respectively. The observed RSS variations are caused mainly by multipath. Note again that the distribution of is approximately to a Gaussian as in the open field environment and that σ_ψ increases from 1.56 dB to 2.82 dB when the position of the node in relation to ground goes from $h = 2$ m to $h = 0\ 3$ m. Therefore, the same explanation for the open field environment applies in this environment.

In Tables 3.2 and 3.3 we summarize the obtained model parameters with the corresponding 95% confidence bounds as well as the goodness of fit in terms of R^2 and the $RMSE$ errors of the obtained models for both environments.

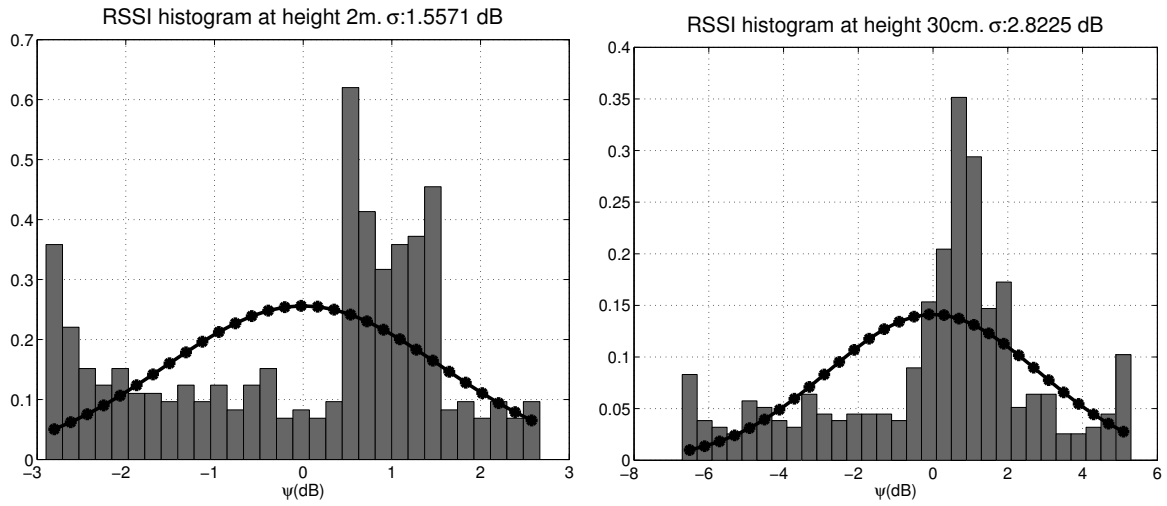

(a) $h = 2$ m (b) $h = 0.3$ m

Figure 3.15: Ground to ground histograms for heights $h = 2$ m and $h = 0\ 3$ m in urban park environment.

3.7.2 Ground to Air

For this communication scenario, we carry out the same procedure than in the ground to ground scenario keeping the RX position fixed at $h = 3$ m. We start in Section 3.7.2.1 analyzing $RSS(d0\ h)$ as a function of the TX position in relation to ground. We follow in Section 3.7.2.2 evaluating the model characteristics in the same environments in terms of $RSS(d0\ h)$, $\gamma(h)$ and . We end the evaluation of this scenario introducing a smart city application example that takes into account the L_e model parameter.

Table 3.3: Ground to ground model parameters (γ and $RSS(d0)$ with its 95% confidence bounds). Urban park.

h	**2 m**	**0.7 m**	**0.3 m**
γ	2.033(1.84, 2.225)	2.132(1.922,2.343)	3.467(3.157,3.777)
$RSS(d0)$	-15.27(-17.4,-13.13)	-13.91(-16.24,-11.58)	-11.58(-15.01,-8.145)
μ	0	0	0
σ_ψ	1.56	1.78	2.82
R^2	96.90	96.65	97.23
$RMSE$	1.72	1.87	2.76

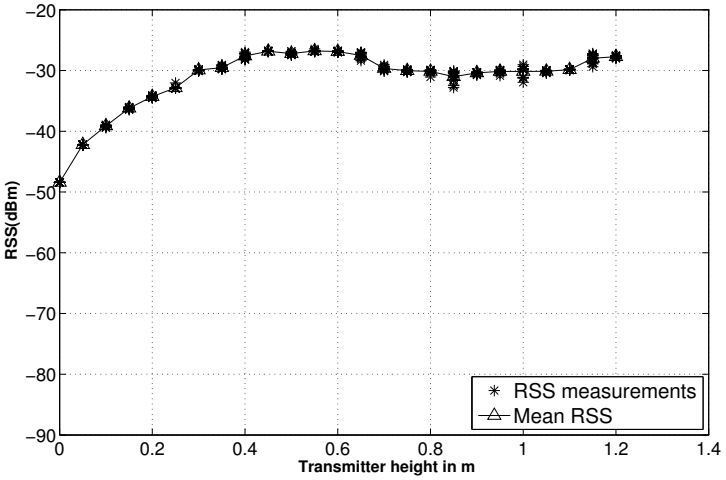

Figure 3.16: $RSS(d0)$ variation as a function of TX position in relation to ground.

3.7.2.1 Measurement Campaign I

This measurement campaign is also carried out in an open field environment. The results illustrated in Figure 3.16 show that in comparison to the ground to ground scenario, $RSS(d0\ h)$ is higher in this scenario because the LOS is never obstructed by ground. Thus, the $RSS(d0\ h)$ evolution from -30 dBm to -50 dBm is resulting from variations caused by a change of the TX and RX antennas gain (from 0 dB to 20 dB) in the propagation direction: θ at TX and $-90-\theta$ at RX. We remind that the antenna gains are included in $RSS(d0)$ in our generic model. Thus when deploying wireless devices it is important to take into account the antenna orientation.

3.7.2.2 Measurement Campaign II

In this section we show and discuss the obtained model parameters $RSS(d0\ h)$, $\gamma(h)$ and by adopting the Least Squares approach (see Equation (2.14)) for the different TX antenna heights as described in Section 3.6.2.2. The experimental results are validated in the same environments than in Section 3.7.1.2.

- **Open field environment:** As the height of the TX and RX is always different, the antenna gain in the propagation direction changes with the distance. As a result, in Figure 3.17 we observe the following: a slight increase of the RSS occurs at the first measurement distances. As the distance increases the elevation angle θ formed between TX and RX decreases conducing to an increase of either the TX or RX antenna gain in the propagation direction. At $log(d\ d0) = 0$ we can see a lower $RSS(d0\ h)$ in comparison to the ground to ground scenario discussed in Section 3.7.1.2. It accounts for the null of the RX whip antenna. If both TX and RX were at the same height we would obtain

a similar propagation model than in the ground to ground scenario. In order to obtain the corresponding propagation models depicted in Figure 3.18a we remove in Figure 3.17 the first 7 empiric RSS measurements that increase with distance to avoid obtaining an inconsistent γ and an inaccurate propagation model. In general, the set of $\gamma(h)$ shown in Figure 3.18a are lower in general than the ground to ground scenario. As stated above, this is because there is a contribution of the antennas gain in the propagation direction to the propagation model slope, i.e. at each distance the antennas gain change. Despite the LOS is always satisfied, values of $\gamma(h)$ for the different heights are much lower than those corresponding to free space ($\gamma = 2$). For example, we have obtained a value of $\gamma \ll 2$ for $h = 0$ m and $h = 0\ 3$ m respectively whereas the ground to ground scenario have $\gamma > 3$. Nevertheless an increase of γ from 1.79 to 2.35 is observed from $h = 2$ m to $h = 70$ cm.

It is worth noting that the multipath effects are smaller in comparison to the ground to ground scenario since there is no diffraction caused by ground. At $log10(d\ d0) = 0\ 7$ in Figure 3.18a we observe a slope breakpoint for the heights $h = 0$ m, 30 cm. Similarly with the two ray model, after a breakpoint distance the direct signal and the reflected signal are destructive (out of phase) causing a slope change from 2.11 to 4.4 for $h = 30$ cm, and from 1.68 to 3.32 for $h = 0$ m. The reduction of the TX height deals with a reduction of $RSS(d0\ h)$. For example $RSS(d0\ h = 2) = -26\ 98$ dBm whereas $RSS(d0\ h = 0) = -48\ 78$ dBm. It corresponds to a factor of 21.8 dB, which is close to the empirical value presented in Figure 3.16 (in that experiment the maximum transmitter height was set to $h = 1\ 2$ m). On its behalf, and as expected it is possible to state that this scenario is better than the ground to ground since the fact of not having a Fresnel zone obstructed by ground, it deals with a higher wireless range, as shown in Figure 3.18b with all the measurement positions appearing inside the connected region (a PDR of one hundred per cent).

Figures 3.19a and 3.19b illustrate the distribution of the variable in Equation (3.1) from the RSS measurements taken in this experiment. As aforementioned, in this communication scenario and environment the observed RSS variations are caused by both ground reflections and a change of antennas gain. For this reason the distribution of is not so close to a Gaussian distribution as in the ground to ground scenario. This distribution includes the RSS variations due to reflections from ground as well as the TX/RX antennas gain variation with distance. The value of σ_ψ for $h = 2$ m is 3.32 dB whereas the value of of σ_ψ for $h = 30$ cm is 2.18 dB.

- **Urban park environment:** The corresponding results are depicted by Figure 3.20. As observed the same effect is shown here: the RSS slightly increases in the first distances because an increase of the antennas gain, and then lineally decreases. Avoiding the first 7 measurements inducing error in the slope we obtain the results in Figure 3.21a. The contribution of the antenna gains affect the value of $\gamma(h)$. As observed $\gamma(h = 2\ \text{m}) = 1\ 67$

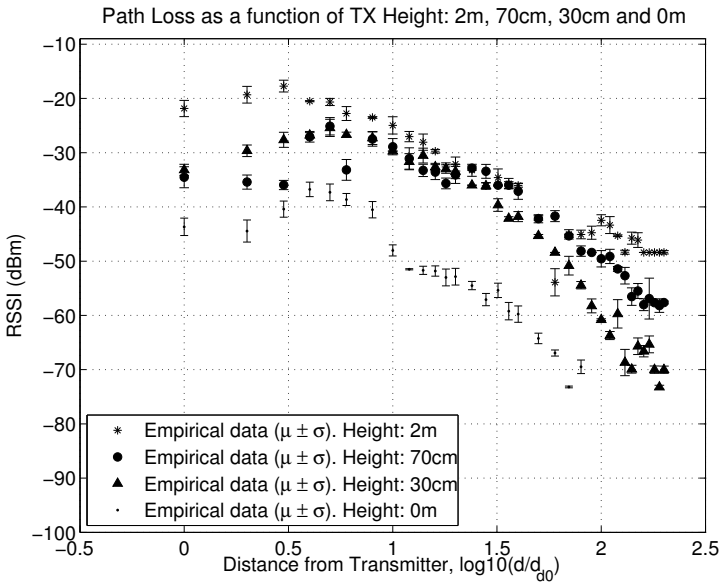

Figure 3.17: Ground to air empiric RSS measurements for different TX heights: h = [2 m,0.7 m,0.3 m,0 m]. Open field environment.

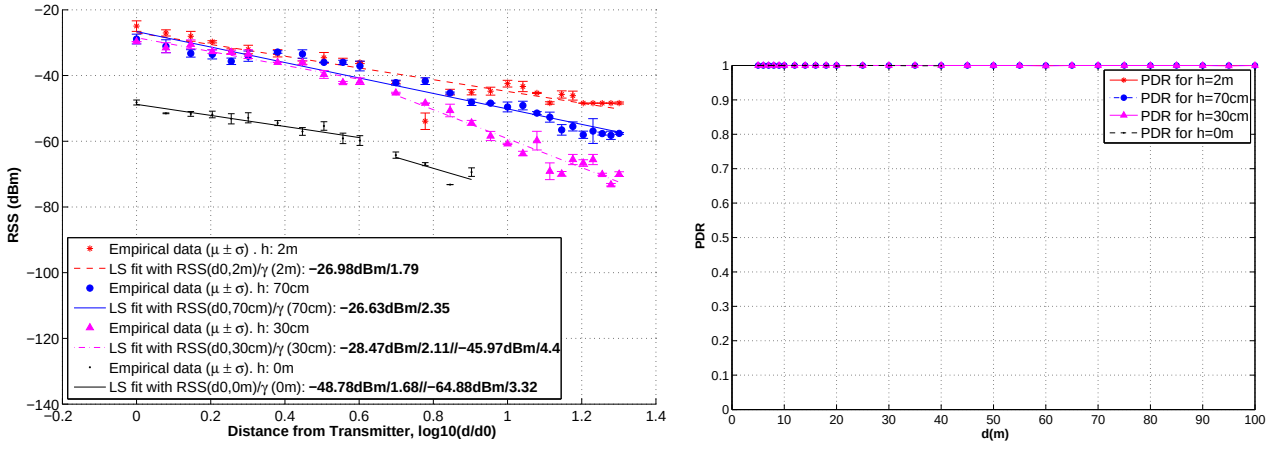

(a) (b)

Figure 3.18: 3.18a: Figure 3.17 avoiding the first 7 measurements with the corresponding propagation models. Open field environment. 3.18b: Empiric representation of the PDR as a function of the distance.

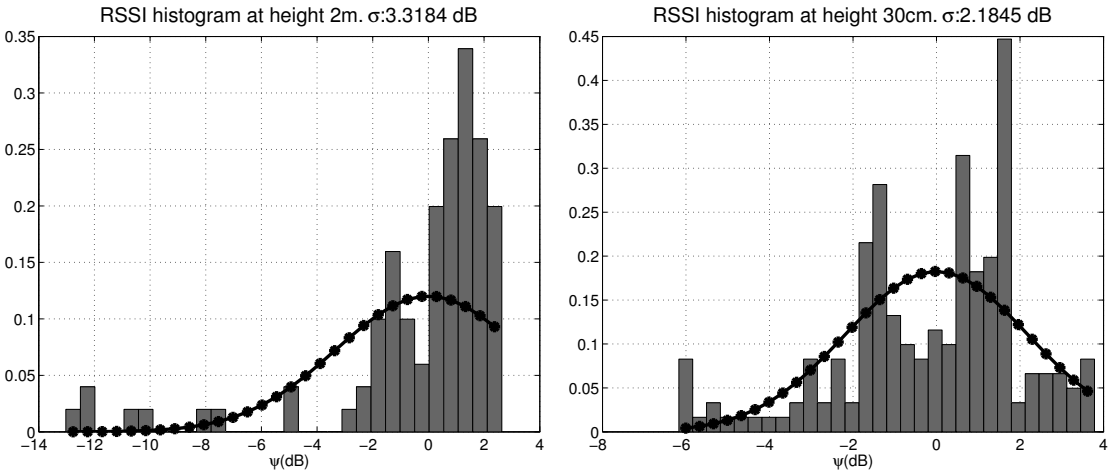

(a) $h = 2$ m (b) $h = 0.3$ m

Figure 3.19: Ground to Air histograms for $h = 2$ m and $h = 0\ 3$ m in open field environment

increases to $\gamma(h = 0\ 3\ \text{m}) = 2\ 38$. The value of $\gamma(h = 0\ \text{m})$ does not present a significant variation with $\gamma(h = 0\ 3\ \text{m})$. Nevertheless, it is surprising that $\gamma(h = 0\ 7\ \text{m}) = 0\ 74$. The fact that $\gamma(h = 2\ \text{m}) = 1\ 67$ instead of $\gamma(h = 2\ \text{m}) = 2$ in LOS condition is as discussed above caused by the mismatching of elevation angles between TX and RX with the distance inducing changes in the antennas gains at the propagation direction for each distance. As empirically demonstrated in the ground to ground scenario $\gamma(h = 2m) \sim 2$ because the elevation angles between both nodes is allways the same. Note that in this environment a critical distance does not appear since it occurs at larger distances. On its behalf, the PDR as a function of distance is shown in Figure 3.21b. As expected, the PDR is always one, as in the open field environment.

Figures 3.22a and 3.22b show the RSS histograms for this experiment and this environment. The conclusions given for the open field environment are the same in this environment scenario since the communication scenario is the same. The distribution of the variable and the values of σ_ψ are different than in the open field due to a change in the physical environment.

In Tables 3.4 and 3.5 we summarize the obtained model parameters with the corresponding 95% confidence bounds as well as the goodness of fit in terms of R^2 and the $RMSE$ errors of the obtained models for both environments.

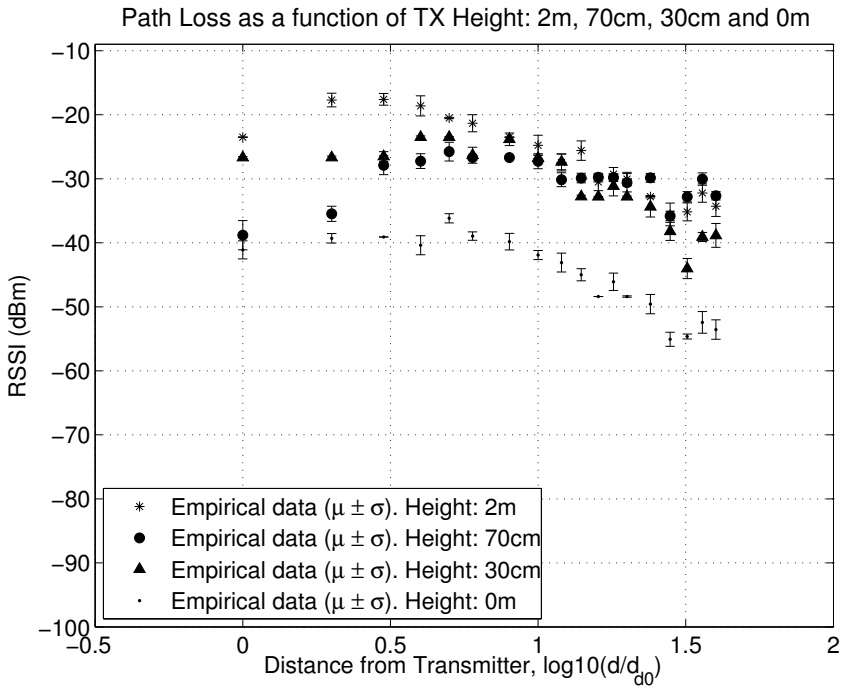

Figure 3.20: Ground to air empiric RSS measurements for the same TX heights: h = [2 m,0.7 m,0.3 m,0 m]. Urban park environment.

3.7.2.3 Measurement Campaign III

Dynamic near ground effects can be modeled by the model parameter L_e which accounts for the attenuation caused by any object that blocks temporally the LOS or the first Fresnel zone. As an example we introduce this parameter to traffic sensing applications. Under this example L_e is the additional power losses caused by cars, which temporally blocks the LOS between the transmitter and the receiver. In order to obtain this parameter we consider two cases: with and without car. The results presented in Table 3.6 are the mean RSS for each radius between both cases. The L_e parameter does not present significant variations from one distance to another. We conclude that L_e can be considered as a constant to the general propagation model in Equation (3.1).

If we take the RSS measurements for a specific circle, for instance 15 m, we obtain a cut of the TX radiation pattern at $\theta = 0\ 1974$ rad under the conditions with and without car. As observed in Figure 3.23, the car changes significantly the TX radiation power pattern.

On the other hand, Figures 3.24a and 3.24b present the histogram of the RSS measurements taken in this experiment. It is worth noting that the observed variations are owing to the radiation pattern as we are considering the simplest scenario. The reason to take into account the histogram of RSS for different angles is to provide a generalized model independent of the angle between the transmitter and the receiver. In other words, the histogram is considered

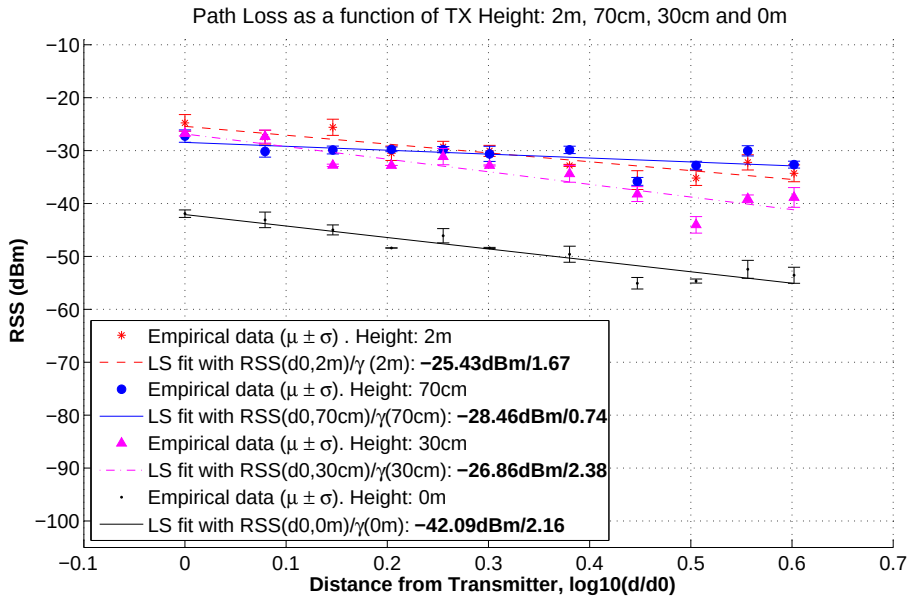

(a)

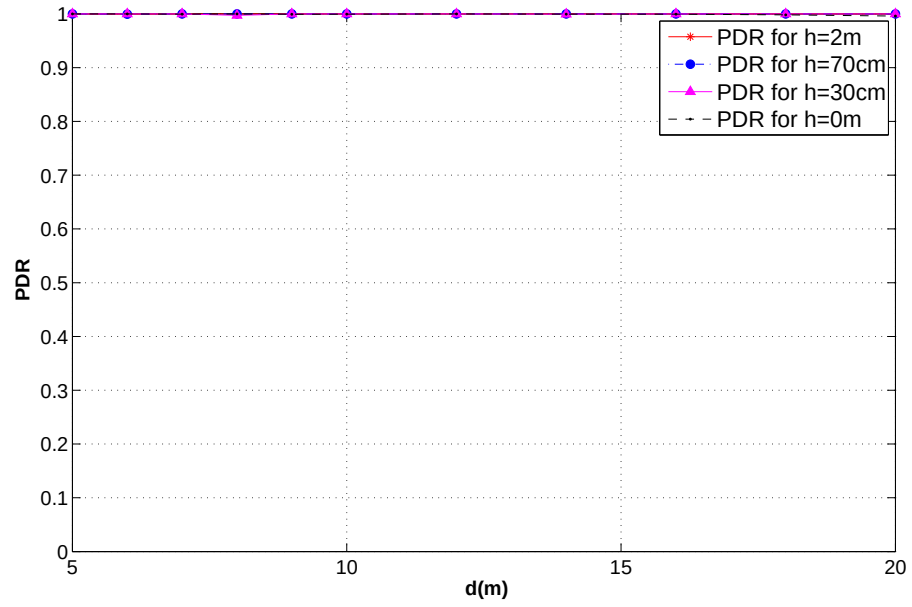

(b)

Figure 3.21: 3.21a: Figure 3.20 avoiding the first 7 measurements with the corresponding propagation models. Urban park environment. 3.21b: Communication distance in terms of Packet Delivery Ratio.

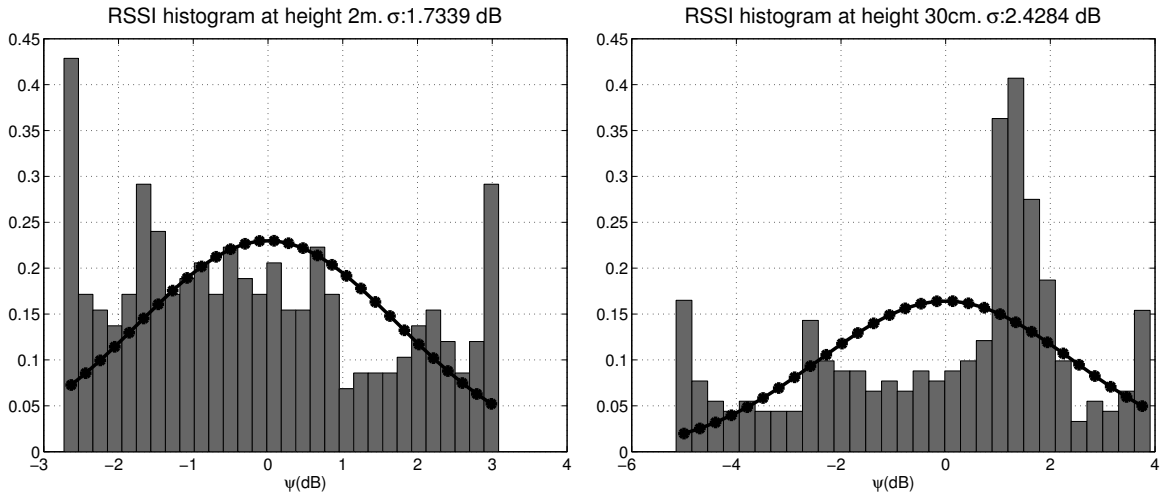

(a) $h = 2$ m (b) $h = 0.3$ m

Figure 3.22: Ground to Air histograms for heights 2 m and 0.3 m in urban park environment.

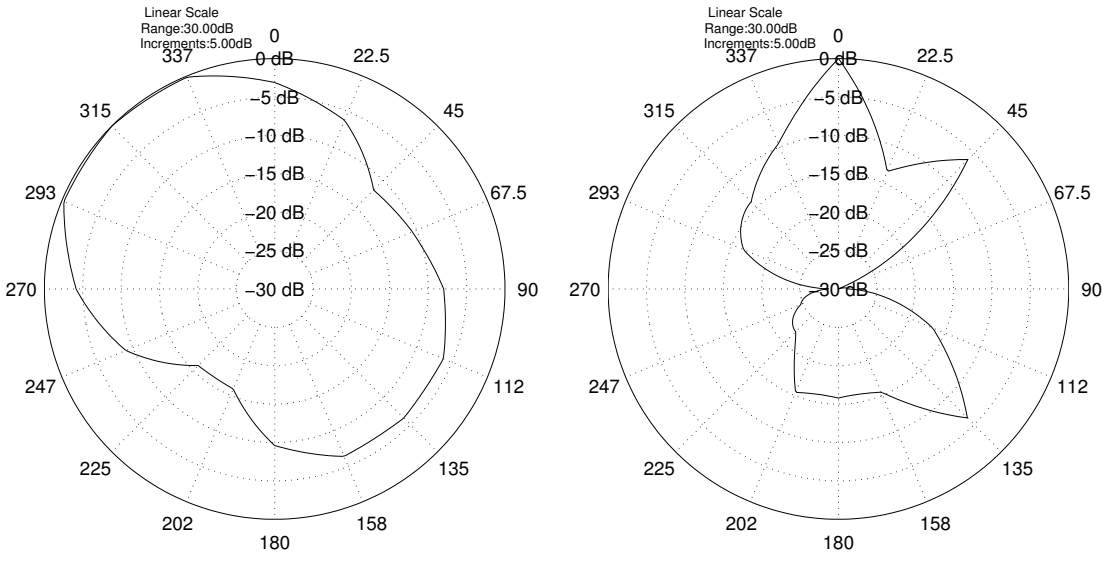

(a) Without car (b) With car

Figure 3.23: A cut of the radiation power pattern for the cases without car and with car.

Table 3.4: Ground to air model parameters (γ and $RSS(d0)$ with its 95% confidence bounds). The values of R^2 for h=0.3 m and 0 m correspond to each of the slopes. Open field.

h	**2 m**	**0.7 m**
γ	1.786(1.49,2.082)	2.353(2.129,2.577)
$RSS(d0)$	-26.98(-29.53,-24.43)	-26.63(-28.57,-24.7)
μ	0	μ:0
$\sigma_\psi(dB)$	3.32	2.27
R^2	86.07	94.92
$RMSE$(dB)	3.06	2.32
h	**0.3 m**	**0 m**
γ_1	2.11(1.648,2.572)	1.683(1.304,2.061)
$RSS(d0)$	-28.47(-30.17,-26.77)	-48.78(-50.17,-47.38)
γ_2	4.399(3.621,5.178)	3.324(-5.126,11.77)
μ	0	0
$\sigma_\psi(dB)$	2.18	1.41
R^2	92.22/91.3	91.84/58.89
$RMSE$(dB)	1.29/2.60	1.05/3

in order to obtain the distribution of variable in 3.1. By doing so, we can provide system designers with a channel model that takes into account the variations of the received power due to different antenna orientations. As observed in Figure 3.24, a Gaussian distribution can be adopted for a simple and approximate modeling of the received power distribution.

3.7.3 Air to Air

The purpose of this section is to evaluate and compare the propagation characteristics in urban streets with different widths. Under this scenario, γ is only dependent on the environment since the first Fresnel zone is not obstructed by ground, satisfying LOS condition and $\theta = 0$. The model parameter L_e is set to 0 dB since in this scenario the environment is less dynamic than in the above discussed communication scenarios. Higher the nodes less signal blockage, less power variations and thus a more robust communication. The generic propagation model for this scenario is simplified to Equation (3.14). Note γ and $RSS(d0)$ parameters do not depend on height.

Table 3.5: Ground to air model parameters (γ and $RSS(d0)$ with its 95% confidence bounds). Urban park.

h	**2 m**	**0.7 m**
γ	1.669(1.051,2.288)	0.7373(0.101,1.374)
$RSS(d0)$	-25.43(-27.71,-23.15)	-28.46(-30.81,-26.11)
μ	0	μ:0
$\sigma_\psi(dB)$	1.74	1.78
R^2	80.56	43.29
$RMSE$(dB)	1.72	1.77
h	**0.3 m**	**0 m**
γ	2.382(1.539,3.224)	2.162(1.553,2.77)
$RSS(d0)$	-26.86(-29.96,-23.75)	-42.09(-44.34,-39.85)
μ	0	0
$\sigma_\psi(dB)$	2.43	1.65
R^2	81.96	87.76
$RMSE$(dB)	2.35	1.7

$$RSS(d) = RSS(d0) - 10\gamma log10\ \ d\ \ d0) + \tag{3.14}$$

Two kind of urban streets are considered: narrow street and wide street. Empirical RSS measurements are collected in both streets. As a reference, the propagation model characteristics are obtained in an open field environment. In all environments we take RSS measurements every 5 m from the transmitter up to $d = 110$ m, as shown in Figure 3.9.

- **Open field:** the results in Figure 3.25a show that the power decay factor $\gamma = 1\ 79$ for $h = 4\ m$ is close to free space and $\gamma = 2\ 41$ for $h = 3\ m$. It is observed that γ still has some

Table 3.6: Attenuation due to a car.

Radius	**5m**	**10m**	**15m**	**25m**	
Without car RSS	-51.55	-56.53	-61.81	-67.18	
With car RSS	-63.53	-66.32	-74.37	-76.53	Mean
$L_e(dB)$	11.98	9.8	12.56	9.35	10.92

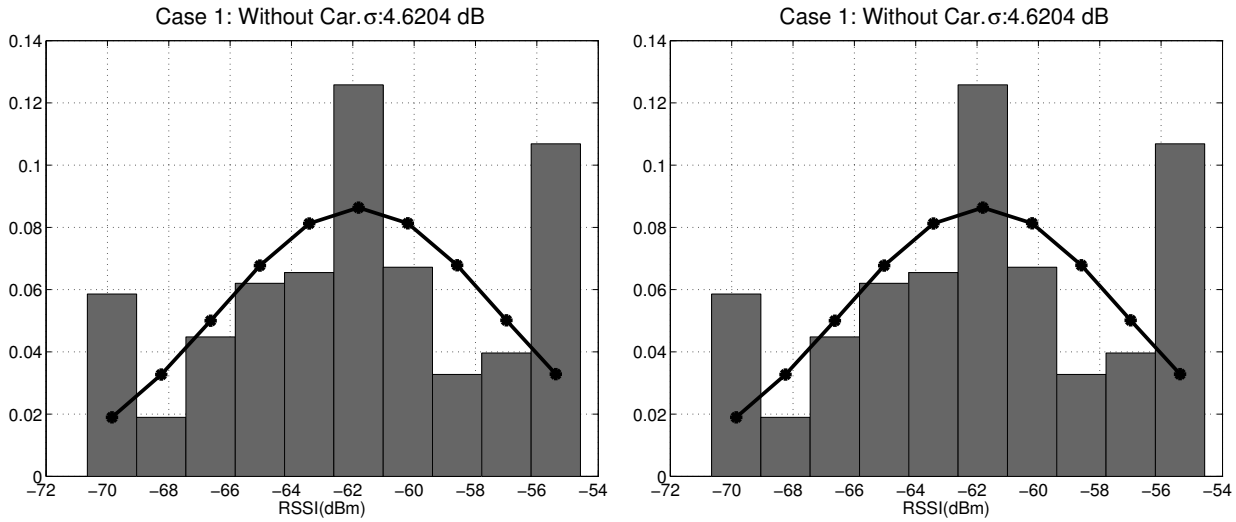

(a) Without car RSS distribution

(b) With car RSS distribution

Figure 3.24: RSS distributions for the cases without car and with car

influence on height. We believe that this influence is attributed to reflections from few surrounding trees other than ground. On its behalf, Figure 3.25b shows that as expected the start of the transition region is quite above 100 m.

The received power distribution of the propagation models in Figure 3.25 are represented by Figures 3.26a and 3.26b for the heights $h = 3$ m and $h = 4$ m respectively. The conclusions given by the ground to ground scenario can be given as well in this scenario since there is no effect of antennas gain, and there is no obstruction by ground to the first Fresnel zone. Note that both distributions are close to a Gaussian and in accordance with the Central Limit Theorem the distribution of the variable can be considered as Gaussian. It can be seen that lower the height higher the σ. For $h = 3$ m, $\sigma = 4\,9$ dB whereas for $h = 4$ m, $\sigma = 2\,97$ dB.

- **Wide street:** The corresponding empiric propagation model is shown in Figure 3.27. It is of 2-slope: one slope accounting for the propagation losses in the LOS region and another slope accounting for the propagation losses caused by building blockage (NLOS region). A value of $\gamma \ll 2$ in this experiment indicates that street acts as a waveguide. The literature demonstrates that either in an urban street or in an indoor corridor there exists are waveguide effects that reflects in a path loss exponent lower than the free space [40, 41].

  The RSS distribution corresponding to the measurements in 3.27 is depicted in Figure 3.28. As we did for previous set of histograms, we approximate the distribution of the taken measurements as normal distribution $\mu = 0$ dB and a standard deviation of $\sigma = 3\,18$ dB. The

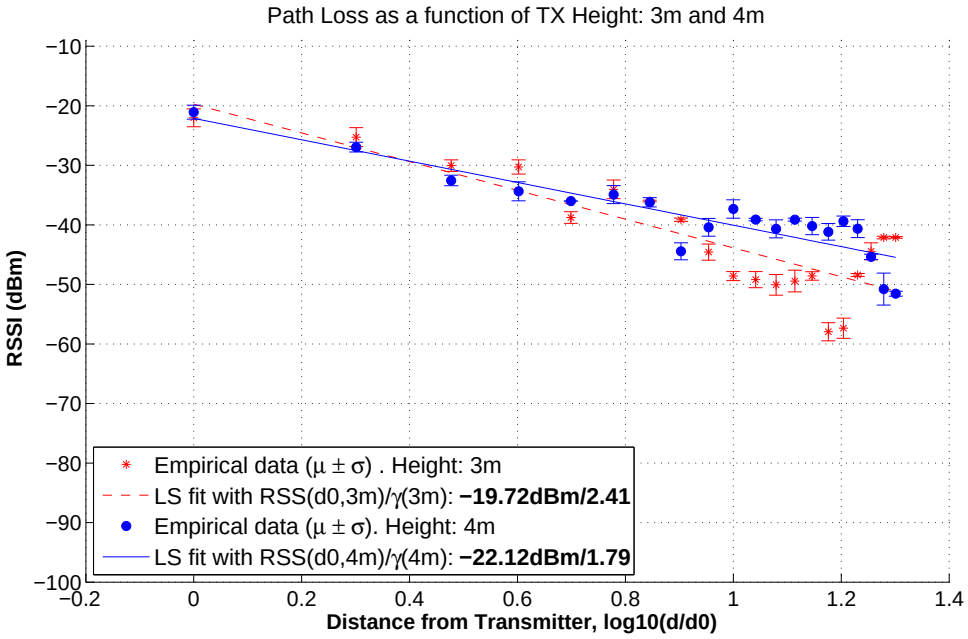

(a)

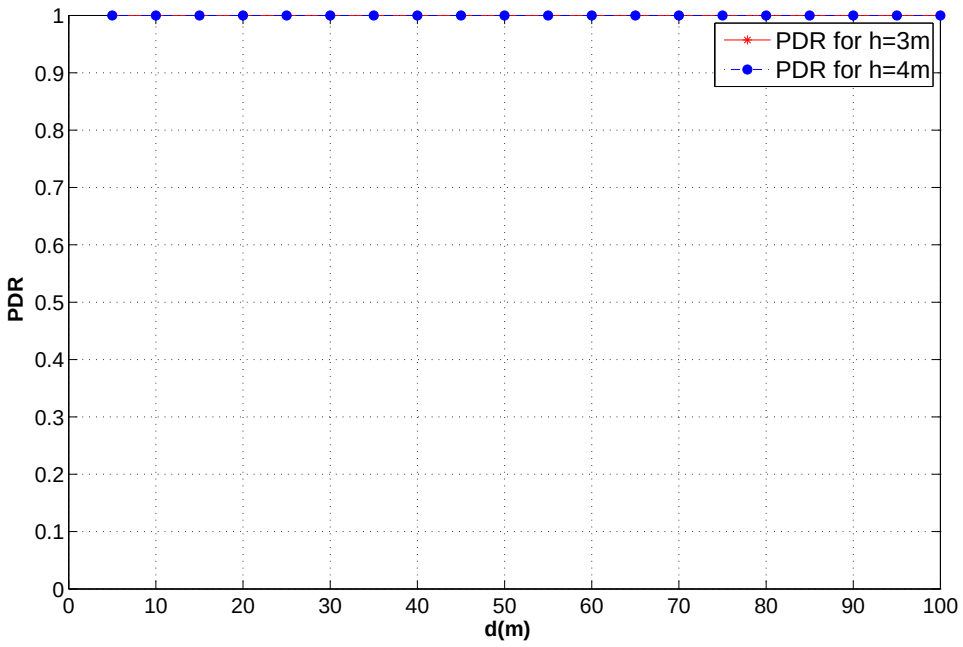

(b)

Figure 3.25: 3.25a: Air to air propagation model in open field. 3.25b: Wireless range in terms of the Packet Delivery Ratio.

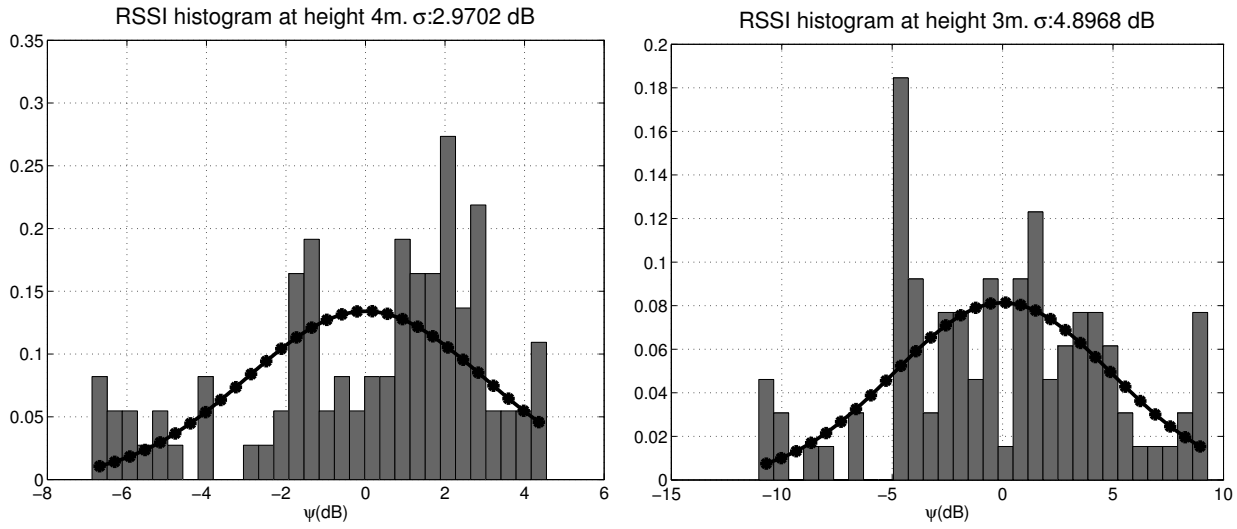

(a) $h = 4$ m (b) $h = 3$ m

Figure 3.26: Air to air histograms for heights $h = 4$ m and $h = 3$ m in open field environment.

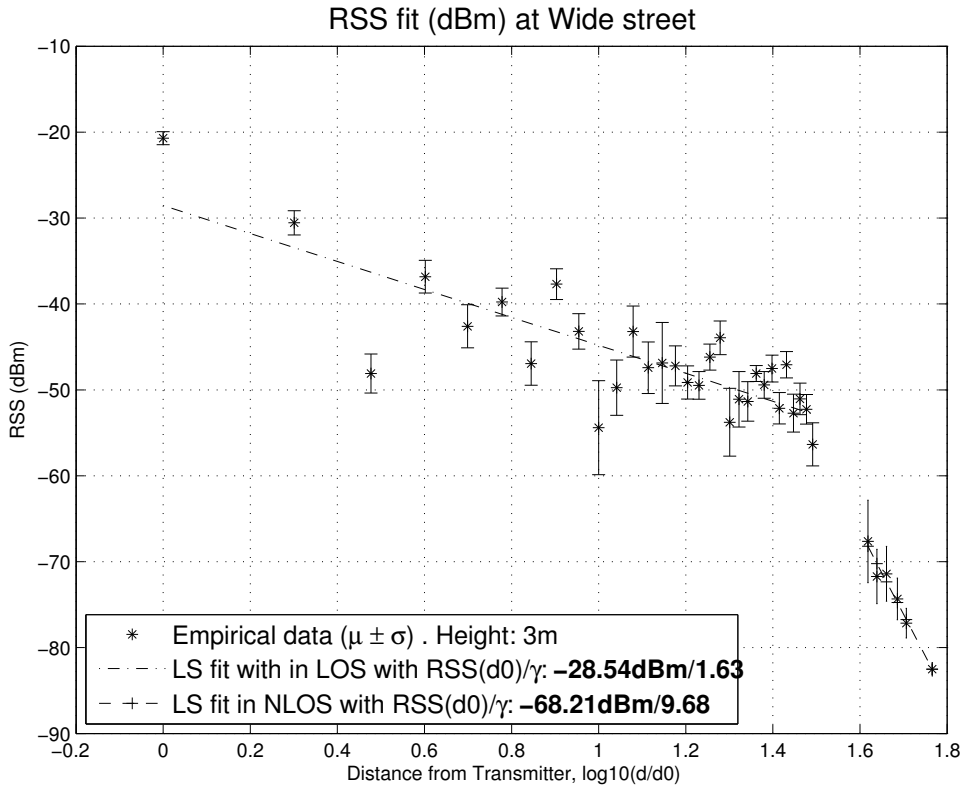

Figure 3.27: Air to air propagation model in wide street.

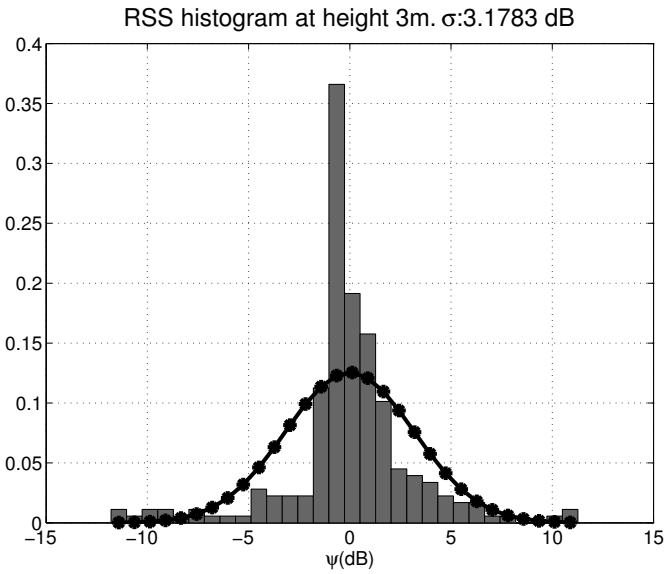

Figure 3.28: Air to air histogram for $h = 3$ m. Urban wide street.

RSS variations in this environment is attributed mainly to multipath (multiple reflections from surrounding buildings, trees, etc) and shadowing.

- **Narrow street:** The corresponding empiric propagation model is given in Figure 3.29. In comparison to the wide street, the surrounding objects are less dispersed leading to an increase of the power losses and thus an increase of γ from 1.63 to 3.06.

  Concerning the distribution of the RSS measurements, the same conclusions in the wide street can be given in this environment. The histogram of the RSS measurements is illustrated in Figure 3.30. As observed, the distribution of the measurements is clearly Gaussian with a higher standard deviation $\sigma = 5\,65$ dB. The fact that σ is bigger than in the wide street is because as observed in Figure 3.29 in some positions the mean of the RSS is 10 dB lower than the value given by the propagation model. All the empiric measurements that fall outside the propagation model are caused by either multipath or blockage of the first Fresnel zone by surrounding things. In Table 3.7 and 3.8 we summarize the obtained model parameters with the corresponding 95% confidence bounds. We also show the goodness of fit in terms of R^2 as well as the $RMSE$ errors of the obtained models for these environments.

3.7.4 Reference model for low power wireless devices deployment under Urban environments.

In this section we provide a reference model for the smart wireless devices deployment in the considered scenarios from the obtained propagation models. The reference model depicted by

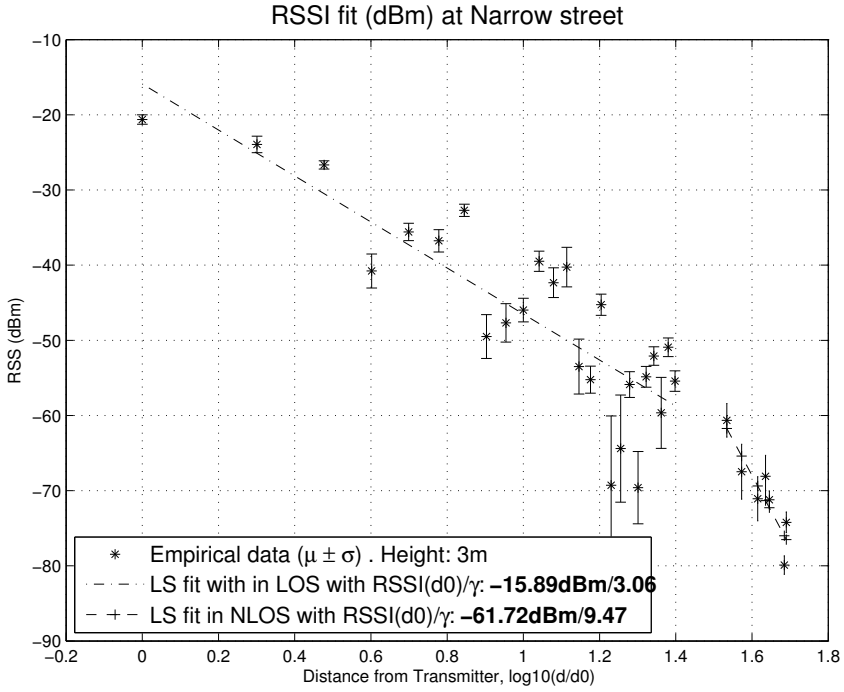

Figure 3.29: Air to air propagation model in narrow street.

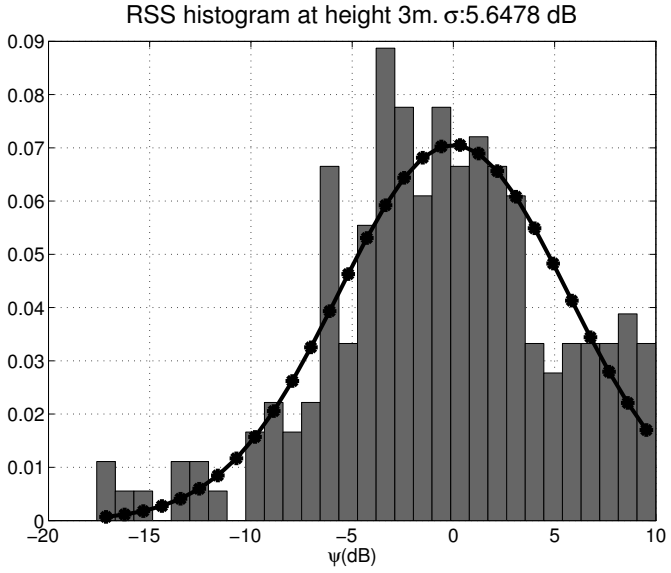

Figure 3.30: Air to Air histogram for $h = 3$ m. Urban narrow street.

Table 3.7: Air to air model parameters (γ and $RSS(d0)$ with its 95% confidence bounds). Open field.

h	**3 m**	**4 m**
γ	2.415(1.695,3.135)	1.794(1.359,2.228)
$RSS(d0)$	-19.72(-26.79,-12.64)	-22.12(-26.38,-17.86)
μ	0	0
σ_ψ	4.9	2.97
R^2	73.38	80.70
$RMSE$	5.26	3.18

Figure 3.31 shows the possible range or communication distances, represented on the x-axis, that can be reachable as a function of TX/RX height, represented on the vertical axis. The results are obtained from the propagation models of all communication scenarios discussed above. The air to air scenario does not have measurements between the heights 0 m-3 m. In practice wireless devices are deployed high enough from ground to increase the wireless range for the near ground nodes as well as to prevent vandalism with reduced costs. All in all, the ground to air scenario presents higher communication capabilities than the ground to ground scenario.

3.8 Model validation

In this section we validate the model presented in Equation (3.1) from the set of carried measurement campaigns. Our model presented in Equation (3.15) is aligned with the theory of wireless propagation and the experimental results. We state that the proposed model is suitable for the studied smart city communication scenarios.

$$\begin{aligned} RSS(d\ h)(dBm) = RSS(d0) - 10\gamma(h)log(d\ d0) \\ -L_g^{dB}(h) - L_e(dB) + \quad (h)(dB) \end{aligned} \tag{3.15}$$

Hence:

- When h γ towards the free space. γ $[\sim 1\ 6 - 3\ 5]$ h(m) $[\sim 4 - 0]$ for any scenario.
- h $L_g^{dB}(h)$. For h(m) $[1\ 2 - 0]$, $L_g^{dB}(h)$ $[0 - 40]$. This parameter measured in independent campaign is observed in real data.
- L_e(dB) is also measured in independent campaign and is observed to be a independent with distance with a value of 10.91 dB.

Table 3.8: Air to air model parameters (with its 95% confidence bounds). Wide street and narrow street.

	Wide street	**Narrow street**
γ_{LOS}	1.628(1.205,2.051)	3.061(2.243,3.879)
γ_{NLOS}	9.679(7.39,11.97)	9.47(4.23,14.71)
$RSS(d0)$	-28.54(-33.42,-23.66)	-15.89(-24.63,-7.157)
μ	0	0
$\sigma_{\psi}(dB)$	3.18	5.65
$R^2(\%)$ in LOS	68.11	72.28
$R^2(\%)$ in NLOS	97.18	81.19
$RMSE$(dB) in LOS	4.20	7.02
$RMSE$(dB) in NLOS	0.97	2.84

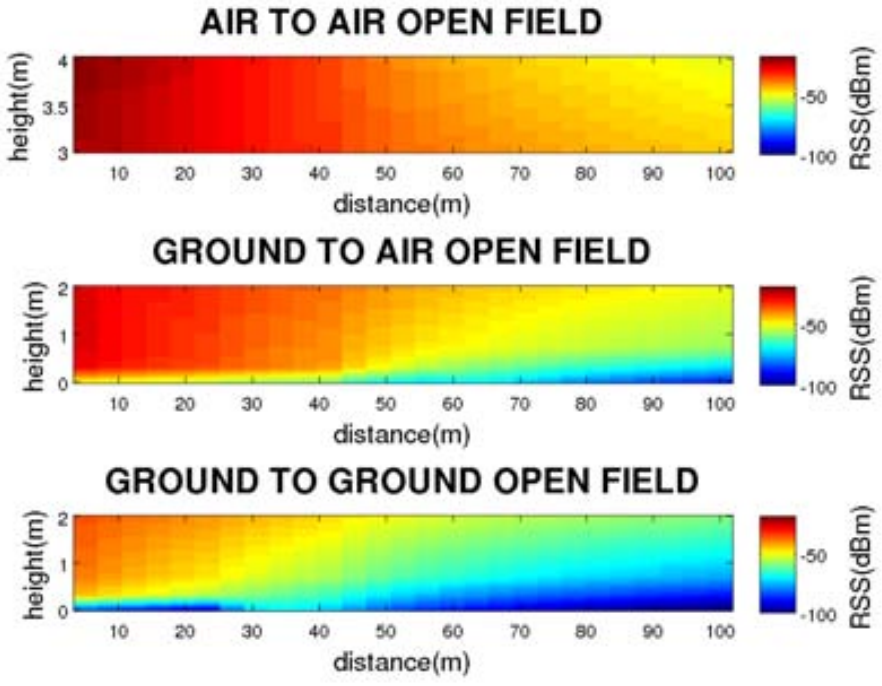

Figure 3.31: Range in open field of all communication scenarios as a function of height

- is confirmed to follow a Gaussian distribution with $\mu = 0$ dB and σ(dB) $[\sim 1\ 6 - 5\ 7]$.

3.9 Conclusions

This Chapter has modeled typical communication scenarios that can be found in a smart city, namely ground to ground, ground to air and air to air. In this context, air refers to the nodes placed high enough from ground whereas ground refers to the nodes that can be placed near ground and high enough from ground. In that sense, we have provided a unified propagation model derived from the theoretical knowledge focused on the described communication scenarios. Our developed channel model takes into account the node position in relation to ground as well as the environment. This propagation model has been used to evaluate the propagation characteristics for each of the above communication scenarios.

It is demonstrated that the signal propagation differs between the aforementioned communication scenarios because they are completely different. A path loss exponent is found for each height h satisfying that $h - r < 0$, being r the Fresnel zone radius. The ground to air link in LOS conditions experiences a $\gamma \ll 2$ owing to the height mismatching that leads to a change of the antennas gain with distance in the propagation direction. The communication between near ground nodes experiences a $\gamma \sim 3$. It is demonstrated that the received power decay with distance depends on the node height once the first Fresnel zone becomes obstructed. This happens for heights below 1 m corresponding to 3λ at the band 868 MHz. Additionally, our model takes into account external power losses due to other objects that blocks temporally the LOS between air nodes and ground nodes.

An empirical evaluation of the communication distance in terms of PDR for the different communication scenarios as well as environments is presented. The results demonstrate that the sizes of the connected region as well as the transition region of the PDR are dependent of both the surrounding environment and the propagation characteristics. In addition to the RSS, the PDR provide information about the exact communication distance that leads to a specified PDR threshold. This is also demonstrated in Figure 3.32, which the mapping between the RSS and the PDR is environment dependent. Thus, the RSS only is not only a measure to indicate the quality of a wireless link, it is both the RSS as well as the PDR. Moreover the results depicted in Figure 3.32 does not mean that the receiver sensitivity is environment dependent but the number of multipath components as well as external interferences may distort the received signal causing an increase of the lost packets and the number of received corrupted packets and hence leading to a low Packet Delivery Ratio.

To this end, we have provided a model as a reference to deploy smart wireless devices from the aforementioned scenarios. This reference model is derived from the set of obtained empirical

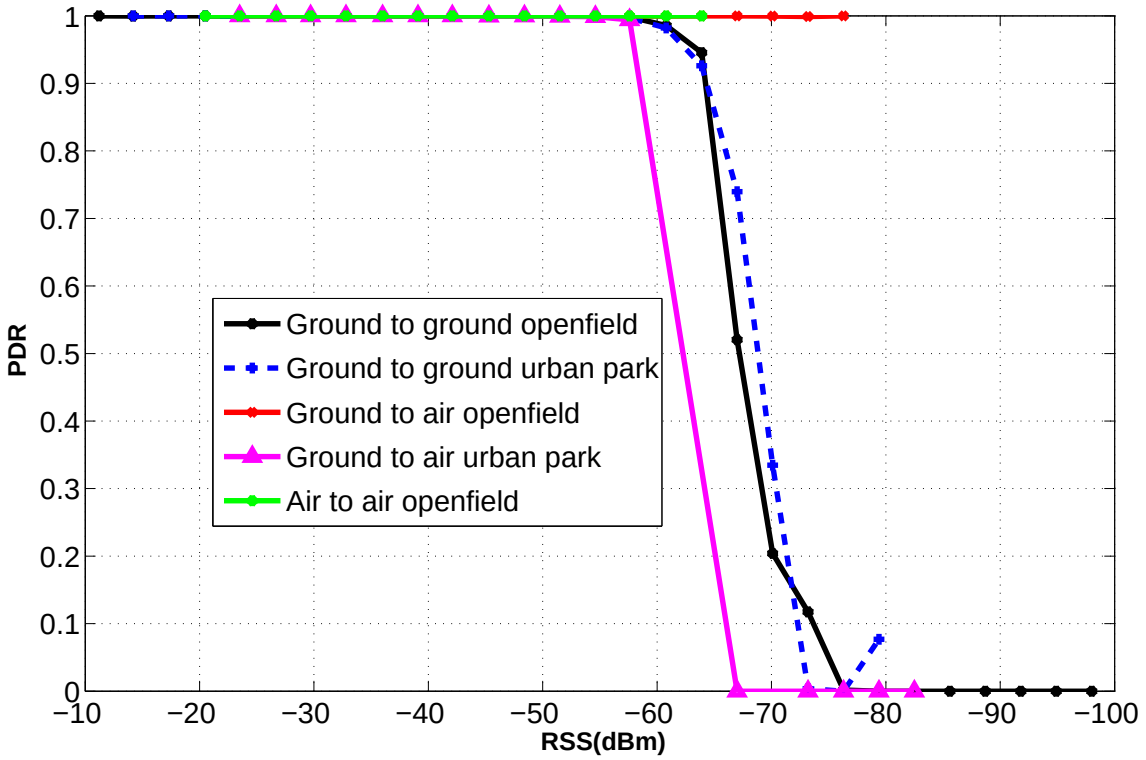

Figure 3.32: PDR to RSS mapping as a function of the environment and communication scenario.

propagation models.

Chapter 4

On the suitability of the 433 MHz band for M2M wireless communications: propagation aspects

4.1 Introduction

The previous Chapter of this thesis have focused in evaluate the propagation aspects at the European non ISM 868 MHz band for typical smart city communication scenarios by developing a generalized channel model for typical smart city applications, where the antenna height from ground is considered. In this Chapter we follow a similar approach, considering the antenna height and using an ISM band that a priori provides longer range because the frequency is lower. This is the emergent 433 MHz ISM band, which is available worldwide. The 433 MHz band present the following advantages in comparison to the 868 MHz band:

- The 433 MHz band has fifteen narrowband channels whereas the 868 MHz band only has one channel. This great advantage offers channel hopping to overcome external interferences.

- The path loss at the 433 MHz is 6 dB lower than at the 868 MHz band. Thus considering a similar transmit power and similar receiver sensitivity at both frequency bands, the wireless range at the 433 MHz is longer than at 868 MHz.

- The 433 MHz can be used worldwide since it is an ISM-band. The non ISM 868 MHz band is only available in Europe.

All these advantages makes the 433 MHz band suitable and with great potential for low power wireless communications, typically focused on smart city applications. For this reason we are interested in this Chapter to evaluate the propagation aspects for this emergent band and comparing it with the worldwide 2.4 GHz ISM band, which also offers fifteen channels and channel hopping.

Machine-to-Machine (M2M) communications refer to the set of technologies that are used to connect systems for the purpose of remote monitoring and control without human intervention. To connect end devices with the surrounding infrastructure, M2M communications typically rely on cellular or low-power wireless technologies. For low-power wireless technologies the 2.4 GHz band is commonly used for two main reasons. First, the 2.4 GHz band is part of the ISM (Industrial, Scientific and Medical) bands meaning that it is available world-wide without requiring a license. Second, the IEEE 802.15.4 standard [12] defines the use of the 2.4 GHz band for Low-Rate Wireless Personal Area Networks (LR-WPAN) and, thus, many off-the-shelf transceivers are readily available from different manufacturers. Today IEEE 802.15.4 networks have already been successfully deployed in various environments, i.e. industrial monitoring, but there are several factors that may limit its suitability. For example, in industrial environments IEEE 802.15.4 suffers from high attenuations caused by concrete walls and metallic surfaces. In addition, in such scenarios IEEE 802.15.4 networks have to cope with interferences coming from other narrowband and broadband wireless technologies operating at the same band with higher transmit power [42, 43], e.g. IEEE 802.11 and IEEE 802.15.1.

To overcome these limitations two approaches are used in IEEE 802.15.4 networks. First, the use of DSSS (Direct-Sequence Spread Spectrum) helps improving coexistence with narrowband and broadband interferences. Second, channel hopping also contributes to mitigate the effects of interferences, either narrowband or broadband, and also combats the effects of multi-path propagation [21]. In that sense IEEE 802.15.4e [14] has recently been approved as part of the IEEE 802.15.4 standard and an open source reference implementation already exists [44]. In addition to spread spectrum techniques, the use of the 868 MHz and 915 MHz bands has also been devised as an alternative to overcome the limitations of the 2.4 GHz band in certain environments. These bands are also part of the IEEE 802.15.4 standard and offer better propagation and interference characteristics thanks to its lower operating frequency and data rate, as well as because fewer wireless systems currently make use of these bands. However, these bands do not represent a true alternative to the 2.4 GHz band because ubiquitous deployment is limited by existing regulations [45, 46]. The 868 MHz band allows a transmit power up to 14 dBm (25 mW) but is not a part of the ISM bands and, thus, it is only available in the European Union (EU). Moreover, channel hopping is not available at the 868 MHz band because only one channel is available. On its behalf, the 915 MHz band enables transmit powers up to 30 dBm (1 W) and is part of the ISM bands, but usage is limited to the United States (US).

Recently the 433 MHz band has re-gained momentum as an alternative to the 868/915 MHz and 2.4 GHz bands. Compared to the former, the 433 MHz band is a true ISM band and, thus, it is available (almost) world-wide without requiring a license. Compared to latter, the 433 MHz band has better propagation characteristics due to its lower operating frequency and is currently less affected by external interferences due to the lower number of systems operating at the band. Given its interesting properties and the possible impact in M2M communications, there are two standardization organizations that are currently defining physical layers that operate at the 433 MHz band, e.g. DASH7 Mode 2 [47] and IEEE 802.15.4f [2]. Nevertheless, despite the efforts that have already been conducted, there are still aspects at the physical layer that require further investigation in order to understand its properties and determine which frequency band is more suitable depending on application requirements. Thus, we currently focus in evaluating the physical layer characteristics of the 433 MHz band and compare it to the 2.4 GHz band. Specifically, we focus this Chapter in evaluating and comparing the propagation aspects of both bands in different environments, e.g. indoor and outdoor, to determine its suitability for M2M communications using low-power wireless technologies. For example, better propagation may lead to a reduction in the requirements of multi-hop communications and, thus, decrease the overhead caused by routing protocols [48].

The contributions of the Chapter are the following. First, it presents an overview of the low-power standards currently being developed at the 433 MHz band for M2M wireless communications. Second, it conducts empirical measurements to demonstrate the benefits and drawbacks of the 433 MHz band compared to the 2.4 GHz band in both outdoor and indoor scenarios at different node heights from ground level. Third, it evaluates the behavior of channel hopping against multi-path propagation at the 433 MHz band both in LoS (Line of Sight) and NLoS (Non-Line Of Sight) indoor environments. Therefore, our results contribute to the understanding of the propagation properties of the 433 MHz band and demonstrate that, under similar conditions, 433 MHz propagation is better in terms of range than 2.4 GHz. In addition, the obtained empiric propagation models can be useful for the deployment of M2M wireless communications in both outdoor and indoor environments where nodes have to be deployed at different heights.

The remainder of the Chapter is organized as follows. Section 2 presents the work related to propagation at the 433 MHz and 2.4 GHz bands and introduces the different low-power wireless communication standards that are currently developed at the 433 MHz band. Section 3 presents the theoretical background related to the propagation aspects of wireless communications. Section 4 presents the experimental methodology that we have used to evaluate and compare the propagation aspects of the 433 MHz band with the 2.4 GHz band. The corresponding results of the experiments are presented and discussed in Section 5. Finally, Section 6 concludes the Chapter.

4.2 Related work

4.2.1 Propagation models at 433 MHz and 2.4 GHz

There are some studies that have already conducted experimental propagation measurements at the 433 MHz band and 2.4 GHz bands. Thelen et al. [49] carried out measurements in a potato field at the 433 MHz band. In their study they took two series of measurements that expanded over a two week period each and checked three main aspects. First, the reception rate depending on the received power to determine the receiver sensitivity. Second, the variation of the received power according to the distance between the transmitter and the receiver with the growth stage of the potato crop. Third, the influence of micro-climate (temperature, relative humidity and rain) on the received power. Whilst the paper verifies that the foliage and micro-climate has an impact on the propagation of radio waves, it fails to validate how well the proposed model fits the empiric data in the specific environment. At the 2.4 GHz band, Holland et al. [50] investigated radio propagation aspects using Tmote Sky motes. In the experiments they measured received power, signal quality and packet reception as a function of distance, angle and transmit power, in both indoor and outdoor environments taking into account environmental conditions. The results show that mote position and height have a great impact on received power and link quality, but the authors do not present any propagation model that can be useful for link budget planning. Finally, in [51] the authors conduct propagation measurements in the military UHF bands, which include the 433 MHz band, to characterize path loss of narrowband channels in urban terrain for ground based communications. The results, obtained using RF equipment, show that the mean received power in LoS conditions matches two-ray propagation theory and is not affected by street width.

More recently, Zhang et al. [52] measured propagation characteristics at the 433 MHz and the 2.4 GHz bands in an orchard environment with different peach tree heights and fruit densities. Specifically, they evaluated the channel fading and the packet loss rate for different antenna heights. From the results they conclude that the antenna height influence at the 433 MHz band is slightly larger, but the initial path loss at the 2.4 GHz band is greater. In addition, they found that for their particular environment the optimal antenna height is 3.5 m. Nevertheless, they also fail to present a propagation model that can be useful for link budget planning. Wennerström et al. [53] focused on the PRR (Packet Received Ratio) and RSS (Received Signal Strength) behavior against meteorological conditions (temperature and humidity) in a two week period using TelosB motes. Their experimental results demonstrate that temperature and humidity variations influence the PRR. They assume that the RSS variations are correlated with temperature and humidity variations but fail to take into account that the RSS variation can be also attributed to multipath propagation (shadowing and fading). Finally, in [54] the authors present empirical path loss models at different frequencies for an environment of stacked

shipping containers. In particular, they conducted measurements for intra- and inter-container communications at the IEEE 802.15.4 bands, e.g. 433 MHz, 868 MHz and 2.4 GHz, as well as for extra-container communications using the GSM/UMTS bands, e.g. 900 MHz, 1850 MHz and 2100 MHz. For the inter-container measurements the results show that path loss is lowest at 433 MHz band in the pathways between container rows, and lowest at 2.4 GHz band in the small gaps between adjacent containers.

Other interesting articles related to propagation aspects at the 433 MHz and the 2.4 GHz bands in different environments include [55, 56, 57, 58].

4.2.2 Overview of 433 MHz standards

As stated earlier, the 433 MHz band has recently gained relevance as an alternative to the 868/915 MHz and 2.4 GHz bands for different reasons. First, compared to 868/915 MHz it is available (almost) world-wide without the need of a license. Second, compared to 2.4 GHz it has better propagation characteristics due to its lower operating frequency. Nevertheless the 433 MHz band has some downsides as well. The band is not harmonized, e.g. different regulations in different countries. In the European Union (EU) the transmission power is 10 dBm with a 10% duty cycle or 0 dBm with a 100% duty cycle [45], whereas in the United States (US) the transmission power is -14 dBm for periodic control applications and -23 dBm for other periodic applications [46]. However, a Duty Cycle Correction (DCC) of up to 20 dB can be applied to enable higher transmit powers as long as the average transmit power during the averaging time frame, i.e. pulse train or worst case 100 ms, is kept within the regulatory limits. Furthermore, the 433 MHz band is more limited in terms of bandwidth than the 2.4 GHz band is, e.g. 1.74 MHz and 100 MHz respectively. Finally, the optimal antenna size for the 433 MHz band is larger compared to an equivalent antenna for the 2.4 GHz band.

The 433 MHz band extends from 433.05 MHz to 434.79 MHz and is organized into fifteen 108 kHz narrowband channels for two reasons. First, support for multiple channels enables different systems located in the same physical domain to coexist, e.g. a narrowband channel can be allocated between two consecutive narrowband or broadband systems without either causing or receiving interference. Second, using narrowband channels enables to comply with specific regional regulations that have more strict bandwidth limitations, e.g. China. Currently two standards are being developed that use the 433 MHz band for low-power wireless communications: DASH7 Mode 2 and IEEE 802.15.4f. Despite of these standards are targeted at active RFID applications, they can also be used for WSN applications. Although the content presented in this Chapter is focused on the propagation aspects of the 433 MHz band with narrowband channels, we show in Figures 4.1 and 4.2 the philosophy of these standards. As observed, there are different data rates associated to different channel bandwidths which can be used according to

the application requirements and specific regulations. For a detailed overview of these standards please refer to [47, 2].

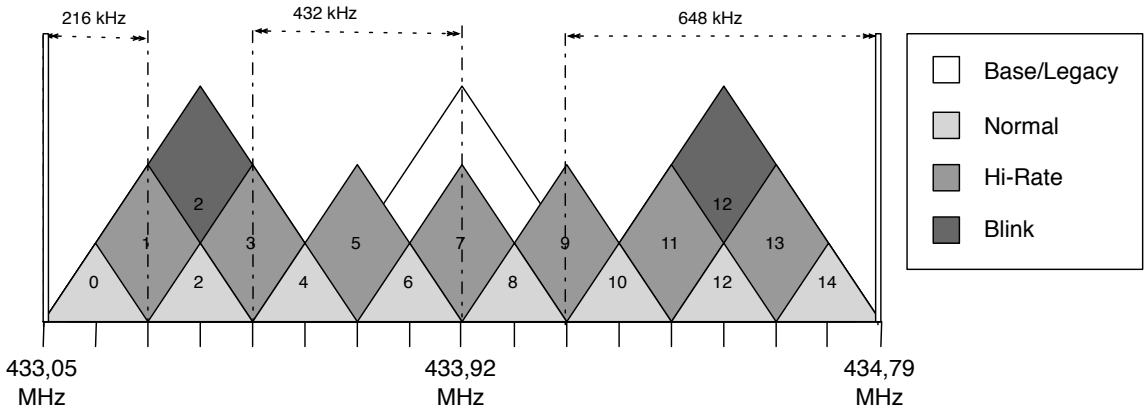

Figure 4.1: DASH7 Mode 2 physical layer channel organization. In DASH7 Mode 2 only the Normal and Blink channel types are orthogonal, that is, neighboring channels of the same type do not cause and receive interference to/from each other. The remaining channel types are non-orthogonal and, thus, neighbor channels cause and receive interference to/from each other and also to the Normal and Hi-Rate channel types. For example, the Blink channel type centered at channel 2 interferes with Normal and Hi-Rate channel types centered at channels 0, 2, and 4.

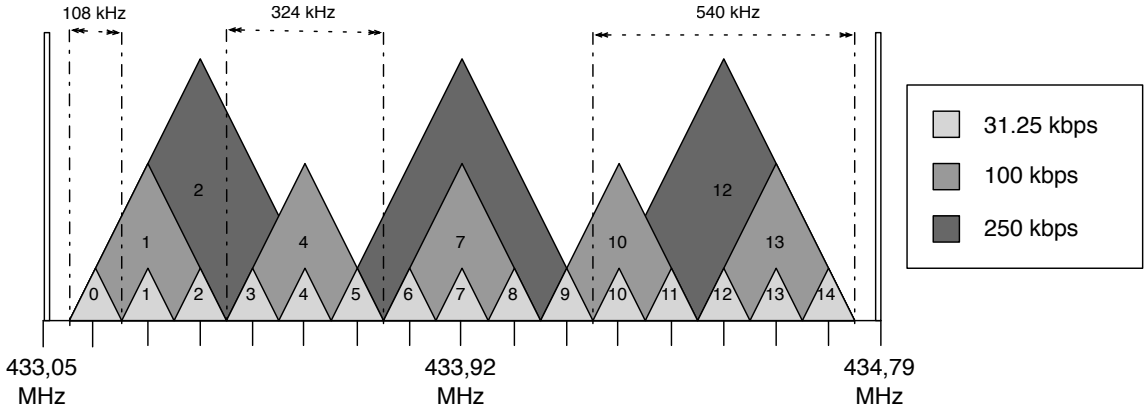

Figure 4.2: IEEE 802.15.4f physical layer channel organization. In IEEE 802.15.4f operating at the 433 MHz band all channel types are orthogonal with channels of the same type but non-orthogonal between different channel types. For example, the 250 kbps channel centered at channel 2 will cause and receive interference to/from all channels types centered at channels 0, 1, 2, 3 and 4 but not to/from all the remaining channels.

4.3 Theoretical propagation aspects

The main characteristics that determine the ultimate performance of any wireless communication system are interference and propagation. Interference determines how noise and other wireless systems operating at or near the carrier frequency affect the performance of the system under consideration. On its behalf, propagation determines how the power of an electromagnetic wave that propagates through space falls off depending on the distance between the transmitter and the receiver, as well as the characteristics of the surrounding environment. In the following subsections we provide a brief theoretical overview of the propagation phenomenons that determine the performance of a wireless system, namely free-space propagation, shadowing and multipath, as this is the main focus of this Chapter.

4.3.1 Free-space propagation

Free-space propagation is a model that describes the effects of how electromagnetic waves propagates through space with no obstacles causing reflection or diffraction. In that particular case, the received power falls off following an inverse square law that depends on the distance between the transmitter and the receiver.

On the one hand, in order to exist propagation there must exist a source acting as a wavefront such as a transmitter antenna. The reference antenna is an isotropic antenna which spreads out the power in equal magnitude in all spatial directions, mathematically described by (4.1). Note that propagation is not dependent on the wavelength (or the wave's frequency).

$$S = P_{TX} \frac{1}{4\pi d^2} \tag{4.1}$$

where P_{TX} is the transmitted power (in W) and S is the power density (in $W\ m^2$) at distance d. On the other hand, in order to exist communication there must exist both a transmitter (or a propagating electromagnetic wave) and a receiver antenna with an effective area A_{eff} which describes how well the receiver antenna can pick up the incident power from an incoming electromagnetic wave. For an isotropic antenna, the aperture is given by (4.2)

$$P_{RX} = SA_{eff} = S\frac{\lambda^2}{4\pi} \tag{4.2}$$

where P_{RX} is the received power. Note that the effective area is entirely dependent on wavelength, which is how the frequency-dependent behavior arises. Hence (4.2) demonstrates that the more power to pick up from an incident electromagnetic wave, the larger the antenna must be or the lower the frequency. From (4.1) and (4.2) the free space path loss (FSPL) is

defined as ratio between the transmitted power and received power (4.3), or as the power loss in free space as a function of the square of the distance.

$$FSPL = \frac{P_{TX}}{P_{RX}} = (\frac{4\pi d}{\lambda})^2 \tag{4.3}$$

In addition to path loss, the nature of the environment in which the wireless communications operates causes random variations in the received power at the receiver around the mean value (path loss). These variations occur at any distance from the transmitter and they are attributed to the contribution of either slow fading (shadowing) or fast fading (multipath) experienced in the wireless media in the time domain, in the space domain and in the frequency domain.

4.3.2 Shadowing

In the time domain, the slow fading usually occur when the variation of the channel magnitude is in the period of minutes or even hours, i.e. the coherence time T_c of the channel $T_c >> L_p$ where L_p is the packet length. These kind of fading is due to the shadowing phenomenon. The shadowing phenomenon is common when the visibility between TX and RX is temporary obstructed (from LOS to NLOS scenarios or vice versa). The shadowing phenomenon induces high fluctuations over the path loss producing attenuations or gains in the received signal [15]. The statistical distribution of the random received power due to shadowing is log-normal with mean μ_{dBm} in dBm units and standard deviation σ_{dB} in dB units. The mean can be based on empirical measurements which equals the averaged received power in order to remove the multipath and shadowing components. The statistic distribution of the shadowing is log-normal with zero-mean and standard deviation $\sigma_{shad}(dB)$ [16, 17, 18]. In contrast, the fast fading occur when the channel variation is within the symbol length T_s or the packet length L which can be the order of ms or μs. Fast fading arises from multi-path propagation effects and they are more emphasized when the environment changes dynamically, i.e. when either the transmitting or receiving node is moving.

In the space domain the shadowing phenomenon can also be experienced as observed in Figure 2.1 over long distances. Since variations due to path loss combined with shadowing occur over relatively large distances $(100 - 1000m)$, these variations are sometimes refereed to as large-scale fading. Contrarily, small-scale fadings occur over distances the order of λ 2. We call this short movement as coherence length [21, 18]. Since these variations over path loss occur every short distances, these variations are also referred to as fast fading.

In the frequency domain the power spectral density of the transmitted signal may or may not be affected according if the channel is [18]:

- **Flat fading**: when $\tau_s << B_u^{-1}$ where τ_s is the root mean square (RMS) delay spread of

the channel and B_u is the bandwidth of the transmitted signal. Another way to ensure flat fading is when $B_c >> B_u$ where $B_c = \tau_s^{-1}$ is the channel coherence bandwidth and B_u is the bandwidth of the transmitted signal. Flat fading channels are common in narrowband systems.

- **Frequency selective**: it is the opposite to flat fading. Thus a channel is frequency selective when $\tau_s >> B_u^{-1}$ or when $B_c << B_u$. Frequency selective channels are common in wide-band systems, i.e. at 2 4 GHz, where the channel bandwidth is much larger than the coherence bandwidth.

4.3.3 Multipath

Fast fading is a common characteristic in any wireless communication in that that the transmitted signal impinge the receiver with other m replicas (m extends from 0 to) due to surface reflection. Each of these replicas impinge the receiver through different paths or angles γ and different path lengths L_m with a delay of τ_s. The maximum τ_s is referred to as the channel delay spread as commented above. All the received signals from paths other than the direct path become attenuated experimenting a phase shift of $\pm\theta_n$ radiants in each reflection. This phase shift is Gaussian distributed from $[-\pi \ \pi]$ [18]. If the m received interference signals are in-phase the result is the sum of these m signal replicas causing an large increase in the received power (a.k.a constructive interference); if they are out-of phase they cancel each other causing hence deep fade (a.k.a destructive interference). These kind of interferences occur over short distances the order of λ 2 aforementioned. A model for the received signal in a multi-path wireless channel is defined by (4.4) [18, 20]:

$$r(t \ \tau) = \mathbb{R}\left\{ s(t)e^{j(2\pi f_c t+\phi)} \left(\sum_{n=1}^{M} \alpha_n(t) e^{-j\theta_n} \delta(\tau - \tau_n(t)) \right) \right\} \tag{4.4}$$

being $s(t)$ the transmitted signal at the center frequency f_c with an arbitrary phase γ, α_n is the attenuation coefficient associated to the n signal replica, θ_n is the phase shift of the n signal replica and $\delta(t - \tau_n)$ is the Dirac delta delayed τ_n. If TX and RX are fixed in a certain position and the surrounding environment is not highly dynamic we can approximated (4.4) by (4.5).

$$r(\tau) = \mathbb{R}\left\{ se^{j(2\pi f_c+\phi)} \left(\sum_{n=1}^{M} \alpha_n e^{-j\theta_n} \delta(\tau - \tau_n) \right) \right\} \tag{4.5}$$

A way to to take advantage of multi-path is the use of spatial diversity with several antennas separated λ 2 [22]. Nevertheless such approach is not used in low-power wireless communications

due to physical constraints: at the 433 band, $\lambda\ 2 = 35cm$ is much bigger than the dimensions of the electronic devices.

The FSPL is a standard model but not generic. A more generic propagation model known as log-normal propagation model takes into account whether the free space propagation is satisfied or not. Additionally, it takes into account that the propagation characteristics are dependent on either the environment and the height of the node with respect to ground. The log-normal propagation model is given in Equation 4.6 [13, 17, 18, 24]:

$$\begin{aligned} RSS(d\ h) = RSS(d_0\ h) - 10\gamma(h)log_{10}(d\ d_0) + \\ +\ _{shad};\ d \geq d_0 \\ RSS(d_0\ h) = P_t + G_{TX} + G_{RX} - A - L_g(h) \end{aligned} \tag{4.6}$$

where $P_t(dBm)$ is the transmitted power, G_{TX} and G_{RX} in dBi are the transmitter and receiver antenna gains, and A is a constant called intercept factor, expressed in dB, which depends on the receiver antenna effective area (and hence the wavelength) as well as the average channel attenuation at a given initial distance d_0, as shown in Equation 2.13 [18]. $L_g^{dB}(h)$ models the diffraction losses, i.e. the power losses attributed to the first Fresnel zone obstruction. As stated in 2.3.3, the Fresnel zone is a concept related to the diffraction of waves that determines the region of the space that defines the condition of visibility between the transmitter and receiver antennas. In LOS conditions, the first Fresnel zone is free and thus the received power is proportional to the propagation losses in free space. In NLOS conditions, the first Fresnel zone is obstructed by an obstacle that causes diffraction.

All the parameters presented above are combined by $RSS(d_0\ h)$ at $d = d_0$. γ is known as path loss exponent which represents the falloff of the received power with the distance, i.e. the slope. The path loss exponent is frequency independent and environment specific. For environments close to free space $\gamma = 2$, which in turn transforms Equation 2.12 to the free space propagation model [18]. For more complex environments such as near ground, it is best to estimate γ together with $RSS(d_0\ h)$ to minimize the mean square error between the model and the empirical measurements. In such environments the value of γ is typically between 2 and 4, or more, depending on whether the path is LoS or NLoS [17, 13]. Finally, $_{shad}(dB) \sim N(0\ \sigma_{shad})$ is a zero mean log-normally distributed random variable with standard deviation $\sigma_{shad}(dB)$ which models the received power variations around the propagation model caused by multipath propagation [16], either shadowing or fading. Most empirical studies show standard deviations between 0 $4dB$ and $4dB$ [17, 19].

$$A = 20log_{10}(\frac{4\pi d_0}{\lambda}) \tag{4.7}$$

As the carried experiments are obtained with the antenna at different heights from ground as well as in different environments, we use the model presented in Equation 4.6 because it accurately describes the $RSS(d\ h)$ behavior with the antenna height and the environment.

4.4 Experimental setup

Given the theoretical propagation models described in Section 4.3, our experiments aim to evaluate the propagation aspects of the 433 MHz band and compare it to the 2.4 GHz band in different environments, e.g. indoor and outdoor. In order to conduct these experiments we use COTS (Custom Off The Shelf) devices, namely COU24-A2 and OpenMote-433 motes. For that reason in the current section we present a detailed description of the devices and the configuration parameters (e.g. transmit power, receiver sensitivity, signal modulation, data rate, etc.) that have been used to conduct the different experiments. Finally, as we use COTS devices, we also present the procedure that we have used to calibrate the motes and ensure they operate under the configured parameters.

4.4.1 Equipment

The set of experiments at the 2.4 GHz band are conducted using two COU24-A2 motes, as depicted in Figure 4.3. The COU24-A2 motes are equipped with an Atmel 8-bit ATmega-1281 microcontroller and an Atmel AT86RF230 transceiver. The microcontroller operates at 4 MHz and features 8 Kbytes RAM, 128 Kbytes of Flash and 4 Kbytes EEPROM memory respectively. The transceiver is fully compliant with IEEE 802.15.4-2006 standard, e.g. 250 kbps with OQPSK modulation and DSSS, and is connected to an onboard 0 dBi chip antenna.

To conduct the experiments at the 433 MHz band we use two OpenMote-433, as depicted in Figure 4.4. OpenMote-433 boards feature a 32-bit ARM Cortex-M3 STM32F103 microcontroller from ST Microelectronics and a Texas Instruments CC1101 transceiver. The microcontroller operates at 72 MHz with 20 kBytes of RAM and 128 kBytes of Flash memory respectively. The transceiver operates at the Sub-1 GHz band with full support for both DASH7 Mode 2 and IEEE 802.15.4f standards, e.g. FSK/GFSK/MSK modulations with bit-rates up to 250 kbps, and is connected to a 0 dBi λ 2 helix antenna using a SMA connector.

4.4.2 Configuration Parameters

The configuration parameters of both devices used in the experimental measurements campaign are presented in Table 4.1. The chosen data rate and modulation scheme for the OpenMote-433 are in accordance with DASH7 Mode 2 Normal channel type, as presented in Section 4.2.2. In

Figure 4.3: A CC1124-A2 development board featuring an Atmel ATmega-1284 microcontroller and an Atmel AT86RF20 transceiver.

Figure 4.4: An OpenMote-433 development board featuring a ST Microelectronics STM32F103 microcontroller and a Texas Instruments CC1101 transceiver.

both cases the transmit power is configured to be the same, e.g. 0 dBm, for comparison purposes.

Two metrics have been used throughout the measurement campaign to evaluate the propagation aspects of the 433 MHz and the 2.4 GHz bands, the RSS (Received Signal Strength) and the PDR (Packet Delivery Ratio). The RSS measures the received power level at the input of the signal demodulator given the receiver filter bandwidth and Low Noise Amplifier (LNA) gain. On its behalf, the PDR indicates the percentage of packets that have been successfully received at the receiver normalized to one.

	COU24-A2	**OpenMote-433**
Standard	IEEE 802.15.4	DASH7 Mode 2
Modulation	OQPSK	GFSK
Data rate (kbps)	250	200
Transmit power (dBm)	0	0
Channel number (MHz)	18 (2450)	7 (433.92)
Channel bandwidth	5 MHz	432 kHz
Antenna type	0 dBi λ 2 chip	0 dBi λ 2 helix
RSSI resolution (dB)	3	0.5

Table 4.1: Configuration parameters for COU24-A2 and OpenMote-433 motes.

4.4.3 Calibration

Prior to start the measurements campaign we have conducted a set of preliminary measurements to calibrate the transmitter and receiver used during the experiments campaign at the 433 MHz and 2.4 GHz bands to ensure that they operate under the configuration parameters, e.g. transmit power, modulation scheme and channel bandwidth, presented in Table 4.1.

At the 433 MHz band we have connected the OpenMote-433 board to a Rigol DSA-815 spectrum analyzer. The peak output power, measured at the output of the SMA connector, is about -3 dBm and the overall power in the given bandwidth, i.e. 432 kHz for a DASH7 Mode 2 Hi-Rate channel, is 0 dBm. In addition, we have also calibrated the receiver node. In particular, we have measured the linearity of the RSS according to a known transmit power, e.g. $P_t = 0\ dBm$, and channel attenuation using a JWF 50PA-51 programmable attenuator. The obtained results are in accordance with the configured parameters in Table 4.1 and, thus, the transmitter node configuration is validated. Despite, the results are not shown due to lack of space.

At the 2.4 GHz band an extensive calibration of the COU24-A2 has not been possible because the motes use an integrated chip antenna and, thus, it is not possible to connect them to any measurement equipment. Therefore to ensure that node operation is consistent with configured parameters we have compared the RSS at a distance of 1 m in outdoor with other available motes. In all the devices the measured signal is quasi identical regardless of the selected. Hence we consider that the COU24-A2 motes used for the experimentation campaign are calibrated.

Finally, we have also conducted measurements to determine the sensitivity of the DASH7 Mode 2 and IEEE 802.15.4f standards at 433 MHz using the OpenMote-433 motes and the IEEE 802.15.4 standard at 2.4 GHz using the COU24-A2 motes. The measurements have been

conducted sending 1024 packets with a 23 byte payload for each channel type. Notice that the sensitivity parameter is defined as the RSS value such that the $PDR >= 90\%$. The results of the measurements are depicted in Figure 4.5 and summarized in Table 4.2.

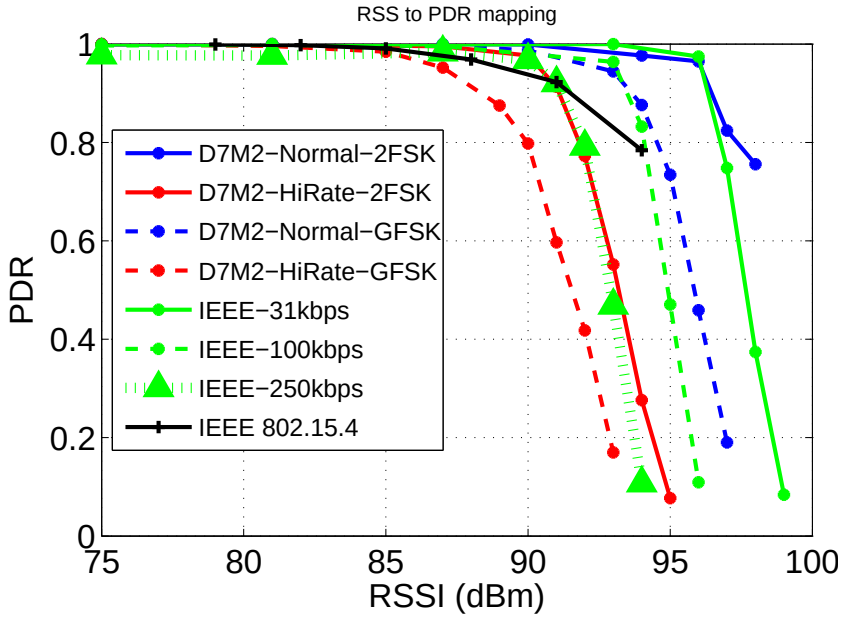

Figure 4.5: RSS to PDR mapping for both COU24-A2 and OpenMote-433 motes. For the IEEE 802.15.4 standard operating at 2.4 GHz the COU24-A2 achieves a sensitivity of -91 dBm. On its behalf, using DASH7 Mode 2 Hi-Rate channel type at 433 MHz with a GFSK modulation the OpenMote-433 achieves a sensitivity of -88 dBm.

Standard	Channel type	Modulation	Sensitivity
DASH7 Mode 2	Normal	2FSK	-97 dBm
DASH7 Mode 2	Normal	GFSK	-94 dBm
DASH7 Mode 2	Hi-Rate	2FSK	-91 dBm
DASH7 Mode 2	Hi-Rate	GFSK	-88 dBm
IEEE 802.15.4f	31 kbps	MSK	-96 dBm
IEEE 802.15.4f	100 kbps	MSK	-93 dBm
IEEE 802.15.4f	250 kbps	MSK	-91 dBm
IEEE 802.15.4	250 kbps	OQPSK	-91 dBm

Table 4.2: Sensitivity summary for the DASH7 Mode 2 and IEEE 802.15.4f channel types at 433 MHz using OpenMote-433 and for the IEEE 802.15.4 standard at 2.4 GHz using COU24-A2. These figures combined with the propagation models presented in Section 4.5 enable to estimate the effective communication range for each standard and channel type.

4.5 Experiments and results

In this section we first experimentally evaluate the diffraction phenomenon for 433 MHz and 2.4 GHz, i.e. from which height the Fresnel zone is not obstructed by the effect of being close to the ground. With the knowledge of the height such that the first Fresnel zone is free, we then experimentally validate the large scale propagation for both bands. Additionally, we validate the dependence of height to the propagation characteristics, ($RSS(d0\ h)\ \gamma(h)$) according to the propagation model described in Equation 4.6, since the closer to the ground, the more obstructed the Fresnel zone is and, hence, the higher the power losses are. Finally, we also validate the small scale propagation effects (known as multipath) for the 433 MHz band and compare it with the results at the 2.4 GHz band obtained in [21]. The goal is to validate if channel hopping can combat multipath at the 433 MHz band since the band is flat fading, i.e. the coherence bandwidth of the wireless channel is higher than the bandwidth of the transmitted signal. It is important to mention that in all the experiments the antennas were positioned to ensure proper polarization and the locations were carefully measured to ensure repeatability.

Concerning the large scale propagation effects they have been carried out in two different environments: outdoor and indoor (in a 4 mx80 m corridor), both without obstructions in the path.

4.5.1 Diffraction modeling

First we focus in obtaining and evaluating the diffraction models for the 433 MHz and 2.4 GHz bands. The diffraction models are useful to analyze the power losses attributed to the penetration of a certain obstacle inside the first Fresnel zone [18]. In our case we analyze the power losses attributed to the penetration by ground, modeled by the parameter $L_g(dB)$. As we are interested in finding the variation of the RSS with the height with respect from ground, we fix the distance between the transmitter and the receiver, for instance $d0 = 5$ m, and we vary the height of nodes. For this scenario the model in Equation 4.6 simplifies to Equation 4.8 taking into account that $\overline{_{shad}} = 0$ dB and $h0 = h_{free}$.

$$\overline{RSS(d0\ h)} = \overline{RSS(d0\ h0)} - Lg(h);\ h \leq h0 \tag{4.8}$$

The corresponding diffraction models for the 433 MHz and 2.4 GHz bands are depicted in Figure 4.6 for two environments, outdoor and indoor. In general terms it is possible to see that the 433 MHz band is less affected by diffraction losses when compared to the 2.4 GHz band in both environments. The diffraction results are combined with the effects of multi-path propagation and the 9-16 dB deltas are expected from the Friis equation dependence on the wavelength. Despite, it is possible to observe that the first Fresnel zone becomes free after a

height of $h = 2\ 1$ m for 433 MHz and a height of $h = 36$ cm for 2.4 GHz. Hence, the rule of thumb $h_{free} = 3\lambda$ to ensure a free first Fresnel zone is satisfied for both bands. In addition, it is possible to see that in the outdoor environment the magnitude of this interference is lower than in indoor.

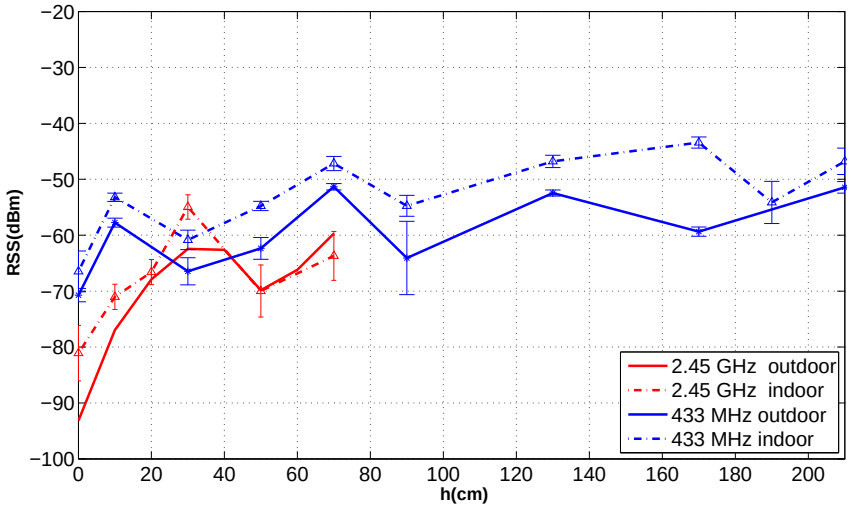

Figure 4.6: Diffraction modeling for the 433 MHz and 2.4 GHz bands in indoor and outdoor environments. The error bars represent the temporal RSS variation attributed to diffraction and multipath, i.e. reflections from ground and other surrounding objects. Also, the rule of thumb $h_{free} = 3\lambda$ to ensure a free first Fresnel zone is satisfied for both bands.

4.5.2 Large-scale propagation

This section deals with the empirical evaluation of the large scale propagation characteristics of the 433 MHz and 2.4 GHz bands in outdoor and indoor environments. For each measurement the transmitter sends 1024 packets of 33 bytes (including a preamble of 4 bytes, a synchronization word of 4 bytes, 23 bytes of data and a 2-byte CRC) to the receiver at the configured channel, while the receiver is continuously listening for incoming packets.

4.5.2.1 Outdoor

This section is devoted to analyze the propagation effects and compare the wireless range between the 433 MHz and the 2.4 GHz bands in an outdoor environment. This environment is depicted in Figure 4.7 and is found at the GPS coordinates (+41°31 39 27 ; +2°26 7 92). The ground is asphalt and the environment did not have obstructions in the path. The measurements were taken along the yellow line.

The methodology to conduct the measurements is the following: RSS measurements are taken

Figure 4.7: Outdoor propagation environment. The measurements were taken along the yellow line and the columns are not obstructions.

for each received packet at the following distances, where the notation (yy:xx:pp) means from yy meters to pp meters every xx meters.

- For heights from $h = 2$ 10 m to $h = 70$ cm: [1 m, 5 m:5 m:70 m, 80 m:10 m:120 m].
- For heights from $h = 0$ cm to $h = 70$ cm: [1 m:1 m:10 m, 15 m:5 m:70 m, 80 m:10 m:120 m].

The results of the RSS over distance for the 433 MHz and 2.4 GHz bands are depicted in Figure 4.8. As expected the RSS falls off linearly with $log10(d\ d0)$ and γ increases when the height with respect to ground decreases due to the Fresnel zone obstruction caused by ground. The $RSS(d0\ h0)$ of the propagation model at 433 MHz is 10 dB higher than $RSS(d0\ h0)$ of the 2.4 GHz propagation model. Also, for $h = 0$ and $log10(d\ d0) = 0$, the RSS for 433 MHz is 28 dB higher than 2.4 GHz. This is traduced to a higher wireless range at 433 MHz. To find the wireless range in meters using the propagation models the following procedure is used. First, according to Table 4.2, the PDR is $> 90\%$ when $RSS > -91$ dBm for 2.4 GHz and when $RSS > -88$ dBm for 433 MHz. Then, for a height of $h = 10$ cm, the maximum range at 2.4 GHz such that the $RSS > -91$ dBm is $log10(d\ d0) = 0\ 8 \quad d = 8$ m, and the maximum range at 433 MHz such that the $RSS > -88$ dBm is $log10(d\ d0) = 1\ 65 \quad d = 45$ m. Similarly, for a height of $h = 70$ cm at 2.4 GHz and a height of $h = 2$ 10 m at 433 MHz the maximum range is 70 m and 160 m respectively.

The corresponding values for $RSS(d0\ h)$, $\gamma(h)$ and σ_{shad} for all the propagation models are presented in Table 4.3 and Table 4.4 respectively. Additionally we include the coefficient of determination R^2 which is a statistical measure of how well the regression line approximates to the measurements. An R^2 of 1 0 indicates that the regression line perfectly fits the data. As observed,

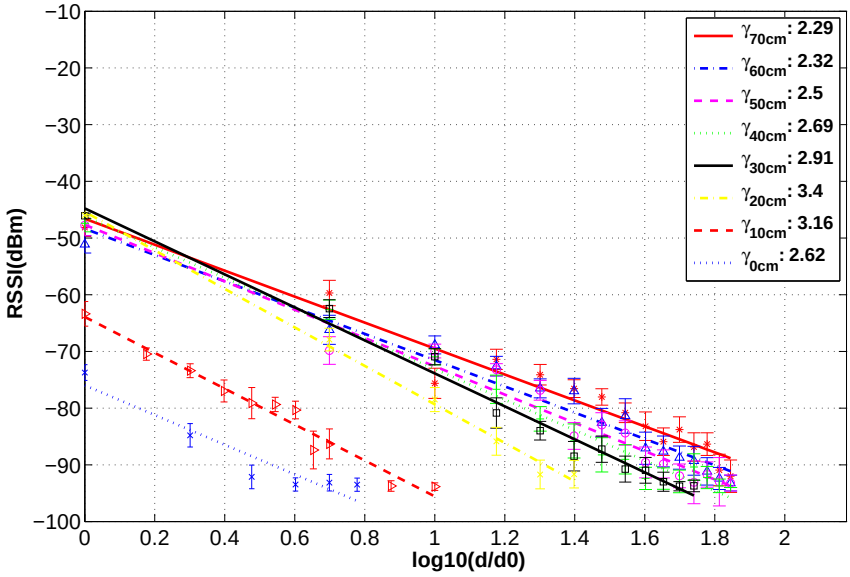

(a)

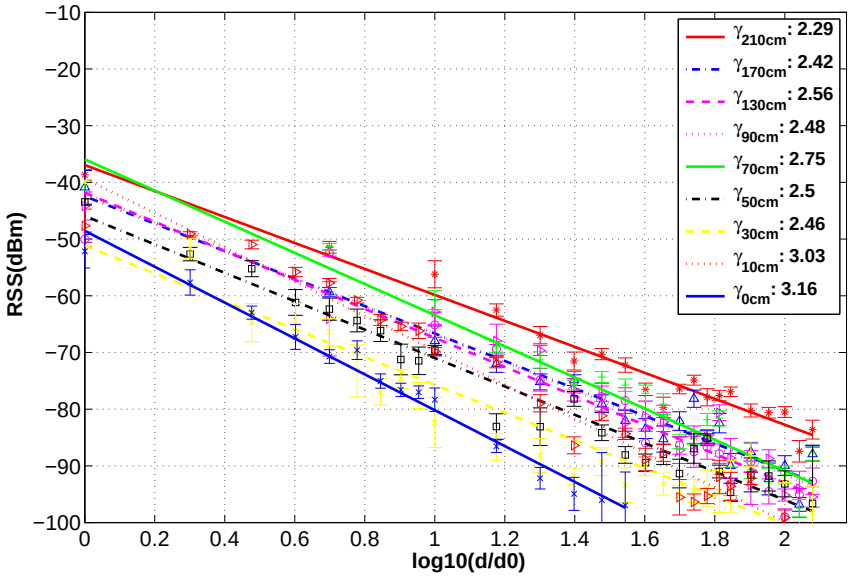

(b)

Figure 4.8: Propagation models for 2.4 GHz and 433 MHz in an outdoor environment.

the path loss exponents are more or less similar. However, a significant difference is shown by $RSS(d0\ h)$. This effect is because, according to Equation 4.6, $RSS(d0\ h)$ is proportional to the intercept factor which is inversely proportional to λ (Equation 2.13) and, thus, the lower the λ the higher the received power. Moreover as A is related to the effective area of the receiver antenna, the larger it is the more energy it can pick up. An average gain of 11.6 dB is given by the 433 MHz band which is close to the theoretical value of 14 87 dB obtained from the difference of Equation 2.13 between both frequency bands.

Concerning the shadowing, the respective statistical distributions are shown in Figure 4.9 and Figure 4.10 for both bands. We only show the shadowing distribution for near ground and away from ground heights, due to space constraints. As illustrated, the distribution of the shadowing follows approximately a Gaussian distribution.

$h(m)$	0.7	0.6	0.5	0.4	0.3	0.2	0.1	0
$RSS(d0\ h)$(dBm)	-46.6	-48.36	-47.67	-46.26	-44.77	-45.39	-63.92	-75.97
γ	2.29	2.32	2.5	2.69	2.91	3.4	3.16	2.62
$\sigma_{shad}(dB)$	2.58	2.21	2.37	1.95	1.82	1.34	1.64	2.52
R^2	0.95	0.97	0.97	0.98	0.98	0.99	0.97	0.9

Table 4.3: Propagation model characteristics for 2.4 GHz in an outdoor environment.

$h(m)$	2.1	1.7	1.3	0.9	0.7	0.5	0.3	0.1	0
$RSS(d0\ h)$(dBm)	-36.94	-42.45	-41.83	-42.02	-35.95	-45.93	-51.15	-39.35	-48.55
γ	2.29	2.42	2.56	2.48	2.75	2.5	2.46	3.03	3.16
$\sigma_{shad}(dB)$	2.18	2.82	3.54	3.03	3.4	2.93	4.85	3.27	1.80
R^2	0.97	0.95	0.93	0.95	0.94	0.96	0.9	0.97	0.98

Table 4.4: Propagation model characteristics for 433 MHz in an outdoor environment.

4.5.2.2 Indoor

The large-scale propagation measurements in an indoor environment were taken in a 80 m corridor at the same measurement distances of outdoor measurements. An illustration of the indoor scenario, including a brief description of the environment, is shown in Figure 4.11.

The corresponding propagation models for this environment are depicted in Figure 4.12. The waveguide effects can be observed at the 2.4 GHz band since the path loss exponent γ is smaller than 2. In fact 1 2 $< \gamma <$ 2 [59, 40]), that is, the actual path loss exponent is lower than the free space path loss exponent. However the waveguide effects cannot be appreciated in the 433 MHz

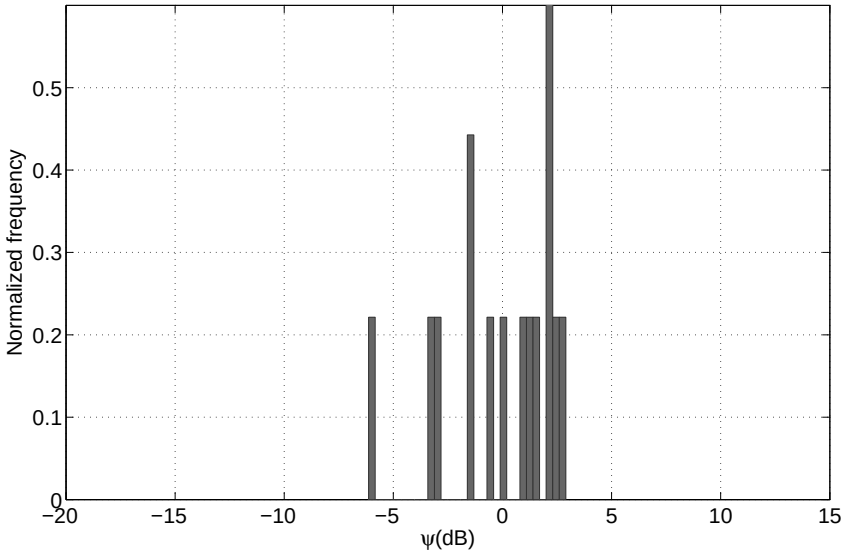

(a)

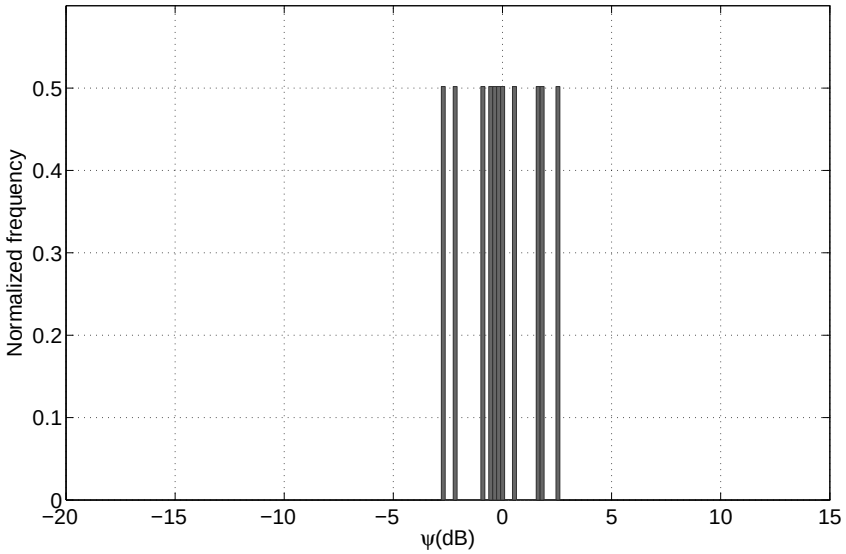

(b)

Figure 4.9: Shadowing distribution for 2.4 GHz in outdoor environment, 4.9a: $h = 0\ 7$ m with σ_{shad} :2.58 dB, 4.9b: $h = 0\ 1$ m with σ_{shad} : 1 64 dB.

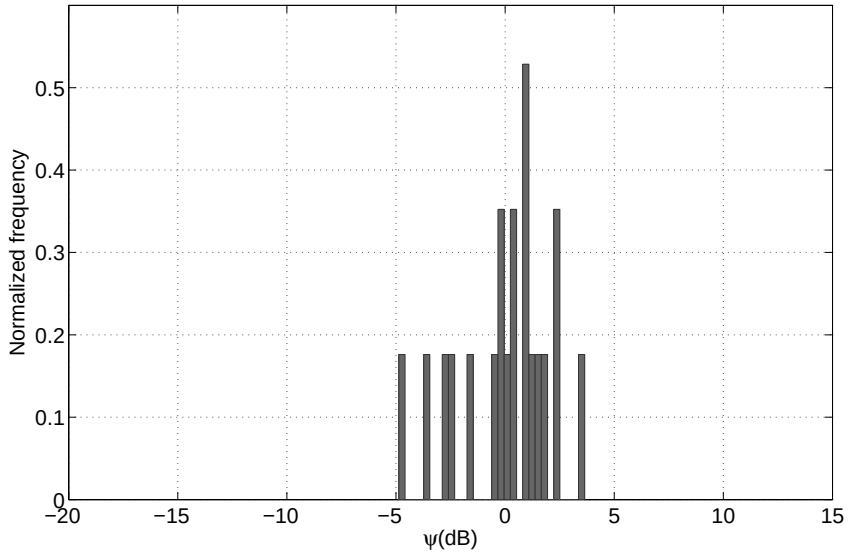

(a)

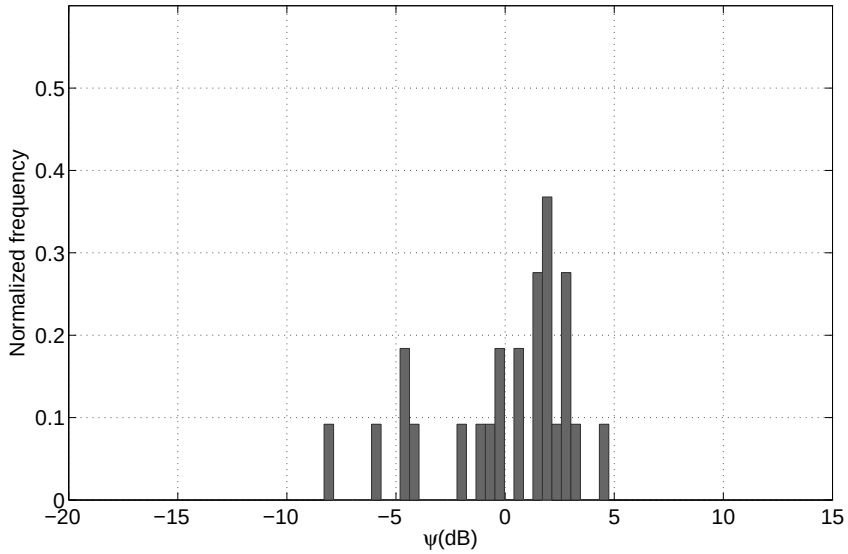

(b)

Figure 4.10: Shadowing distribution for 433 MHz in outdoor environment, 4.10a: $h = 2\ 10$ m with $\sigma_{shad} : 2\ 18$ dB, 4.10b: $h = 0\ 1m$ with $\sigma_{shad} : 3\ 27$ dB.

Figure 4.11: Indoor propagation environment. The outer of the building and the floor partitions are made by reinforced concrete, whereas the wall partitions are made by plaster and the floor is made of stoneware. Finally, it is important to mention that there are metal structure in the ceilings used to conduct the electricity and communications wiring.

band due to two reasons. First, the reflection of an electromagnetic wave in an obstacle only occurs when the size of the obstacle is large compared to the wavelength [60]. Thus, as the wavelength at 433 MHz is around 69 cm the waves are not reflected but propagate along the objects. Second, the size of a waveguide depends on the wavelength of the electromagnetic wave [61]. Hence, the required dimension of the corridor to act as a waveguide is larger at the 433 MHz band.

The results for $RSS(d0\ h)$, $\gamma(h)$, σ_{shad} and R^2 for this environment are depicted in Table 4.5 and Table 4.6. Again, a significant difference can be observed for the values of $RSS(d0\ h)$ between both bands. The average gain at the distance $d0$ is 14.4 dB which matches with the value obtained using Equation 4.7. The corresponding distributions of the shadowing for the 2.4 GHz and 433 MHz bands are illustrated in Figure 4.13 and Figure 4.14. Again, most of the distributions demonstrates that the shadowing approximates to a Gaussian distribution, which in turns validates the theory presented in Section 4.3. Therefore, the 433 MHz band provides an increase of the received power with respect to 2.4 GHz by around 14 dB which approximately means doubling the wireless range, despite of the waveguide effects not being contemplated.

4.5.3 Small-scale propagation

This subsection analyzes the effects of multipath propagation at the 433 MHz band and evaluates if multipath can be combated using channel hopping, as presented in [21] for the 2.4 GHz band. In their experiments the receiver is fixed at a certain location and the transmitter is displaced

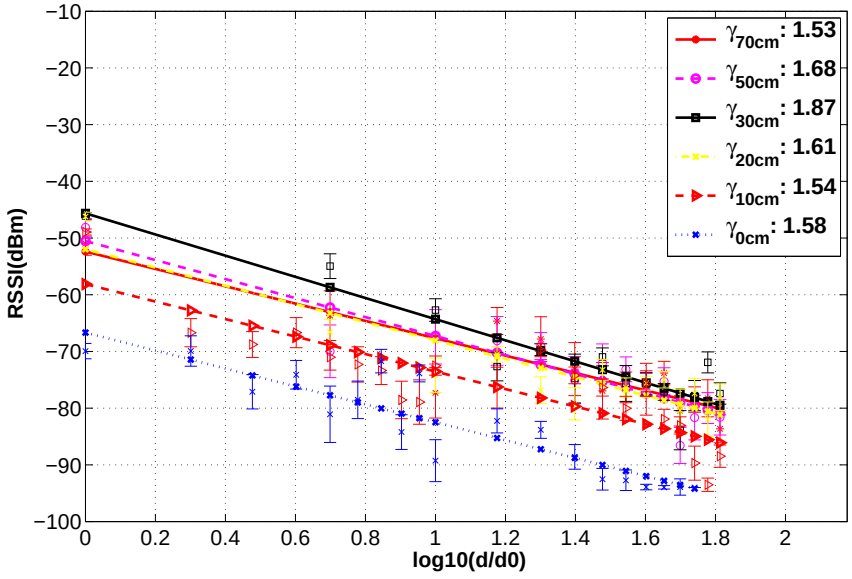

(a)

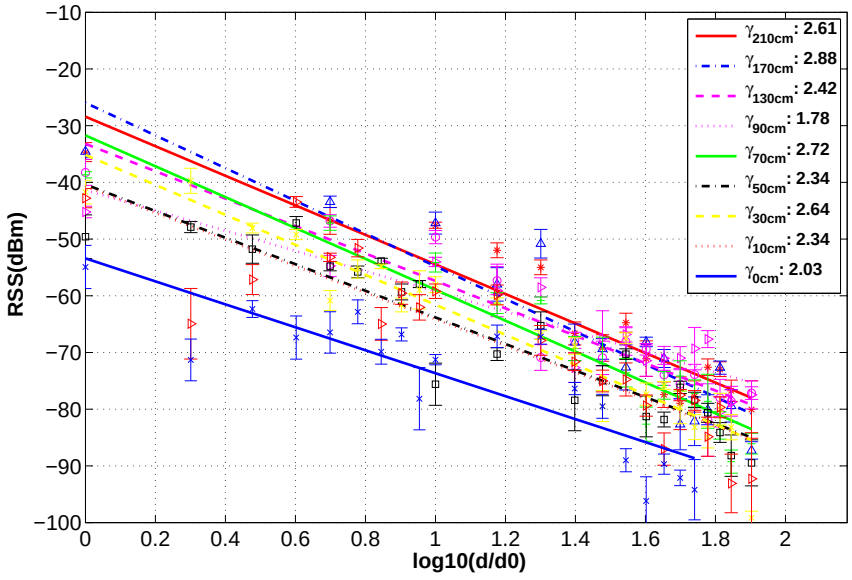

(b)

Figure 4.12: Propagation models for 2.4 GHz and 433 MHz in and indoor environment.

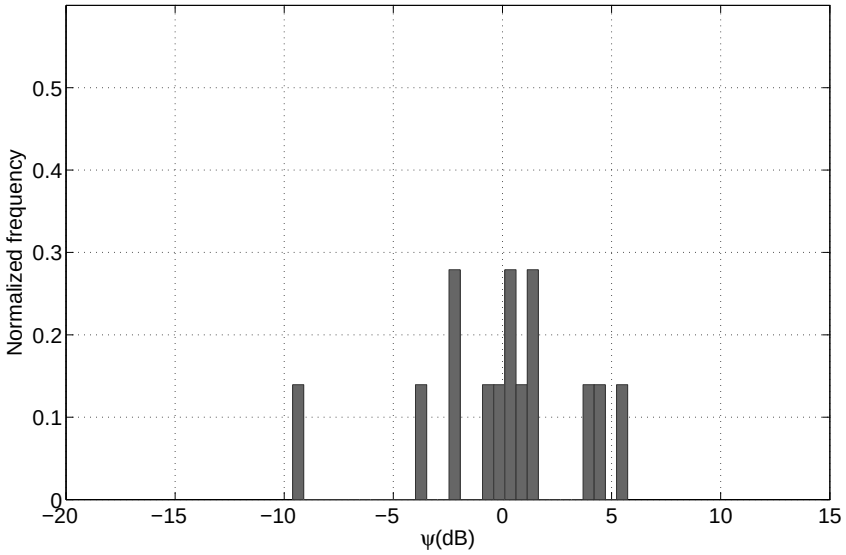

(a)

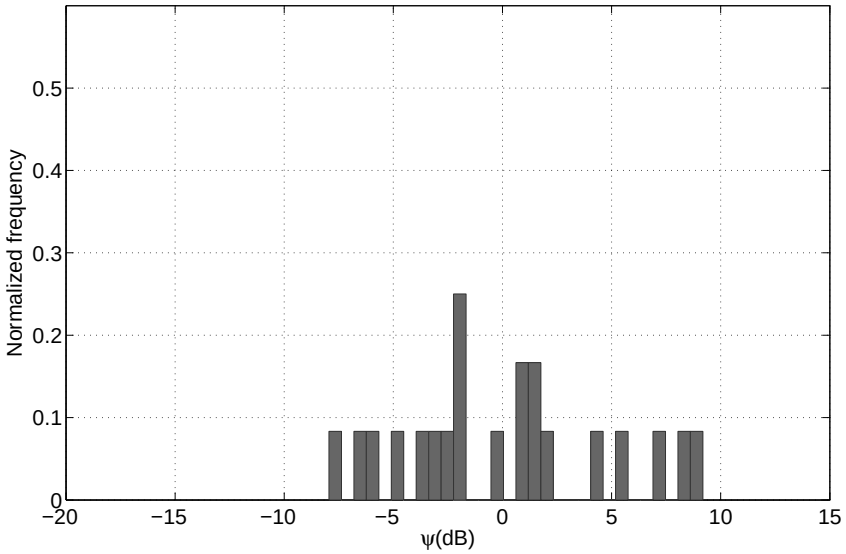

(b)

Figure 4.13: Shadowing distribution for 2.4 GHz in indoor environment, 4.13a: $h = 0\ 7$ m with σ_{shad} :3.78 dB, 4.13b: $h = 0\ 1$ m with σ_{shad} : 4 89 dB.

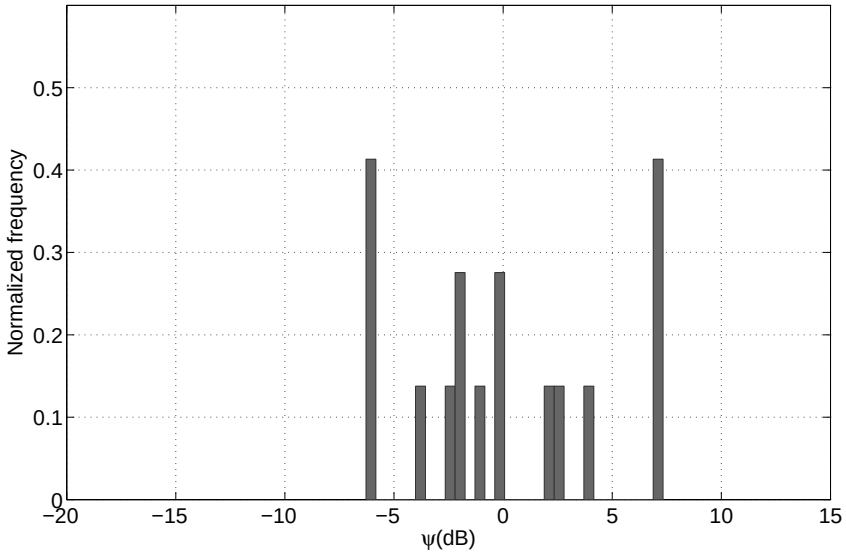

(a)

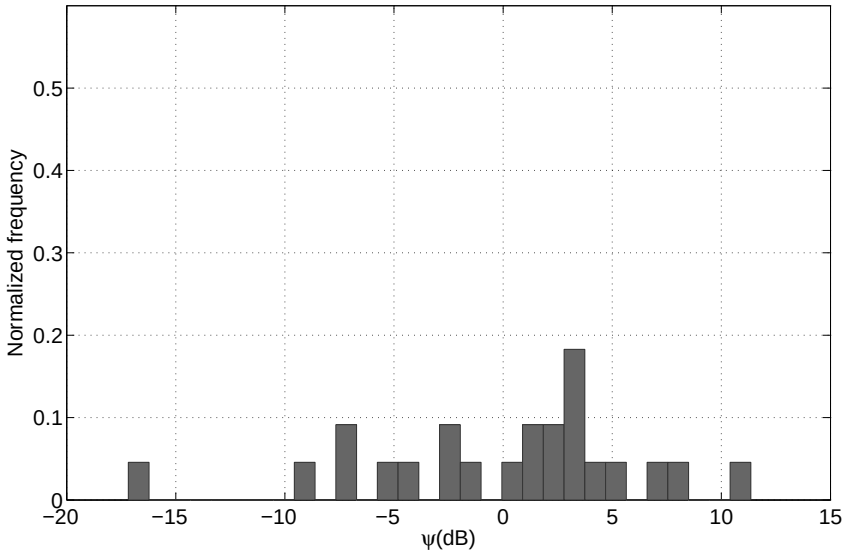

(b)

Figure 4.14: Shadowing distribution for 433 MHz in indoor environment, 4.14a: $h = 2\ 10$ m with $\sigma_{shad} : 4\ 64$ dB, 4.14b: $h = 0\ 1$ m with $\sigma_{shad} : 6\ 37$ dB.

$h(m)$	0.7	0.5	0.3	0.2	0.1	0
$RSS(d0\ h)$(dBm)	-52.39	-50.53	-45.64	-51.98	-58.12	-66.68
γ	1.53	1.68	1.87	1.61	1.54	1.58
$\sigma_{shad}(dB)$	3.78	3.69	3.44	3.55	4.89	3.80
R^2	0.81	0.84	0.88	0.84	0.74	0.82

Table 4.5: Propagation model characteristics for 2.4 GHz in an indoor environment.

$h(m)$	2.1	1.7	1.3	0.9	0.7	0.5	0.3	0.1	0
$RSS(d0\ h)$(dBm)	-28.42	-25.96	-33.21	-41.4	-31.72	-40.37	-35.15	-40.7	-53.41
γ	2.61	2.88	2.42	1.78	2.72	2.34	2.64	2.34	2.03
$\sigma_{shad}(dB)$	4.64	5.83	3.77	4.06	4.23	5	4.78	6.38	6.37
R^2	0.89	0.86	0.91	0.83	0.91	0.87	0.90	0.80	0.72

Table 4.6: Propagation model characteristics for 433 MHz in an indoor environment.

every 1 cm on a 20 cm x 35 cm area, corresponding to λ 12 24. According to the results, multipath propagation at 2.4 GHz can be combated with channel hopping, since the channel is frequency selective, or with antenna diversity.

In our case, the methodology to conduct the experiments is similar but with a displacement of 5.66 cm corresponding to the same order of magnitude of λ for the 433 MHz band. The receiver is fixed and the transmitter is placed at the appropriate location in a 113.2 cm x 198 cm square. For each position 1024 packets with the same structure of the large scale propagation measurements are transmitted over the first channel with an inter-packet delay of 3 ms. Upon finishing a channel the transmitter waits for 10 ms and changes to the following channel and the process is repeated until all channels are completed. Once all the channels are completed the process is repeated for all the remaining positions in the square. Using such setup, two different experiments have been conducted to evaluate the suitability of channel hopping at the 433 MHz band, one in Line-of-Sight (LoS) conditions and the other in Non-Line-of-Sight (NLoS) conditions. Both experiments have been conducted in a domestic environment with concrete floor and plaster walls and ceilings, as depicted in Figure 4.15.

4.5.3.1 Line of Sight (LoS)

In this experiment the transmitter and the receiver are located in the same room at a distance of 5 meters and with clear line of sight as illustrated in Figure 4.15. The results in terms of RSS depending on node position and channel are shown in Figure 4.16. The results from channels 1,

7 and 14 are presented.

Figure 4.15: Indoor domestic environment. The transmitter and the receiver are in Line-of-Sight.

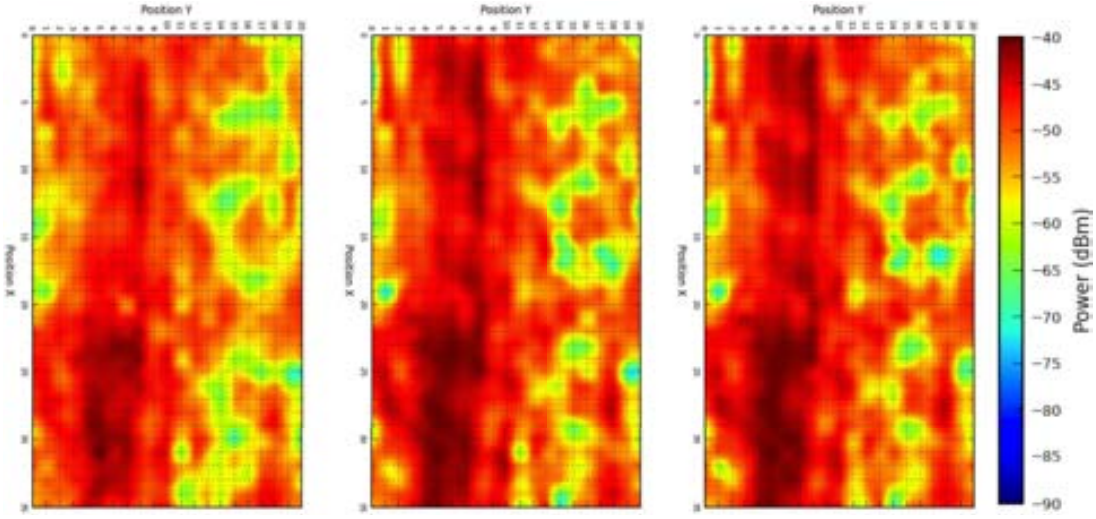

Figure 4.16: RSS for LOS conditions. From left to right: channels 1, 7 and 14 respectively.

In LoS conditions the PER (not shown) is always the minimum because the received signal is well-above the receiver sensitivity. As observed in Figure 4.16, there are fadings with a magnitude of 20-25 dB approximately in some positions. These fadings are caused by multipath propagation. Moreover, it is possible to see that the magnitude of the RSS is more or less constant within the different channels regardless of node position. This is because the wireless channel is flat fading (the channels are narrowband). Flat fading channels occur when the channel delay spread (the order of τ_s =10 ns, 100 ns for indoor environments) is much lower than the time delay of the

transmitted signal or the channel coherence bandwidth B_{wc} is larger than the bandwidth of the transmitted signal B_s. Mathematically this is expressed as $B_s^{-1} = 1/108KHz = 9.26\mu s >> \tau_s$. In comparison to the results presented in [21], at the 2.4 GHz band the wireless channel is frequency selective ($B_{wc} << B_s$ or $\tau_s >> B_s^{-1}$) and hence the magnitude of the wireless channel is different for each single channel (5 MHz of bandwidth) and, thus, channel hopping can combat multipath. However in our case, the wireless channel is not frequency selective but flat fading ($B_{wc} >> B_s$ or $\tau_s << B_s^{-1}$) and the magnitude of the wireless channel is almost the same for each single channel. Thus, channel hopping cannot combat multipath.

4.5.3.2 Non Line of Sight (NLoS)

In this second experiment the transmitter is located in the same place as in the previous experiment and the receiver is located at the furthest room of the building, where NLoS conditions exist. The experiments presented above are repeated to verify the effects of multipath propagation in NLoS conditions.

The results obtained from this experiment are depicted in Figure 4.17 for channels 1, 7, and 14. Contrarily to the previous results, PER in NLoS conditions fact showed greatly varies from one hundred percent to zero percent depending on the transmitter position due to the effects of fadings, which are caused by multipath propagation. The magnitude of the RSS is more or less constant within the different channel regardless of node position. This is because the wireless channel is flat fading and, thus, in NLoS conditions channel hopping cannot combat the negative effects of multipath either.

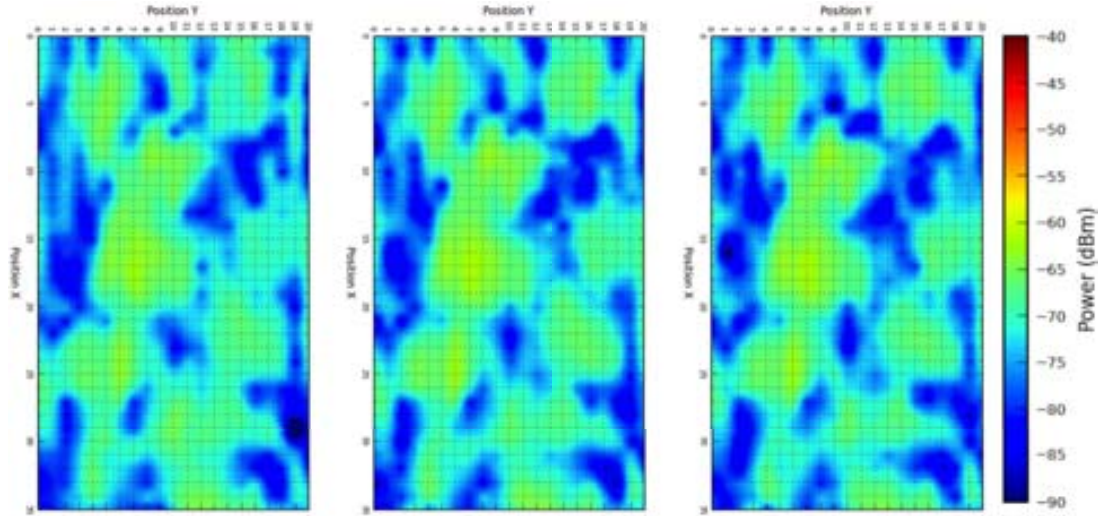

Figure 4.17: RSS for the NLOS conditions. From left to right: channels 1, 7 and 14 respectively.

Finally, if we average the PER for the different positions, over all deep fades in the data set where the PER $\leq 5\%$ we obtain the results shown in Figure 4.18. As it is possible to observe, in

the case of NLoS the transition from a deep fade (PDR $\leq 5\%$) to a *good* position (PDR $\geq 95\%$) the node has to move an average of 30 cm. This is *quasi* the half wavelength λ 2 or the coherence length, and confirms the theory and results given by [21, 18]. Therefore the only way to combat multipath at the 433 MHz band is by means of a spatial displacement of λ 2 to any direction or by means of using antenna diversity.

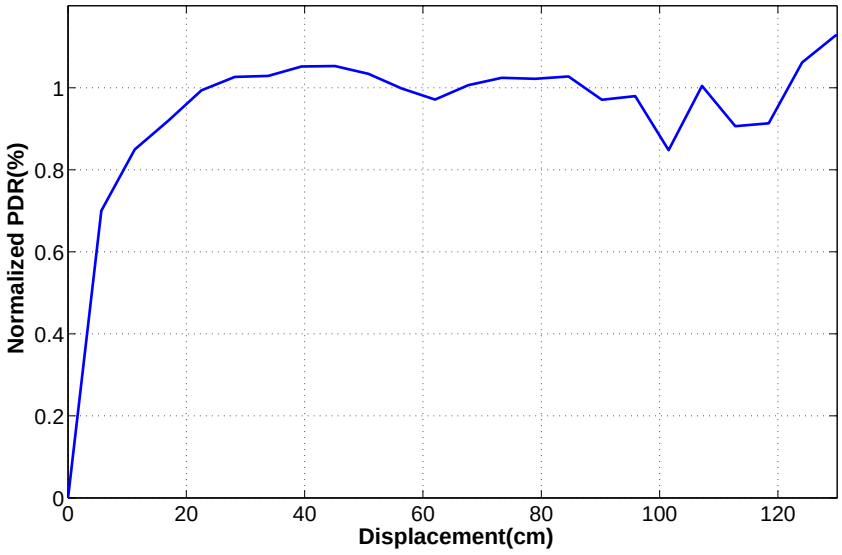

Figure 4.18: Channel coherence length obtained from the averaged PDR for all channels and node displacements.

4.5.4 Discussion

From the diffraction results presented in Section 4.5.1 we confirm that the received power at the 433 MHz is well above 2.4 GHz despite of the larger Fresnel zone. At ground level, the RSS at 433 MHz is 20 dB above the RSS at 2.4 GHz, whereas in LoS the RSS is 10 dB above.

Regarding the propagation results presented in Section 4.5.2, the results confirm that the wireless range is dependent both on the frequency, node height and the environment. The adopted propagation model in Equation 4.6 demonstrates that the path loss exponent γ is height dependent and that $RSS(d_0\ h)$ is frequency band dependent because of the intercept factor. We find the corresponding model parameters ($RSS(d0\ h)$, $\gamma(h)$ and σ_{shad}) by line fitting for the 433 MHz and 2.4 GHz bands. The obtained propagation models depicted in Figure 4.8 and Figure 4.12 are useful to compare the different frequency bands.

In addition, it is important to mention that in indoor environments there is less contribution due to multipath propagation at 433 MHz. The path loss exponent at the 433 MHz band is higher than at 2.4 GHz because the larger wavelength reduces the effects of multipath propagation, e.g.

waveguide phenomenon in corridors. Despite of a higher γ, the 433 MHz band has an advantage of 14 dB at $d = d0$ with respect to the 2.4 GHz band. If we assume that both 2.4 GHz and 433 MHz receivers have the same sensitivity, at the distance where both 433 MHz and 2.4 GHz propagation models crosses, the RSS at the 2.4 GHz band may be below the receiver sensitivity and hence $PDR << 1$, whereas the RSS at the 433 MHz band will be above with $PDR = 1$. Moreover, the propagation model characteristics are height dependent and the shadowing follows a Gaussian distribution.

Finally, from the small-scale results presented in Section 4.5.3 we confirm that, contrarily to the results presented by Watteyne et al. [21] for the 2.4 GHz band, channel hopping does not improve robustness against multipath propagation for the 433 MHz band. The rationale behind that fact is that, as expected, the channel coherence bandwidth, the inverse of the channel delay spread, at the 433 MHz band is larger than the whole bandwidth itself and, thus, all the channels are highly correlated.

4.6 Conclusions

In this Chapter we have developed an empiric propagation model as a tool to evaluate the performance at the PHY layer of the 433 MHz with respect to the 2.4 GHz band. It is worth to note that the use of lower frequency bands may also be able to offer higher wireless range without the need to embed an additional Front End to the original design, and thus lowering total cost and energy consumption of the system.

Given the discussion above this Chapter has presented a short overview of the low-power wireless standards currently being developed at the 433 MHz for M2M communications, namely DASH7 Mode 2 and IEEE 802.15.4f, and extensively evaluated the propagation characteristics of the 433 MHz and the 2.4 GHz bands in both indoor and outdoor environments. The results obtained show that the communication range at 433 MHz is better than at 2.4 GHz despite the effects of having a larger Fresnel zone. The results also demonstrate that, contrarily to the 2.4 GHz band, the use of channel hopping does not combat the effects of multipath propagation because the channel coherence bandwidth is larger than the whole 433 MHz band bandwidth and, thus, all channels are highly correlated.

From the obtained results we conclude that the 433 MHz band has a great potential for M2M communications using low-power wireless technologies such as WSN or RFID. Besides being available world-wide, for a similar environment the better propagation characteristics enable to reduce multi-hop communication requirements, which in turn has a direct impact on the node and network energy consumption and, thus, its overall battery life. Nevertheless, the fact that multipath propagation cannot be combated through channel hopping needs to be taken into

account when designing low-power wireless systems for M2M communications that operate at the 433 MHz band. For example, antenna diversity may need to be considered to improve link robustness against multipath propagation. Similarly, despite the better range it is still advisable to incorporate packet routing mechanisms at the network layer that are capable of sending packets over disjoint paths to circumvent the effects of multipath propagation. In addition, there are other important physical layer aspects that need to be considered to design upper layer protocols, e.g. Media Access Control (MAC) protocols, that operate at the 433 MHz band. For example, better signal propagation also leads to an increased level of interference to/from adjacent wireless systems operating at the same band and, thus, dynamic power allocation mechanisms may be required to improve spatial coexistence and further reduce node and network energy consumption.

Chapter 5

Conclusions and Future Work

5.1 Conclusions

This PhD dissertation focused on wireless communications with power constraints has explored in depth the physical layer phenomenons that occur in wireless links under typical deployments in real environments. This analysis has been carried out from an extensive measurements campaign. Specifically the behavior of the large scale propagation, multipath and diffraction has been analyzed for different environments. Two metrics have been used in order to evaluate the wireless link reliability: the Received Signal Strength, and the Packet Delivery Ratio. Both terms are dependent on the distance as well as the environment. The second term specifies the wireless range that leads to a specified number of successfully received packets i.e. packets that are detected, received and have a correct CRC. The PDR has been demonstrated to be modeled with three regions: connected with PDR above 90%, transition with a PDR between 0 and 90% and disconnected with 0 received packets. The size of these regions is shown experimentally to be dependent mainly on the environment. The environment influences the sizes of the aforementioned regions. For instance the lower the height of the nodes with respect to the ground, the higher the power losses due to the diffraction caused by ground and hence the reduction of the communication distance. We can state also that in terms of propagation, as the environment influence the model parameters, i.e. path loss exponent, intercept factor, etc., the higher the propagation losses the lower the connected region.

Given the above discussion this thesis contributes and provides a useful empiric channel model focused on low power applications in urban environments operating at the 868 MHz band (Chapter 3). The model has been obtained in scenarios close to real applications, specifically the height of the node with respect to the ground has been considered. Since WSN has stringent power constraints and taking the consideration that the nodes can be deployed near ground in certain applications, it was important to quantify the amount of additional losses and how them

affect the communication distance. Specifically, the provided model takes into account these additional losses that are caused mainly by the Fresnel obstruction by ground. Furthermore, other frequency bands are also considered and investigated (Chapter 4). The ISM 433 MHz band as a contribution is evaluated and compared with the well known 2.4 GHz ISM band in terms of propagation. This contribution demonstrates that the 433 MHz band besides of being a less crowded band than either 868 MHz and 2.4 GHz it has the advantage of a lower propagation losses. Specifically for a a given distance, the 433 MHz band provides a path gain of 14 dB with respect to 2.45 GHz, i.e. an external RF front end should be considered at the 2.45 GHz band to reach the same communication distance than the 433 MHz band.

All in all, this thesis has demonstrated that the communication distance is fairly reduced when the Fresnel zone is obstructed by ground due to the high amount of additional power losses. The 433 MHz band plays an important role because of the following: first despite of having a bigger Fresnel zone than 868 MHz and 2.45 GHz the lower the path loss counteracts with diffraction losses, i.e. even in LOS conditions at 2.45 GHz the communication distance is fairly smaller than the 433 MHz band for the same configuration parameters (transmit power, packet length, antenna).

5.2 Future research work

In this section we mention possible works for the future research. We are aim to follow in the same research field since the low power wireless technologies in the context of the future Internet of Things is interesting and presents a big challenge.

- Given the advantage of using channel hopping at the 433 MHz band to combat external narrowband interference, the future work is intended to evaluate its performance in terms of PDR in different environments such as office and industrial.
- Given the performance of the 433 MHz band at the physical layer and the fact that currently two standards are being developed (DASH7 and 802.15.4f) that focus on this band the future work is intended to focus on the upper layers. The idea is to evaluate the impact of the physical layer phenomenons to the upper layers, e.g how propagation characteristics affect routing protocols behavior in multi-hop communications.
- Given the advantage of having propagation losses 6 dB lower at the 433 MHz in comparison to the 868 MHz band which in turn traduces to a lower communication distance, as well as the characteristic of offering data rates up to 250 kbps, the future work is devised to evaluate this frequency band for commercial solutions.
- One of the interesting future works is to evaluate the performance of the 433 MHz, 868 MHz

and 2.45 GHz frequency bands in terms of propagation for other environments: ice, snow and water.

Bibliography

[1] Dohler M, Vilajosana I, Vilajosana X, Llosa J. Smart Cities: An Action Plan. In: Barcelona Smart Citiy Congress;. .

[2] IEEE Draft Standard for Local and Metropolitan Area Networks Part 15.4: Low Rate Wireless Personal Area Networks (LR-WPANs) Amendment: Active Radio Frequency Identification (RFID) System Physical Layer (PHY); 2011.

[3] Atmel. AT86RF212 Datasheet; 2010. Available from: `http://www.atmel.com/Images/doc8168.pdf`.

[4] (UNFPA) UPF. State of World Population 2007, Unleashing the Potential of Urban Growth. UNFPA; 2007. Available from: `http://www.unfpa.org/public/publications/pid/408`.

[5] Kinver M. The challenges facing an urban world; 2006. Available from: `http://news.bbc.co.uk/2/hi/science/nature/5054052.stm`.

[6] Tam L. Smart Cities, Limited Resources. SPUR The Urbanist Is Information Making Our Cities Smarter? 2012;517. Available from: `http://www.spur.org/publications/library/article/smart-cities-limited-resources`.

[7] OUTSMART EP. Provisioning of Urban-Regional Smart Services and Business Models Enabled by the Future Internet, Future Internet-Public Private Partnership (FI-PPP); 2011-2013. Available from: `http://www.fi-ppp-outsmart.eu/en-uk/about-project/Pages/Vision.aspx`.

[8] Kehua S, Jie L, Hongbo F. Smart City and the applications. International Conference on Electronics, Communications and Control (ICECC). 2011;p. 1028–1031.

[9] Lugaric L, Krajcar S, Simic Z. Smart City - Platform for Emergent Phenomena Power System Testbed Simulator. In: Innovative Smart Grid Technologies Conference Europe (ISGT Europe), IEEE PES; 2010. p. 1–7.

[10] Feltrin G, Saukh O, Bischoff R, Meyer J, Motavalli M. Structural monitoring with wireless sensor networks: Experiences from field deployments; 2011. .

[11] Xu N, Rangwala S, Chintalapudi KK, Ganesan D, Broad A, Govindan R, et al. A Wireless Sensor Network for Structural Monitoring. In: In Proceedings of the ACM Conference on Embedded Networked Sensor Systems(Sensys04); 2004. .

[12] IEEE Standard for Information Technology- Telecommunications and Information Exchange Between Systems- Local and Metropolitan Area Networks- Specific Requirements Part 15.4: Wireless Medium Access Control (MAC) and Physical Layer (PHY) Specifications for Low-Rate Wireless Personal Area Networks (WPANs); 2011.

[13] Yang Y, Hu J, Song T, Shen L. A Study of Near Ground Channel Model for 2.4GHz IEEE 802.15.4 Signal in Outdoor Environment. In: ICISE 2009, o 1st International Conference on Information Science and Engineering; 2009. .

[14] IEEE Draft Standard for Local and Metropolitan Area Networks Part 15.4: Low Rate Wireless Personal Area Networks (LR-WPANs) Amendment to the MAC sub-layer; 2011.

[15] Andrews J, Ghosh A, Muhamed R. Fundamentals Of Wimax. Understanding Broadband Wireless Access. 1st ed. Prentice Hall; 2007.

[16] Ghassemzadeh S, Larry L, Greenstein J, Kavcic A, Sveinsson T, Tarokh V. An Empirical Indoor Path Loss Model For Ultra-Wideband Channels. Communications Networks. 2003;5:303–308.

[17] Pardo J, Sala A, Delgado M, Lopez EE, Llacer L, Haro J. Channel Model at 868 MHz for Wireless Sensor Networks in Outdoor Scenarios. In: International Workshop on Wireless Ad hoc Networks; 2005. .

[18] Goldsmith A. Wireless Communications. 1st ed. Cambridge University Press; 2005.

[19] Sohrabi K, Manriquez B, Pottie G. Near ground wideband channel measurement in 800-1000 MHz. In: IEEE 49th Vehicular Technology conference (VTC); 1999. .

[20] Saleh A, Valenzuela R. A Statistical Model for Indoor Multipath Propagation. IEEE Journal on Selected Areas in Communications. 1987;5(2):128–137.

[21] Watteyne T, Lanziseram S, Mehta A, Pister K. Mitigating Multipath Fading Through Channel Hopping in Wireless Sensor Networks. In: IEEE International Conference on Communications (ICC); 2010. .

[22] Aaberge T. Low Complexity Antenna Diversity For IEEE 802.15.4 2.4 GHz PHY. Norwegian University of Science and Technology; 2009.

[23] Seybold J. Introduction to RF Propagation. Wiley-Interscience.; 2005.

[24] Sawant R, Liang Q, Popa D, Lewis F. Experimental Path Loss models For Wireless Sensor Networks. In: Military Communications Conference; 2007. .

[25] Aslam MI. New channel path loss model for near-ground antenna sensor networks. IET Wireless Sensor Systems. 2008;2-2:103–107.

[26] Sala AM, Pardo J, Lopez E, Alonso JV, Llacer L, Haro JG. An Accurate Radio Channel Model for Wireless Sensor Networks Simulation. Communications and Networks. 2005 December;7(4).

[27] Walden MC, Jackson T, Gibson WH. Development of an empirical path-loss model for street-light telemetry at 868 and 915 MHz. In: IEEE Int. Symposium on Antennas and Propagation. Great Chesterford, UK; 2011. p. 3389–3392.

[28] Ndzi DL, Arif MA, Shakaff AY, Ahmad MN, Harun LM A Kamarudin, Zakaria A, et al. Signal Propagation Analysis for Low Data Rate Wireless Sensor Network Applications in Sport Grounds and On Roads. Progress in Electromagnetics Researc. 2012;125:1–19.

[29] Stoyanova T, Kerasiotis F, Prayati A, Papadopoulos G. A Practical RF Propagation Model for Wireless Network Sensors. In: Third International Conference on Sensor Technologies and Applications (SENSORCOMM); 2009. p. 194–199.

[30] See CH, Abd-Alhameed RA, Hu YF, Horoshenkov KV. Wireless sensor transmission range measurement within the ground level. In: Antennas and Propagation Conference. Bradford,UK; 2008. p. 225–228.

[31] Zhang W, He Y, Liu F, Miao C, Sun S, Liu C, et al. Research on WSN Channel Fading Model and Experimental Analysis in Orchard Environment. In: CCTA (2)'11; 2011. p. 326–333.

[32] Wyne S, Santos T, Singh AP, Tufvesson F, Molisch AF. Characterisation of a time-variant wireless propagation channel for outdoor short-range sensor networks. IET Communications. 2010;4-3:253–264.

[33] Valcarce A, Krauss H, Hauck J, Buchholz M, Aguado F. Empirical propagation model for WiMAX at 3.5 GHz in an urban environment. Microwave and Optical Technology Letters. 2008;50-2:483–487.

[34] Walfisch J, Bertoni HL. A theoretical model of UHF propagation in urban environments. IEEE Transactions on Antennas and Propagation. 1988;36-12:1788–1796.

[35] Suzuki H. A Statistical Model for Urban Radio Propagation. IEEE Transactions on Communications. 1977;25-7:673–680.

[36] Xia H. A simplified analytical model for predicting path loss in urban and suburban environments. IEEE Transactions on Vehicular Technology. 1997;46-4:1040–1046.

[37] Zhong J, J K, Medouri A, Salazar M. A survey of various propagation models for mobile communication. IEEE Antennas and Propagation Magazine. 2003;45-3:51–82.

[38] Berkeley. TelosB Datasheet;. Available from: `http://www.willow.co.uk/TelosB_Datasheet.pdf`.

[39] Zolertia. Z1 datasheet; 2010. Available from: `http://zolertia.com/sites/default/files/Zolertia-Z1-Datasheet.pdf`.

[40] Xu D, Gao X, Zhang P, Wu Y. Indoor Office Propagation Measurements and Path Loss Models at 5.25 GHz. In: IEEE 66th Vehicular Technology Conference (VTC); 2007. .

[41] Kivinen J, Zhao X, Vainikainen P. Empirical Characterization of Wideband Indoor Radio Channel at 5.3 GHz. IEEE Transactions on antennas and propagation. 2001;49:1192–1203.

[42] Gil VP, Garcia A. Field Measurements and Guidelines for the Application of Wireless Sensor Networks to the Environment and Security. Sensors. 2009;9(12):10309–10325.

[43] Hongwei H, Youzhi X, Bilen C, Hongke Z. Coexistence Issues of 2.4 GHz Sensor Networks with other RF Devices at Home. In: SENSORCOMM 2009, o 1st International Conference on Technologies and Applications; 2009. .

[44] Watteyne T, Vilajosana X, Kerkez B, Chraim F, Weekly K, Wang Q, et al. OpenWSN: a standards-based low-power wireless development environment. Transactions on Emerging Telecommunication Technologies. 2012;23(1):480–493.

[45] European Telecommunications Standards Institute. Electromagnetic Compatibility and Radio Spectrum Matters (ERM); Short Range Devices (SRD); Radio equipment to be used in the 25 MHz to 1 000 MHz frequency range with power levels ranging up to 500 mW; Part 1: Technical characteristics and test methods. EN 300 220-1; 2000.

[46] Federal Communications Commission. Part 15 - Radio Frequency Devices; 15.231 Periodic operation in the band 40.66-40.70 MHz and above 70 MHz. FCC Part 15.231; 2011.

[47] ISO 18000-7:2009. Radio frequency identification for item management – Part 7: Parameters for active air interface communications at 433 MHz. ISO, Geneva, Switzerland; 2009.

[48] Kuladinithi K, An C, Timm-Giel A, Görg C. Performance evaluation of radio disjoint multipath routing. European Transactions on Telecommunications. 2009;20(7):668–678.

[49] Thelen J, Goense D, Langendoen K. Radio Wave Propagation in Potato Fields. In: 1st Workshop on Wireless Network Measurements; 2005. .

[50] Holland M, Aures R, Heinzelman W. Experimental Investigation of Radio Performance in Wireless Sensor Networks. In: 2nd IEEE Workshop on Wireless Mesh Networks (WiMesh); 2006. .

[51] Hampton JR, Merheb NM, Lain WL, Paunil DE, Shuford RM, Kasch WT. Urban Propagation Measurements for Ground Based Communication in the Military UHF Band. IEEE Transactions on Antennas and Propagation. 2006;54(2):644–654.

[52] Zhang W, He Y, Liu F, Miao C, Sun S, Liu C, et al. Research on WSN Channel Fading Model and Experimental Analysis in Orchard Environment. Computer and Computing Technologies in Agriculture. 2011;369:326–333.

[53] Wennerström H, Hermans F, Rensfelt O, Rohner C, Norden L. A Long-Term Study on the Effects of Meteorological Conditions on 802.15.4 Links. In: 8th Swedish National Computer Networking Workshop; 2012. .

[54] Tanghe E, Joseph W, Ruckebusch P, Martens L, Moerman I. Intra-, Inter-, and Extra-Container Path Loss for Shipping Container Monitoring Systems. IEEE Antennas and Wireless Propagation Letters. 2012;11:889–892.

[55] Mao X, Hui Lee Y, Chong Ng B. Wideband channel modelling in UHF band for urban area. In: IEEE International Symposium on Wireless Communication Systems (ISWCS 2008); 2008. p. 240–244.

[56] Phaebua K, Phongcharoenpanich C, Torrungrueng D, Chinrungrueng J. Short-distance and near-ground signal measurements in a car park of wireless sensor network system at 433 MHz. In: 5th International Conference on Electrical Engineering/Electronics, Computer, Telecommunications and Information Technology (ECTI-CON 2008); 2008. p. 241–244.

[57] Zhang X, Burress TW, Albers KB, Kuhn WB. Propagation comparisons at VHF and UHF frequencies. In: IEEE Radio and Wireless Symposium (RWS 2009); 2009. p. 244–247.

[58] Wu Q, Matolak DW, Apaza RD. Airport surface area propagation path loss in the VHF band. In: Integrated Communications, Navigation and Surveilance Conference (ICNS 2011); 2011. .

[59] Neskovic A, Neskovic N, Paunovic G. Modern approaches in modeling of mobile radio systems propagation environment. IEEE Communications Surveys and Tutorials. 2000;3:2–12.

[60] Balanis A. Antenna Theory: Analysis and Design. 3rd ed. John Wiley & Sons; 2005.

[61] Pozar M. Microwave Engineering. 4th ed. John Wiley & Sons; 2012.